UNIVERSITY OF CALIFORNIA, MERCED

Development of numerical models to predict cycling of mercury and salt in freshwater

A dissertation submitted in partial satisfaction of the requirements
for the degree of Doctor of Philosophy
by
Stefanie Helmrich

Dissertation Committee:
Peggy A. O'Day, Research Advisor
Marc W. Beutel
Charles N. Alpers
Nigel W. T. Quinn
Samuel J. Traina

2022

The Dissertation of Stefanie Helmrich, is approved, and it is acceptable in quality and form for Publication on microfilm and electronically:

Peggy A. O'Day Ph.D.
Research Advisor

Marc W. Beutel Ph.D.

Samuel J. Traina Ph.D.

Nigel W. T. Quinn Ph.D.

Charles N. Alpers Ph.D.

University of California, Merced
2022

Table of Contents

List of Figures

List of Tables

Acknowledgements

This dissertation would not have been possible without the help and support of many people. My family, advisors, and friends helped me to grow as a scientist and as a person.

I would like to express my deepest appreciation to my research advisor Dr. Peggy A. O'Day for her constant encouragement, patient guidance, invaluable advice, and trust. Her enthusiasm for geochemistry and dedication to rigorous science have been an inspiration for me. Thank you for providing me the challenges and opportunities in reaching this stage of my academic career and preparing me for a successful future. I would not be the scientist that I am today if I hadn't had her guidance. I am especially grateful to my committee member Dr. Nigel Quinn for his endless support and trust. He believed in me to excel in academia. The support he offered throughout the years truly made a positive impact on my research. I would like to extend my sincere thanks to my doctoral committee members Dr. Charles N. Alpers, Dr. Marc W. Beutel, and Dr. Samuel J. Traina for their advice during my research work. I was fortunate to have supportive and compassionate committee members.

I would like to thank my committee member Dr. Charles N. Alpers for sharing field data. A special mention goes to Dr. Dimitri Vlassopoulos for experimental data and advice. I acknowledge the financial support from the Delta Stewardship Council Fellowship program (Grant # 5298), the Delta Science Program in partnership with the California Department of Fish and Wildlife (Contract #18208), and UC Merced Environmental Systems Graduate Program.

I am grateful to my former and current colleagues, especially Alex, Ajith, Paul, Danielle, and Edwin. My friends QingQing, Angel, Xiumin, Lixia, Yocelyn, Dominique, Diana, and many others truly enhanced my graduate experience.

Last, but not least, I want to thank my family without whom this dissertation would not have been possible. A heartfelt thank you goes to my mom for her love and teaching me perseverance. A special acknowledgement goes to my husband and best friend, Benjamin who was always there to listen and support me emotionally.

Curriculum Vitae

Education

Doctor of Philosophy 2016-2022
Environmental Systems
University of California, Merced, USA.
Dissertation Title: Development of numerical models to predict cycling of mercury and salt in freshwater
Advisor: Peggy O'Day

Master of Science 2011-2014
Water Management
Technische Universität Dresden, Dresden, Germany.
Thesis Title: Analysis of different rainfall-runoff methods as basis for coupled channel network
and two-dimensional surface-runoff simulation
Advisor: Frank Blumensaat

Bachelor of Science 2008-2011
Water Management
Technische Universität Dresden, Dresden, Germany.
Thesis Title: Measurement of soil hydraulic parameters of agricultural land in Oman
Advisor: Rudolf Liedl

Publications

Tran, V., **Helmrich, S.**, Quinn, N. W. T., O'Day, P. (Forthcoming).
Operationalizing real-time monitoring data in simulation models using the public domain HEC-DSSVue platform. Journal of Water Resources Planning and Management.

Helmrich, S., Vlassopoulos, D., Alpers, C. N., & O'Day, P. A. (2021).
Critical review of mercury methylation and methylmercury demethylation rate constants in aquatic sediments for biogeochemical modeling. *Critical Reviews in Environmental Science and Technology*. https://doi.org/10.1080/10643389.2021.2013073

Quinn, N. W. T., **Helmrich, S.**, Herr, J., & Werkhoven, K. Van. (2018).
Decision Support for Control of Salt and Methylmercury Export from Managed Seasonal Wetlands. 9th International Congress on Environmental Modeling and Software "Modeling for Sustainable Food-Energy-Water Systems."
https://scholarsarchive.byu.edu/iemssconference/2018/Stream-B/8/

Conference Presentations

Quinn N. W. T., Tran V., **Helmrich S**. (2022)
Real-time monitoring data quality assurance for participatory real-time salinity management. iEMS, Brussels, Belgium (Oral).

Helmrich S., Quinn N. W. T., Herr J., Beutel M., O'Day P. (2021)
Improvement of WARMF model to simulate wetland processes leading to increased salinity. Bay-Delta Conference, Virtual, USA (Poster, 3rd place student award).

Helmrich S., Vlassopoulos D., Alpers C., Quinn N. W. T., O'Day P. (2020)
Thermodynamic-kinetic model of net methylmercury production in sediments as a management tool, CWEMF Annual Meeting, Virtual, US (Oral).

Helmrich S., Vlassopoulos D., Alpers C., Quinn N. W. T., O'Day P. (2020)
Biogeochemical simulations to assess the impact of redox processes on mercury cycling in sediment, Goldschmidt Virtual, USA (Oral).

Helmrich S., Vlassopoulos D., Alpers C., O'Day P. (2019)
Development of a kinetic-thermodynamic model to simulate the mercury cycle in freshwater sediments, American Chemical Society National Meeting, San Diego, CA, USA (Oral).

Helmrich S., Vlassopoulos D., Alpers C., O'Day P. (2019)
Simulation of mercury methylation and demethylation coupled to oxidation-reduction reactions in sediments of Delta tributaries, CWEMF Annual Meeting, Folsom, CA, USA (Oral).

Helmrich S., Vlassopoulos D., Alpers C., O'Day P. (2018)
Simulation of biogeochemical processes driving methylmercury production in different sediment habitats of the Delta and its tributaries, 10th Biennial Bay-Delta Science Conference, Sacramento, CA, USA (Oral).

Helmrich S., Vlassopoulos D., Alpers C., O'Day P. (2018)
Critical review of mercury methylation and demethylation rate laws for biogeochemical reaction modeling, Goldschmidt, Boston, MA, USA (Oral).

Helmrich S., Vlassopoulos D., O'Day P. (2017)
Development and application of a biogeochemical reaction-transport model for simulating mercury methylation in sediments at two mercury-impacted sites in California, 13th International Conference on Mercury as a Global Pollutant, Providence, RI, USA (Oral).

Helmrich S., Vlassopoulos D., O'Day P. (2017)
Assessment of the influence of climate change on mercury methylation on a molecular scale with a mechanistic reaction-transport model, 253rd American Chemical Society National Meeting, San Francisco, CA, USA (Oral).

Funding

2019 Southern California Edison Fellowship ($13,065)

2018 Delta Science Fellowship ($151.403)

2017 Environmental Systems Fellowship Summer ($6000)

2016 Environmental Systems Fellowship Summer ($6000)

Professional Development

2020 Reactive Transport Modeling in Geochemical Systems, Goldschmidt

2019 Top 10 finalists GradSLAM UC Merced, UC Merced

2019 Data Carpentry Workshop, UC Merced

2018 Top 10 finalists GradSLAM UC Merced, UC Merced

2016 EXAFS 2016 - SSRL Summer School on Synchrotron X-Ray Absorption Spectroscopy, SLAC

Teaching Experience

Fall 2017	Preparatory Chemistry, Teaching Assistant, Instructor Dr. M. Vidensek, UC Merced
Fall 2016, Spring 2017	Introduction to Earth System Science, Teaching Assistant, Instructor Dr. S. Masclin and P. O'Day, UC Merced
Spring 2016	Engineering Economic Analysis, Teaching Assistant, Instructor Dr. B. Harrison, UC Merced

Dissertation Abstract

Development of numerical models to predict cycling of mercury and salt in freshwater

Stefanie Helmrich

Doctor of Philosophy in Environmental Systems
University of California, Merced
2022

Peggy O'Day, Research Advisor

This dissertation focuses on understanding and quantifying how environmental conditions affect the fate of salinity and mercury in freshwater. Salinity and mercury concentrations are increasing due to anthropogenic activity and threaten ecosystem services of water bodies. Management is important to prevent further degradation. To reconcile management of multiple water quality parameters with ecosystem services, an improved basic knowledge and advanced tools are important. It is still difficult to identify main drivers for elevated salinity at a specific site and there are gaps in our basic understanding of mercury cycling. Therefore, this research focused on development and application of numerical models to improve our understanding of salinity and mercury cycling and to provide tools to plan management measures. The aim of the first chapter was to continue development of a module for seasonally managed wetlands as part of a real-time forecasting tool for salinity in the San Joaquin River watershed. Revising water sources, inflow time series, and model variables that determine the timing of outflow improved model performance by better representing the extensive reuse and recirculation within wetlands. Adequate simulation of conservative water quality parameters such as salinity is a pre-requisite to simulate non-conservative parameters such as mercury. The second chapter focused on critically reviewing published kinetic rate constants for mercury methylation and demethylation including application to a reaction-transport model. Mercury exists in multiple chemical forms and monomethylmercury (MeHg) is one of the most toxic forms. Two important variables that determine MeHg concentrations are the rate of MeHg production and degradation. The critical review informs selection of rate constants from literature and provides a tool to assess rate constants. Experimental conditions and mathematical assumptions were found to cause uncertainty and limit comparability. The aim of the third chapter was to apply a kinetic-thermodynamic model to field data to evaluate how environmental conditions affect MeHg production. The chapter shows how field data can be used to constrain model parameters. A novel rate formulation was developed to simulate precipitation of Hg minerals depending on concentrations of sulfur and organic matter. The addition of the rate improved simulated MeHg under a range of sulfide concentrations. Overall, numerical models proved suitable to identify knowledge gaps and improve basic understanding for both salinity and mercury in freshwater.

Dissertation Introduction

Elevated salinity and mercury concentrations due to anthropogenic activity threaten ecosystem services of water bodies. Salinization is a threat to the ecological functioning of freshwater waterbodies (Herbert et al., 2015) and increased salinity in agricultural irrigation water impedes plant germination (Quinn, 2009). The neurotoxin mercury that is mostly taken up through fish consumption is a significant human health concern (Chumney et al., 2021; Mergler et al., 2007). Anthropogenic activity is exacerbating degradation of water quality (Dodds et al., 2013) and putting water resources are under stress due to altered hydrology, mobilization of contaminants, and global warming. Management actions are necessary to prevent further degradation of water quality and need to consider multiple water quality parameters and reconcile them with ecosystem services.

Advanced tools such as numerical models are crucial to manage contaminants such as salinity and mercury. For salinity, real-time forecasting tools can help to maximize salt export while maintaining water quality objectives (Quinn et al., 2010). For mercury, data collection is expensive, and there are still many knowledge gaps. Models can help to identify main drivers and to test hypotheses.

This research focused on development and application of numerical models to improve understanding of salinity and mercury cycling and to provide tools for planning management measures. General challenges for simulation of contaminant fate are data insufficiency, data aggregation, scale mismatches, scaling from macro- to watershed scale, non-linearity, heterogeneity, transient conditions, model coupling, multiple model objectives and disconnection of models from conceptual models and observed data (Daniel et al., 2011; Fu et al., 2020; Paraska et al., 2014; Steefel, 2019). The presented research addresses some of those challenges for simulation of salinity with a watershed model and simulation of mercury with a reaction-transport model. The objectives were to reconcile aggregated data with the conceptual model for salinity cycling in seasonally managed wetlands, to address data scarcity for mercury methylation and demethylation constants, and to connect observed data to the conceptual model for mercury cycling in freshwater wetlands.

The first chapter is focused on continued development of a module for seasonally managed wetlands as part of a real-time forecasting tool for salinity in the San Joaquin River watershed. Models that adequately simulate salinity in managed wetlands are still under development and no comparable model exists. Available observed data have limitations and are aggregated, which needs to be addressed in the model. Revising water sources, inflow time series, and model variables that determine the timing of outflow greatly improved model performance by better representing the extensive reuse and recirculation within wetlands. Future work needs to address simulation of rain events and groundwater interactions.

The second chapter is focused on critically reviewing published rate constants for mercury methylation and demethylation including application to a reaction-transport model. Mercury exists in multiple chemical forms and monomethylmercury (MeHg) is one of the most toxic forms. Two important variables that determine MeHg concentrations are the rate of mercury methylation and demethylation, but there is considerable variability in published rate constants. Experimental conditions and mathematical assumptions were found to cause uncertainty and limit comparability. The critical review informs selection of rate constants from literature and provides a tool to assess rate constants. The reviews points to a need for more research on demethylation rate constants.

The third chapter is aimed to apply a kinetic-thermodynamic model to field data from floodplains to evaluate how environmental conditions, especially iron and sulfur affect MeHg production. The chapter shows how field data can be used to constrain model parameters and to highlight data needs. Mismatch of simulation results and observed data served to identify potential

flaws in the underlying conceptual model. A novel rate formulation was developed to simulate precipitation of Hg minerals depending on sulfur and organic matter concentration. The addition of the rate formulation greatly improved simulation of MeHg production under a range of environmental conditions and informs the underlying conceptual model.

References

Chumney, L., Klasing, S., & Tran Pham, H. (2021). Statewide health advisory and guidelines for eating fish from California's lakes and reservoirs without site-specific advice. California Environmental Protection Agency (Issue August). https://oehha.ca.gov/media/downloads/advisories/fishadvisorystatewidelakesreport2021.pdf

Daniel, E. B., Camp, J. V., LeBoeuf, E. J., Penrod, J. R., Dobbins, J. P., & Abkowitz, M. D. (2011). Watershed modeling and its applications: A state-of-the-art review. The Open Hydrology Journal, 5(1), 26–50. https://doi.org/10.2174/1874378101105010026

Dodds, W. K., Perkin, J. S., & Gerken, J. E. (2013). Human impact on freshwater ecosystem services: A global perspective. Environmental Science and Technology, 47(16), 9061–9068. https://doi.org/10.1021/es4021052

Fu, B., Horsburgh, J. S., Jakeman, A. J., Gualtieri, C., Arnold, T., Marshall, L., Green, T. R., Quinn, N. W. T., Volk, M., Hunt, R. J., Vezzaro, L., Croke, B. F. W., Jakeman, J. D., Snow, V., & Rashleigh, B. (2020). Modeling water quality in watersheds: From here to the next generation. Water Resources Research. https://doi.org/10.1029/2020wr027721

Herbert, E. R., Boon, P., Burgin, A. J., Neubauer, S. C., Franklin, R. B., Ardon, M., Hopfensperger, K. N., Lamers, L. P. M., Gell, P., & Langley, J. A. (2015). A global perspective on wetland salinization: Ecological consequences of a growing threat to freshwater wetlands. Ecosphere, 6(10), 1–43. https://doi.org/10.1890/ES14-00534.1

Mergler, D., Anderson, H. A., Chan, L. H. M., Mahaffey, K. R., Murray, M., Sakamoto, M., & Stern, A. H. (2007). Methylmercury exposure and health effects in humans: A worldwide concern. Ambio, 36(1), 3–11. https://doi.org/10.1579/0044-7447(2007)36[3:MEAHEI]2.0.CO;2

Paraska, D. W., Hipsey, M. R., & Salmon, U. (2014). Sediment diagenesis models: Review of approaches, challenges and opportunities. Environmental Modelling and Software, 61, 297–325. https://doi.org/10.1016/j.envsoft.2014.05.011

Quinn, N. W. T. (2009). Environmental decision support system development for seasonal wetland salt management in a river basin subjected to water quality regulation. Agricultural Water Management, 96(2), 247–254. https://doi.org/10.1016/j.agwat.2008.08.003

Quinn, N. W. T., Ortega, R., Rahilly, P. J. A., & Royer, C. W. (2010). Use of environmental sensors and sensor networks to develop water and salinity budgets for seasonal wetland real-time water quality management. Environmental Modelling and Software, 25(9), 1045–1058. https://doi.org/10.1016/j.envsoft.2009.10.011

Steefel, C. I. (2019). Reactive Transport at the Crossroads. Reviews in Mineralogy and Geochemistry, 85(1), 1–26. https://doi.org/10.2138/rmg.2019.85.1

1. Salinity forecasting with improved model of seasonal wetlands

1.1. Abstract

Seasonally managed wetlands provide a multitude of ecosystem functions but can affect water quality in receiving tributaries. Salt export from seasonally managed wetlands in arid and semi-arid regions often coincides with germination of salt sensitive crops. To protect irrigated crops and avoid salt build up on soils, salt export can be coordinated with tributary inflows that are low in salinity. Salt export management can be improved with model-based salinity forecasting. Salinity forecasting for seasonal wetlands faces challenges when there are large wetland areas with complex water delivery and drainage system. The Watershed Analysis Risk Management Framework (WARMF) is routinely used for real-time forecasting in the San Joaquin River (SJR) watershed in California, but simulation of seasonal wetland complexes needed improvement. In 2015, WARMF's conceptual wetland module was updated to a bathtub analogue because the bathtub analogue closely resembles management of seasonal wetland ponds. Although the update to the bathtub analogue improved the simulated hydrology, more refinement is needed. Wetland hydrology and drainage salinity simulations for two sub-catchments with differing water sources were performed and compared with previously unused real-time data at the same site. Model input time series were adjusted to represent the aggregation of multiple wetland impoundments into one simulated sub-catchment. It was found that considering the incidental reuse within the water delivery system improved simulated electrical conductivity (EC). Simulations identified the need to further adjust the bathtub analogue for seasonal wetlands to better simulate rain events. The improvements present an important step towards better real-time forecasting for large seasonal wetland areas with complex water delivery and drainage systems.

1.2. Introduction

Seasonally managed wetlands provide important ecosystem functions such as habitat for waterfowl, improve water quality, and sequester carbon. However, wetlands are under threat due to salinization (Herbert et al., 2015) and salt export from seasonally managed wetlands in arid and semi-arid regions often coincides with germination of salt sensitive crops. To protect irrigated crops and avoid salt build up on soils, salt export can be coordinated with tributary inflows that are low in salinity. Simulation models can provide decision support to manage salt export from seasonally managed wetlands. There is currently no commonly used model to simulate seasonally managed wetlands. This research is looking at wetland complexes that cover large areas and have complex water delivery and drainage system that pose challenges for salinity forecasting such as data scarcity and aggregation. Depending on the main drivers and the modeling purpose, different approaches might be suitable to model seasonal wetlands. Some previously developed algorithms for the simulation of seasonal wetland hydrology in arid regions share common features. Kang et al. (2006) adapted the soil and water assessment tool (SWAT) to simulate runoff but not runoff salinity from flooded rice paddy fields when the water level in the rice field exceeded a fixed depth – a bathtub analogue. Flooded rice paddy fields have a similar hydrology to seasonally managed wetlands. Evenson et al. (2018) improved the simulation of wetlands in depression-rich landscapes in which wetlands were represented as separate impoundments instead of aggregating the storage capacity of multiple wetlands. This strategy is less suitable for wetlands that have a high density of impoundments and many small drainage features. Li et al. (2021) developed a model using the popular DRAINMOD software. The lumped DRAINMOD application simulated water and salt balances including subsurface flow to and from wetland ditches. The purpose of the wetland ditches

was to improve agricultural drainage water quality while providing a waterfowl food supply. The water in these wetlands was supplied largely from subsurface accretions into the ditches.

The focus of the current research was a seasonally managed wetland complex in California's Central Valley, which has a semi-arid climate (Figure 1.1). Seasonally managed wetlands in the Grasslands Ecological Area (GEA) are part of the Pacific Flyway and provide food for migrating and overwintering waterfowl (Oppenheimer & Grober, 2002). The wetland complex covers an area of 240,000 acre and water is supplied and drained via s complex system. Increased salinity in drainage flow from GEA wetlands occurs because the hydrology has been altered, underlying groundwater that is naturally high in salts is used for supplemental water supply, and inflowing surface water has already degraded water quality (Oppenheimer & Grober, 2002). Management of salinity is crucial to preserve the water quality of agricultural irrigation diversions and other ecosystem purposes downstream along the San Joaquin River (SJR) and in the southern Delta (Quinn, 2009). The SJR is the second largest tributary to the Delta, which provides drinking water for two thirds of the population in California. The SJR basin is a leading region for agricultural production that generates 50 % of California's agricultural output (Hanak et al., 2019) resulting in more than $5 billion in crop revenue per year (Medellín-Azuara et al., 2015).

The Watershed Analysis Risk Management Framework (WARMF) is used for short-term forecasting of salinity and salt load assimilative capacity in the SJR by the US Bureau of Reclamation (USBR). WARMF is a physically based watershed model that has utility for total maximum daily load (TMDL) analysis (Chen et al., 2008). The WARMF model was derived from the storm water management model (SWMM) and the integrated lake-watershed acidification study (ILWAS) model. In 2006, the WARMF model was enhanced to simulate processes of mercury cycling (Chen et al., 2006). In 2015, WARMF's conceptual wetland module was updated from a slow-moving river analogue to a bathtub analogue (Van Werkhoven, 2015) because the bathtub analogue better represents flooding and draining of seasonal wetlands by pulling weir boards. Although the update to the bathtub analogue improved simulated hydrology, more refinement is needed.

The main goal of this paper was to improve the simulation of seasonal wetland hydrology and water quality by revising water sources, inflow, and prescribed pond depth input time series. Sensor data were used to constrain boundary conditions. Simulations for two sub-catchments with differing water sources were performed for a wet and a dry water year hydrology. A hypothetical simulation scenario with a reduced water supply under drought conditions was performed to verify the utility of the model enhancements.

1.3. Approaches to simulate seasonal wetlands in WARMF

In WARMF, seasonal wetlands were initially simulated with a slow-moving river analogue. In this approach, water that is not subject to immediate runoff either infiltrates or remains on the surface. Water that remains on the surface is calculated as:

$$D = (I_{A1} - I_1)(\frac{d}{100}) \tag{1.1}$$

where D is detention storage (cm), I_{A1} is water available for infiltration into the first soil layer (cm), I_1 is water that will infiltrate into the first soil layer (cm), and d is the percent of surface water that is retained. To simulate wetlands as slow-moving river the percent of retained water (d) had been set to greater than 95 %. In summer, when seasonal wetlands are dry there is no surface water. Water leaving the wetland is calculated using Manning's equation:

$$Q_s = \frac{WZ_0 S^{1/2}}{n \cdot 0.01^{1/3}} \quad (1.2)$$

where Q_S is the runoff (cm), n is Manning's roughness coefficient (day/[$cm^{1/3}$]), W is the width of the catchment parallel to the receiving stream (cm), S is slope of the hydraulic grade line (cm/cm), and Z_0 is the water depth calculated as:

$$Z_0 = I_{A1} - I_1 - D \quad (1.3)$$

Van Werkhoven (2015) updated WARMF's conceptual wetland module to a bathtub analogue where the retained water is calculated with the help of a prescribed pond depth time series and the remaining water is subject to Manning's overland routing as in the previous approach. In the updated approach the retained water is calculated as:

$$V_W = A_W \cdot d_p \quad (1.4)$$

where V_W is water stored in one wetland catchment (cm^3), A_W is the wetland catchment area (cm^2), and d_p is the prescribed pond depth at time t (cm). This approach allows a rapid change in retained water that mimics the actual management of seasonal wetlands. To determine how much water is available as outflow, the water depth at time step t is calculated as:

$$d_t = d_{t-1} + d_1 \quad (1.5)$$

where d_{t-1} is the water depth at the previous time step (cm), and d_I is the inflow depth (cm). When $d_t < d_p$ all water is retained. When $d_t > d_p$, water above d_p is subject to Manning's overland flow. If Manning's N value is greater than zero, water in addition to V_W will be retained and the resulting water depth will be added to the prescribed pond depth.

In WARMF, wetlands in the GEA were divided into 11 large model sub-catchments to simulate water delivery and wetland drawdown (drainage). The update to a bathtub model improved the simulation of wetland drainage (Figure 1.2). Peaks were better matched because the model better represents flooding and draining of seasonal wetlands by pulling weir boards.

Van Werkhoven (2015) noted that further revision of developed input time series would be necessary to further improve the simulation of drainage flow during flood-up and simulation of electrical conductivity (EC) during the whole hydroperiod. Van Werkhoven (2015) had developed a prescribed pond depth time series by averaging and normalizing water depth time series that were measured at inlets and outlets of selected ponds (Figure 1.3) but found that calibration of prescribed pond depth time series would be needed to match prescribed pond depth time series with irrigation volume. The major limitation to the approach to derive pond depth time series from measured depth time series was that it did not consider that sub-catchments simulate average flood-up and drainage conditions. In addition, Van Werkhoven (2015) revised the area of managed wetlands and the inflow based on U.S. Bureau of Reclamation Water Management Plans, and data from the Water Acquisition Program and the Central Valley Operations Office. Available data were limited in that water deliveries to non-wetland areas and water in addition to water service contract deliveries were included. Moreover, water sources and therefore EC were not recorded, and values were monthly instead of daily values. The data limitations resulted in a need to make assumptions affecting initial values of wetland deliveries and the inflow salt loads.

1.4. Study area and model evaluation

Simulated sub-catchments were selected based on available observed data at the inlets and outlets. Observed data were available from the Grasslands Wildlife District (GWD) and are rated excellent and good according to the published U.S. Geological Survey data quality control guidelines (Wagner et al., 2006) (see Suppl. Information for details). The two sub-catchments roughly correspond to drainage areas serviced by the monitoring stations Mud Slough at Gun Club Road (GCR) and Fremont Canal at GCR. These two drainage canals account for more than 80% of the total wetland drainage from GWD. The two sub-catchments are located next to each other within the North GWD (see Figure 1.1) and will henceforth be referred to as Mud Slough and Fremont. The Mud Slough sub-catchment (11,667 acres) receives most of its water supply from the Santa Fe Canal (SFC), a major water supply and drainage conveyance that connects the southern and northern divisions of the district. The SFC conveys water supply from the Delta Mendota Canal, with wetland return flows that are diverted and return to the SFC along its length. This factor complicates the estimation of influent water quality since these returns progressively elevate the influent wetland salinity concentrations as one moves from south to north downstream along the SFC. In addition, Mud Slough receives recirculated water via a new recirculation system that began operation in 2019. The Fremont sub-catchment represents a much smaller wetland area (1,876 acres) and receives water mostly from the San Luis Canal, which receives water from the DMC and minor volumes of local drainage.

Model simulations were performed for two hydroperiods. A hydroperiod describes the time during which an area of land is wetted and, in the current example refers to the time between the end of the flood-up period in the fall (typically in late August/early September) and the end of wetland drawdown in the following spring. The hydroperiod was chosen because flood-up usually starts before the start of the water year on October 1st. The simulated 2018/19 hydroperiod coincided with a wet water year (Anderson, 2019), and the 2019/2020 hydroperiod coincided with a dry water year (Anderson, 2020).

Table 1.1 provides an overview of the WARMF model simulations that were performed to revise input time series of inflow and EC (revised water sources), calibrate prescribed pond depth time series, and assess management options under drought conditions. An evaluation of the input times series was based on a visual comparison of observed and simulated flow, EC and salt, and by calculating the percent difference between simulated and observed flow and salt load for each sub-catchment and hydroperiod.

A hypothetical scenario with reduced water supply under drought conditions was developed for Mud Slough and based on the revised scenario without recirculation for hydroperiod 2019/20. In the hypothetical scenario, water supply was reduced by 25 % during flood-up and there was no maintenance inflow provided after November 30. The hypothetical scenario also assumes a 25 % reduction of the flooded area of seasonal wetlands, which was converted in the model to the category *Barren Land* or *Grassland*. Rain events were assumed to be the same as during hydroperiod 2019/20. The EC of the inflow water was assumed to be the same as in hydroperiod 2019/20, although EC could be elevated in a year with a reduced water supply.

1.5. Simulation results

1.5.1. Flow

The simulation of drainage flow in Mud Slough and Fremont was improved due to a more realistic inflow and prescribed pond depth time series. Revision of prescribed pond depth time

series particularly improved simulated flow during fall flood-up (Figure 1.4A). Table 1.2 shows the percent difference between simulated and observed drainage flow for each hydroperiod. One minor model limitation is that in some cases flow is predicted to occur in summer but is not observed in the field (Figure S1.1A). This is the case when agricultural lands that are located within the wetland sub-catchment are irrigated in summer, which means that water is forced of the model catchment because the prescribed pond depth is zero.

1.5.2. Electrical Conductivity

The simulated EC was improved due to a more realistic blend of inflow sources and higher estimated flow volumes during fall flood-up (Figure 1.4 A, B). Observed EC from the closest monitoring station was used to set inflow EC in the revised model. In the revised model, inflowing water for Mud Slough has a higher EC, which resulted in higher simulated EC in drainage flows (~500 µmho/cm increase). For Fremont, the EC of the inflow was similar in the revised and original model, resulting in similar simulated drainage EC.

It is important to note that the simulated EC depends strongly on the simulated ratio of surface to subsurface drainage flow. The total drainage flow is completely composed of subsurface drainage flow when EC > 3000 µmho/cm. Surface drainage only represents a large percentage of the total drainage flow during drawdown or rain events.

1.5.3 Salt Load

The simulated salt load was improved and matches better with observed salt load for Mud Slough (Figure 1.4 D) and Fremont (Figure S4B, C). Table 1.2 shows the percent difference between simulated and observed salt load for each hydroperiod. The simulated salt load for Mud Slough is close to 100 %, however only when simulated drainage flow per hydroperiod is slightly overestimated. This means that the simulated drainage EC is on average lower than the observed EC. For Fremont, the simulated salt load for each hydroperiod is overpredicted. However, the overprediction is driven by slight overprediction in summer, which is of little relevance when simulating seasonal wetlands as part of the SJR watershed. The salt load prediction is good during fall, winter, and spring.

1.5.4 Scenario with recirculation of water

Consideration of a recirculation system that started operation in 2019 improved the match of simulated and observed EC in Mud Slough for hydroperiod 2019/20 (Figure 1.6). When recirculated water constituted 12 % of the inflow, the simulated drainage EC was on average 100 – 200 µmho/cm higher. The simulated EC in the drainage was 200-300 µmho/cm higher when nearly all drainage was recirculated and constituted 23 % of the inflow (Figure 1.6 A, B, S1.2). Because the percentage of recirculated water on total water volume was highest in January and February, the effect of increased EC was most pronounced at the end of February and start of March.

1.5.5 Hypothetical scenario with reduced water supply

In a hypothetical simulation scenario for Mud Slough the reduced water supply resulted in less drainage and salt load export as would be expected (Figure 1.7A, S1.3). The water that is

released during drawdown has almost the same simulated EC as the inflowing water during fall flood-up (Figure 1.7B).

1.6. Discussion

1.6.1. Assessment of revised model assumptions

Revision of prescribed pond depth time series (Figure 1.5) improved the simulation of flow and EC during fall flood-up. The depth time series was revised to produce a slower increase in pond depth over several months, which more accurately simulates flood-up conditions in sub-catchments and was based on flood-up schedules. Development of a prescribed pond depth profile should consider how many wetland impoundments are aggregated into one model sub-catchment and should make use of any information about timing of flood-up. Only minor revisions to the prescribed pond depth were necessary to improve simulation during drawdown. The revised pond depth profile for Fremont is slightly steeper than the one for Mud Slough during drawdown. The Fremont sub-catchment is smaller than the Mud Slough sub-catchment which may account for the more rapid drawdown.

The simulations showed that the timing of the applied inflow water, not only the amount is crucial. In three out of four revised simulation scenarios, the inflow volume per hydroperiod was smaller than in the original model (Table S1.1). The lower inflow volume still resulted in more drainage volume exported per hydroperiod because the revised inflow time series assumed no inflow during the summer months and more during flood-up. With the original inflow time series, more water would directly evaporate or infiltrate into the soil during the summer months. The water diversions assumed for wetland maintenance over the winter months were similar for both models.

The inflow volume diverted into each wetland impoundment needed to be higher for dry year hydrology than for wet year hydrology. For Mud Slough, the inflow during flood-up was 5 % higher for the dry year, which was expected since less water is supplied via precipitation. For Fremont, it was necessary to increase the maintenance flow, but not the inflow during fall flood-up.

The EC of the inflowing water is an important factor for simulating wetland drainage EC. In the original WARMF model algorithm wetland sub-catchments received water supply from a single source - the DMC via the Mendota Pool, where water could co-mingle with in stream flow from the SJR. This set up did not account for reuse within the GEA and small-scale groundwater pumping.

The bathtub analogue could be further improved to better simulate rain events. In the revised and original approach, sharp simulated drainage peaks coincide with rain events (Figure 1.4C). During simulated drainage peaks the EC was simulated to be several hundred µmho/cm lower than before or after those peaks. The simulated drainage peaks do not match with observed data - drainage increases only lightly after rain events and has no effect on observed EC, which indicates that some rainwater is retained. The reason for the poor simulation of rain events is that storage volume and release of water cannot be set separately with the employed bathtub analogue. To simulate drainage due to maintenance flows the water depth must be set higher than the prescribed pond depth. This means that water from rain events cannot be retained at times when maintenance flows are being simulated. The bathtub analogue should be further modified to allow simulation of maintenance flows at the same time as retention of rainwater.

1.6.2. Assessment of reduced water supply under drought conditions

The simulation of EC for this hypothetical scenario needs further improvement through better estimates for initial conditions. During drawdown simulated EC was equal or lower than with the regular water supply, which is not as expected and likely the result of simplified assumptions (Figure 1.7B). Due to a lack of data the EC of the inflowing water was assumed to be the same with reduced and regular water supply, although the EC will be likely higher when water supply is reduced. This resulted in on average lower EC of inflowing water because the EC in the inflow increases from fall to spring, but in the scenario with reduced water supply the water application stops after November. In addition, precipitation was assumed to be the same in both scenarios and results in stronger dilution with reduced water supply. Moreover, the fluctuation of GW pumping depending on water supply from other sources is not accounted for.

Although in this hypothetical scenario the water is retained in the ponds for several months, the EC is almost unchanged when water is drained in spring, which indicates that some processes that cause an increase in EC over time are too weak in the model. A reason might be that capillary rise from shallow groundwater and salt accumulation on soil is not included in the WARMF wetland module because it is difficult to quantify although it is an important process that affects salinity in seasonal wetlands in semi-arid regions (Crosbie et al., 2009; Jolly et al., 2008; Liu et al., 2019; van der Kamp & Hayashi, 2009).

1.7. Summary

This research gives general guidance on applying the bathtub analogue to simulate seasonal wetlands within a large watershed and it gives recommendations to estimate input time series for wetlands in the San Joaquin River watershed. Simulations for two sub-catchments with differing water sources were performed and compared with observed data. Simulations showed that water inflow to catchments needs to be higher in fall than previously assumed to reproduce observed data. The initial EC affects the simulated drainage EC and was improved by revising water sources to consider reuse and recirculation of water within the simulated wetland system. It was also found that a prescribed pond depth input time series that defines how much water can be held back by a wetland catchment had to be revised to consider the flood-up schedule for all wetland ponds that are represented by one model catchment. Because the simulated area is large, many wetland ponds are aggregated into one catchment, which results in the need for a prescribed pond depth time series that is flatter during flood-up than the actual pond depth for a single wetland pond. The improvements present important steps towards a better real-time forecasting model for salinity management.

1.8. References

Anderson, M. (2019). Hydroclimate report water year 2019. In California Department of Water Resources. https://doi.org/10.1108/dpm.2000.07309aag.019

Anderson, M. (2020). Hydroclimate report water year 2020. In California Department of Water Resources. https://doi.org/10.1108/dpm.2000.07309aag.019

Chen, C., Herr, J. W., & Goldstein, R. a. (2008). Model calculations of total maximum daily loads of mercury for drainage lakes. Journal of the American Water Resources Association, 44(5), 1295–1307. https://doi.org/10.1111/j.1752-1688.2008.00224.x

Chen, C., Herr, J. W., & Tsai, W. (2006). Enhancement of Watershed Analysis Risk Management Framework (WARMF) for mercury watershed management and total maximum daily loads (TMDLs). Electric Power Research Institute.

Crosbie, R., McEwan, K. L., Jolly, I. D., Holland, K. L., Lamontagne, S., Moe, K. G., & Simmons, C. T. (2009). Salinization risk in semi-arid floodplain wetlands subjected to engineered wetting and drying cycles. Hydrological Processes, 23(24), 3440–3452. https://doi.org/10.1002/hyp.7445

Evenson, G. R., Jones, C. N., McLaughlin, D. L., Golden, H. E., Lane, C. R., DeVries, B., Alexander, L. C., Lang, M. W., McCarty, G. W., & Sharifi, A. (2018). A watershed-scale model for depressional wetland-rich landscapes. Journal of Hydrology X, 1, 100002. https://doi.org/10.1016/j.hydroa.2018.10.002

Hanak, E., Escriva-Bou, A., Gray, B., Green, S., Harter, T., Jezdimirovic, J., Lund, J., Medellin-Azuara, Moyle, P., & Seavy, N. (2019). Water and the Future of the San Joaquin Valley. Technical Appendix A: Updated Assessment of the San Joaquin Valley's Water Balance (Issue 83586701). https://www.ppic.org/wp-content/uploads/0219ehr-appendix-a.pdf

Herbert, E. R., Boon, P., Burgin, A. J., Neubauer, S. C., Franklin, R. B., Ardon, M., Hopfensperger, K. N., Lamers, L. P. M., Gell, P., & Langley, J. A. (2015). A global perspective on wetland salinization: Ecological consequences of a growing threat to freshwater wetlands. Ecosphere, 6(10), 1–43. https://doi.org/10.1890/ES14-00534.1

Jolly, I. D., McEwan, K. L., & Holland, K. L. (2008). A review of groundwater–surface water interactions in arid/semi-arid wetlands and the consequences of salinity for wetland ecology. Ecohydrology, 1, 43–58. https://doi.org/10.1002/eco

Kang, M. S., Park, S. W., Lee, J. J., & Yoo, K. H. (2006). Applying SWAT for TMDL programs to a small watershed containing rice paddy fields. Agricultural Water Management, 79(1), 72–92. https://doi.org/10.1016/j.agwat.2005.02.015

Li, S., Wu, M., Jia, Z., Luo, W., Fei, L., & Li, J. (2021). Influence of different controlled drainage strategies on the water and salt environment of ditch wetland: A model-based study. Soil and Tillage Research, 208(November 2020), 104894. https://doi.org/10.1016/j.still.2020.104894

Liu, B., Zhao, W., Wen, Z., Yang, Y., Chang, X., Yang, Q., Meng, Y. Y., & Liu, C. (2019). Mechanisms and feedbacks for evapotranspiration-induced salt accumulation and precipitation in an arid wetland of China. Journal of Hydrology, 568(May 2018), 403–415. https://doi.org/10.1016/j.jhydrol.2018.11.004

Medellín-Azuara, J., MacEwan, D., Howitt, R. E., Koruakos, G., Dogrul, E. C., Brush, C. F., Kadir, T. N., Harter, T., Melton, F., & Lund, J. R. (2015). Hydro-economic analysis of groundwater pumping for irrigated agriculture in California's Central Valley, USA. Hydrogeology Journal, 23(6), 1205–1216. https://doi.org/10.1007/s10040-015-1283-9

Oppenheimer, E. I., & Grober, L. F. (2002). Total maximum daily load for salinity and Boron in the lower San Joaquin River. https://www.waterboards.ca.gov/rwqcb5/water_issues/tmdl/central_valley_projects/vernalis_salt_boron/saltandborontmdljan2002.pdf

Quinn, N. W. T. (2009). Environmental decision support system development for seasonal wetland salt management in a river basin subjected to water quality regulation. Agricultural Water Management, 96(2), 247–254. https://doi.org/10.1016/j.agwat.2008.08.003

van der Kamp, G., & Hayashi, M. (2009). Groundwater-wetland ecosystem interaction in the semiarid glaciated plains of North America. Hydrogeology Journal, 17(1), 203–214. https://doi.org/10.1007/s10040-008-0367-1

Van Werkhoven, K. (2015). Technical Memorandum. Task C3.1. WARMF Model Upgrade to simulate Managed Wetland Operations.

Wagner, R. J., Boulger, R.W., J., Oblinger, C. J., & Smith, B. A. (2006). Guidelines and Standard Procedures for Continuous Water-Quality Monitors: Station Operation, Record Computation, and Data Reporting: U.S. Geological Survey Techniques and Methods. https://doi.org/10.3133/tm1D3

1.9 Figures and Tables

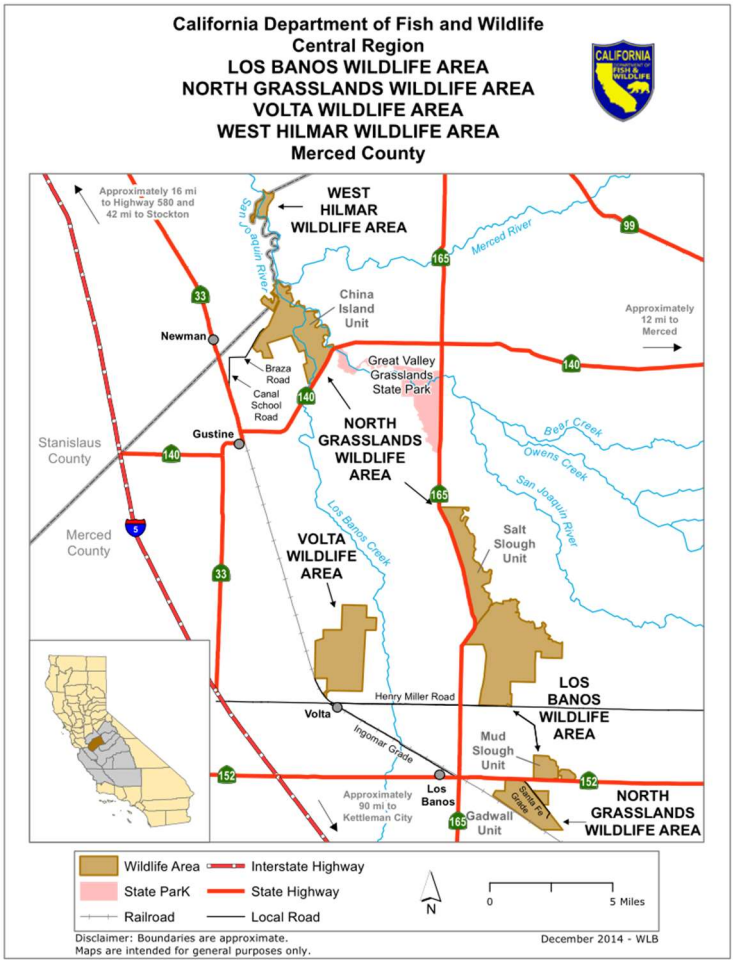

Figure 1.1: Wetlands within the North Grasslands Wildlife Area that is part of the Grasslands Ecological Area in the San Joaquin River basin were simulated.

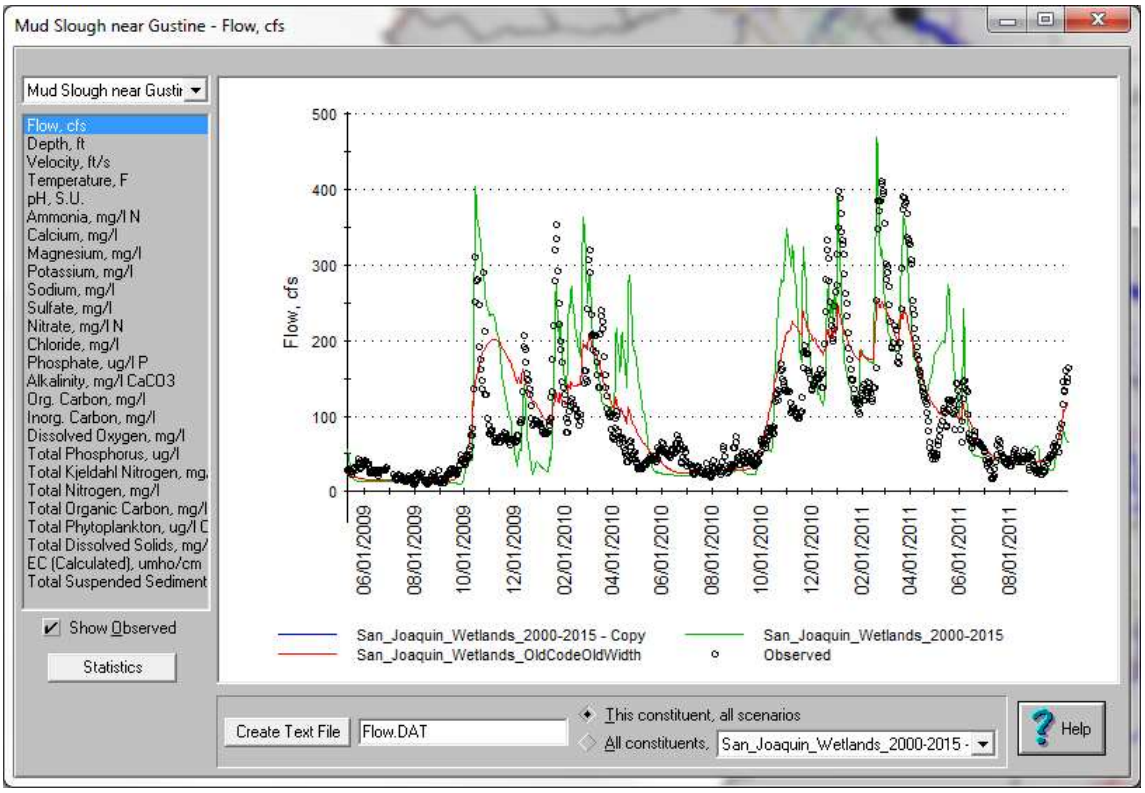

Figure 1.2: Observed flow (black) and simulated flow at Mud Slough near Gustine before the model upgrade (red) and after both the model upgrade and routing adjustment (green). Figure from Van Werkhoven (2015).

Figure 1.3: Figures from Van Werkhoven (2015). Top: Observed pond outlet depth normalized by the maximum depth for each drain along with the average of all 7 drains (red). Bottom: Normalized pond outlet depth (red), smoothed (30-day running average) (blue), and WARMF-adjusted mean areal pond depth (green).

Table 1.1: Overview of revisions to model set up and assumptions of input time series for each simulation scenarios.

WARMF catchment	Simulation scenario	Water source (EC of inflow)	Assumed inflow[a]	Prescribed pond depth profile[b]
Mud Slough at GCR	Original	DMC, MP (simulated)	Original	Original
	Revised	Santa Fe Canal (observed[c])	Revised Mud Slough	Mud Slough at GCR
	Revised + recirculation 12 %	Santa Fe Canal, 12 % recirculated water (observed[c])	Revised Mud Slough	Mud Slough at GCR
	Revised + recirculation 23 %	Santa Fe Canal, 23 % recirculated water (observed[c])	Revised Mud Slough	Mud Slough at GCR
	Hypothetical[e]	Santa Fe Canal, recirculated water (observed[c])	75 % during flood-up, no maintenance	Mud Slough at GCR
Fremont Canal at GCR[f]	Original	San Luis Canal (simulated)	Original	Original
	Revised	San Luis Canal (observed[c])	Revised Fremont	Fremont Canal at GCR

[a] Assumed inflow is included in plots of flow.
[b] Prescribed pond depth profiles are plotted in Suppl. Info Figure S1.2
[c] Observed EC is included in plots of EC. Monitoring station names: Santa Fe Canal: SFC_@_152, Recirculation: SFC_Discharge, San Luis Canal: SL-1
[d] Only Year 2019/2020, since recirculation started in 2019
[e] The area of flooded wetlands was reduced by designating more land are as Grassland or Barren Land.
[f] No scenario with recirculated water was performed because Fremont Canal does not receive recirculated water. No hypothetical scenario was performed because the uncertainty of observed data is high and because the effect of simulated management options would be small because the WARMF catchment is small.

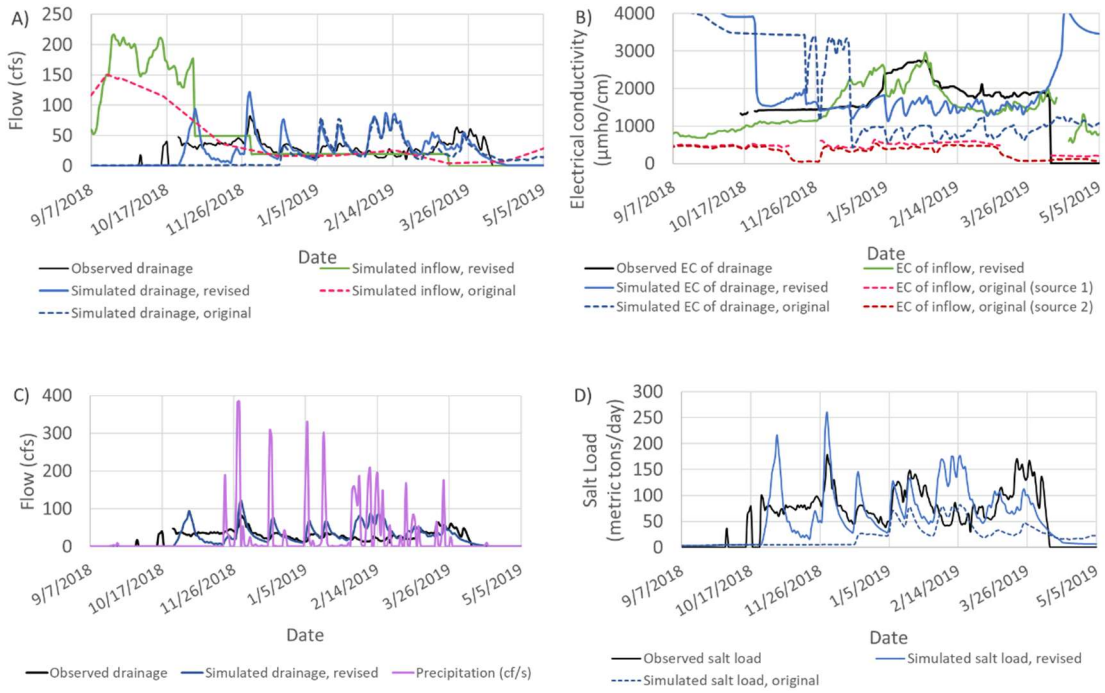

Figure 1.4: Inflow and drainage (A), EC (B), precipitation (C), and salt load (D) observed at Mud Slough at GCR monitoring station or simulated for sub-catchment Mud Slough with scenarios "original" and "revised". Observed drainage and drainage EC at Mud Slough at GCR monitoring station (solid black), assumed inflow and inflow EC in revised model (solid green), assumed inflow and inflow EC in original model (dashed red line), simulated drainage and drainage EC with revised model (solid dark blue) and simulated dainage and drainage EC with original model (dashed blue).

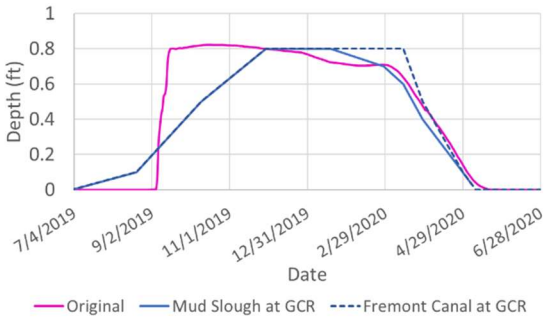

Figure 1.5: Original prescribed pond depth profile for WARMF wetland catchments (solid pink) and revised profiles for Mud Slough (solid blue) and Fremont (dashed blue).

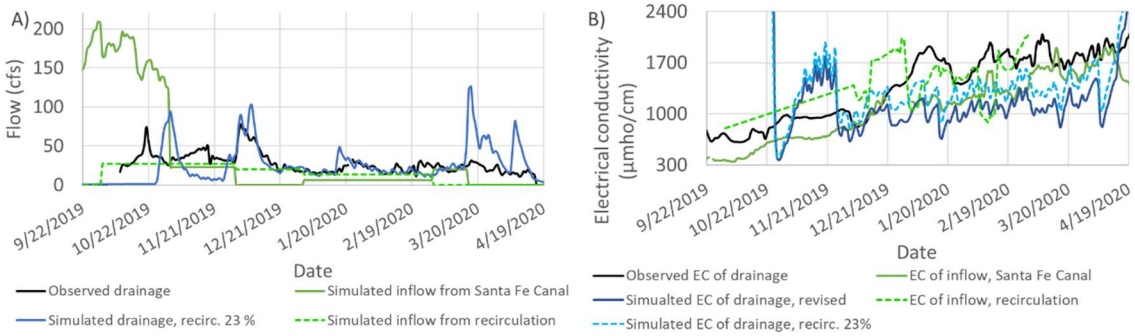

Figure 1.6: Inflow and drainage (A), and EC (B) observed at Mud Slough at GCR monitoring station or simulated for sub-catchment Mud Slough with scenarios "revised" and "recirculation 23 %". Observed drainage and drainage EC at Mud Slough at GCR monitoring station (solid black), assumed inflow and inflow EC from Santa Fe Canal (solid green), assumed inflow and inflow EC from recirculation (23 % of total inflow, dashed light green), simulated drainage and drainage EC with revised model (solid dark blue) and simulated drainage and drainage EC with 23 % recirculated water (dashed green).

Table 1.2: Difference between simulated and observed flow and salt load per hydroperiod.

Catchment	Scenario name	Year	Difference sim. and obs. Drainage flow per hydroperiod (%)[a]	Difference sim. and obs. salt load per hydroperiod (%)[a]
Mud Slough	Original	2018/19	78.9	43.3
		2019/20	76.1	57.5
	Revised	2018/19	110.2	99.2
		2019/20	106.1	96.8
	Revised + recir-culation 1 (12 %)	2019/20	106.1	108.3
	Revised + recir-culation 2 (23 %)	2019/20	106.1	115.7
Fremont[b]	Original	2018/19	101.6	119.5
		2019/20	58.4	92.5
	Revised	2018/19	98.0	131.2
		2019/20	96.7	125.4

[a] Hydroperiod: time that an area if flooded: starts with flood-up in fall and ends with drawdown in spring, Difference = Sum of simulated daily values/ Sum observed daily values times 100
[b] Higher uncertainty in observed data (see discussion in text)

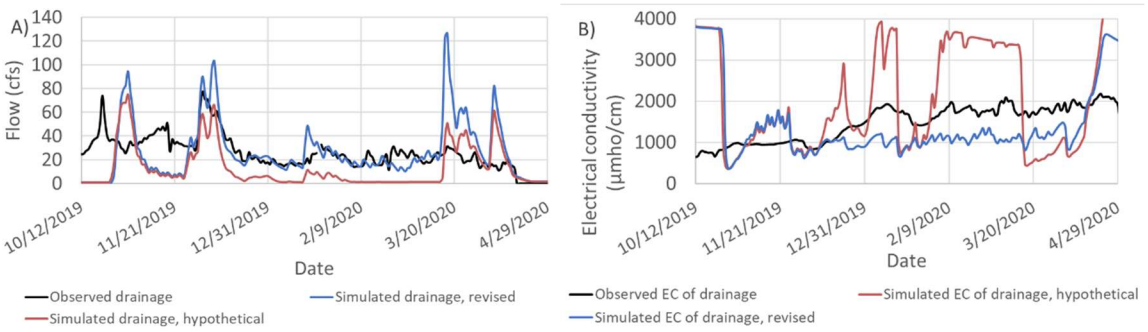

Figure 1.7: Drainage (A) and EC (B) observed at Mud Slough at GCR monitoring station or simulated for sub-catchment Mud Slough with scenarios “revised” and “hypothetical”. Observed drainage and drainage EC at Mud Slough at GCR monitoring station (solid black), simulated drainage and drainage EC with revised model (solid dark blue) and simulated drainage and drainage EC with hypothetical scenario (solid red).

2. Critical review of mercury methylation and methylmercury demethylation rate constants in aquatic sediments for biogeochemical modeling

*This chapter is a reproduction of a published article: Helmrich, S., Vlassopoulos, D., Alpers, C. N., & O'Day, P. A. (2021). Critical review of mercury methylation and methylmercury demethylation rate constants in aquatic sediments for biogeochemical modeling. Critical Reviews in Environmental Science and Technology.

2.1 Abstract

Mercury is a toxin that causes neurological impairments in adults, is particularly harmful for fetuses and children, and is deadly in severe cases, making it a worldwide health concern. Methylmercury (MeHg) is the environmentally relevant form of mercury (Hg) because it biomagnifies along the food chain. Methylmercury is mainly produced in aquatic sediments via methylation of inorganic Hg (Hg(II)) and transformed back via demethylation. Because transformation rates determine MeHg concentrations, quantification of methylation and demethylation rates is needed to inform management of MeHg. Published rate constants for Hg(II) methylation (k_m) and MeHg demethylation (k_d) vary greatly, stemming partly from differences in experimental methods. We conducted a comprehensive review of rate laws, evaluated published rate constants, and performed biogeochemical simulations to assess variability in reported k_m and k_d. Based on selected studies employing the same pseudo-first-order rate law and similar experimental methods, we found that $k_m = 0.04 \pm 0.03\ d^{-1}$ is a reasonable range for wetland sediments. Over a number of environments, maximum k_d was smaller at sites without Hg source ($k_d = 0.5\ d^{-1}$) than at sites with identified Hg source ($k_d = 1.8\ d^{-1}$). Larger variability and higher uncertainty in k_d compared to k_m highlight the need for more research on MeHg demethylation rates. This critical review: a) aids the design of future experimental studies of k_m and k_d; b) provides guidance for comparing rate constants from different studies; c) presents a biogeochemical reaction model to assess rate constants; and d) informs selection of k_m and k_d values from the literature for use in model simulations.

2.2 Introduction

Mercury (Hg) in the environment is mostly present as elemental mercury (Hg(0)) and inorganic mercury (usually as Hg(II) species), but the most toxic forms are methylated Hg species, referred to as methylmercury (MeHg). Monomethylmercury (CH_3Hg^+) and its aqueous complexes are the dominant forms in aquatic systems, with dimethylmercury ($(CH_3)_2Hg$) also observed in marine systems (Loux, 2007; Morel et al., 1998). In contrast to Hg(II), MeHg bioaccumulates and biomagnifies in the food chain (Morel et al., 1998). Human uptake of neurotoxic MeHg via fish consumption (Malm et al., 1995), and in some regions of the world by rice consumption (Feng et al., 2008), results in toxic MeHg concentrations that are particularly detrimental to the development

of fetuses and children but can also cause serious neurological impairments in adults (Clarkson, 1997; Lim et al., 2013; Mergler et al., 2007).

Methylmercury is produced from Hg(II) via methylation facilitated by microorganisms under anaerobic conditions (Gilmour et al., 2018; Podar et al., 2015), which was suspected to be a key step in transformation of inorganic and organic Hg species in early studies (Jensen & Jerneloev, 1969; Wood et al., 1968). Methylmercury is transformed back to inorganic Hg by demethylation processes (also called MeHg degradation) under aerobic and anaerobic conditions (Fleck et al., 2014; Lu et al., 2017; West et al., 2020). Aquatic sediments are hotspots for MeHg production (Fleck et al., 2016), from where MeHg may partition to the water column and become more bioavailable, and thus increase its potential for biomagnification (Mason et al., 2005; Morel et al., 1998). Total Hg(II) concentration and Hg(II) methylation and MeHg demethylation rates determine MeHg concentrations in aquatic sediments, which might be a reason why elevated MeHg concentrations are found in both contaminated and pristine environments (Hintelmann et al., 2000; Schaefer et al., 2004). The lack of a simple correlation between Hg(II) and MeHg concentrations emphasizes the importance of lowering MeHg concentrations by decreasing Hg(II) methylation rates (Eckley et al., 2017; Fuhrmann et al., 2021; Schwartz et al., 2019; Vlassopoulos et al., 2018) or increasing MeHg demethylation rates (Hsu-Kim et al., 2018). However, Hg(II) methylation and MeHg demethylation rates depend on a myriad of biogeochemical processes (Bigham et al., 2016), making it difficult to determine the best management practice for a particular site (Eckley et al., 2020). Speciation and bioavailability of Hg(II) and MeHg are dependent on the reduction-oxidation (redox) potential of an aquatic system and the rate at which it changes, which are determined by coupling of the microbial community and abiotic environmental factors (Graham et al., 2012; Mahalingam Ravichandran, 2004; Schaefer & Morel, 2009; Schartup et al., 2013; W. Zhu et al., 2018). Because Hg and MeHg transformation rates are largely controlled by microbial processes, the amount of labile organic matter (OM) is probably a more important driver of net methylation than the supply of electron accepting species, Cl^- concentration, or pH in many environments (Beckers et al., 2019; Frohne et al., 2012). To understand controls on net MeHg production and manage MeHg concentrations, it is desirable to separately quantify methylation and demethylation rates and relate them to cycling of OM and redox-sensitive species such as sulfur and iron.

Rate constants for Hg(II) methylation (k_m) and MeHg demethylation (k_d) are typically determined experimentally with isotope-tracer assays. Although Hg(II) and MeHg isotope-tracer assays are laborious and time-consuming, rate constants derived from experimental data are useful for quantitative assessment of Hg cycling and development of management strategies to mitigate bioaccumulation, particularly using model simulations that are becoming increasingly popular as decision-making tools (S. Zhu et al., 2018). Published k_m and k_d values derived using isotope tracers vary among studies of different systems and using different experimental conditions. In recent years, several studies tried to theoretically (Olsen et al., 2016) and experimentally (Johnson et al., 2015; Jonsson et al., 2012; Lehnherr et al., 2011; Olsen et al., 2018; Rodriguez Martin-Doimeadios et al., 2004; L. Zhang et al., 2021) elucidate reasons for the large variability when determining k_m and k_d, but there are no recent compilations or critical evaluations of published rate constants. A recent critical review (Regnell & Watras, 2019) discussed derivation of Hg(II) methylation rates from isotope-tracer assays but focused mainly on interpreting field and laboratory studies to better understand pathways of cellular Hg(II) uptake. A prior compilation of Hg(II) methylation rate constants was reported by Merritt and Amirbahman (2009), but they did not evaluate the data or discuss MeHg demethylation rates.

This critical review aims to determine whether variability in k_m and k_d reported in the literature is related to the experimental method or assumed rate law used in different studies and to provide values or ranges of k_m and k_d associated with low uncertainty for application to aquatic sediments. This information is also useful for designing new isotope-tracer assays to avoid pitfalls

and improve consistency. Thus, the goals and outcomes of this review are: 1) review of commonly used rate laws for Hg(II) methylation and MeHg demethylation; 2) compilation and critical evaluation of published rate constants; and 3) assessment of the applicability of k_m and k_d values using biogeochemical reaction simulations compared to experimental data.

2.3 Hg(II) methylation and MeHg demethylation processes

Here we briefly summarize processes and reactions relevant to the formulation of overall rate expressions. In-depth reviews of Hg(II) methylation and MeHg demethylation mechanisms can be found elsewhere (Barkay et al., 2003; Beckers & Rinklebe, 2017; Du et al., 2019; Hsu-Kim et al., 2013; Ma et al., 2019; Ullrich et al., 2001).

Detailed knowledge about Hg(II) methylation mechanisms within microbial cells is limited (Hsu-Kim et al., 2013) and the mechanism for transport of Hg(II) into the cell remains a topic of debate (Adediran et al., 2019). Early on it was found that Hg(II) methylation is promoted by sulfate-reducing bacteria (Compeau & Bartha, 1985; Gilmour et al., 1992; Pak & Bartha, 1998; Wood et al., 1968). Later it was discovered that iron-reducing bacteria (Fleming et al., 2006; Kerin et al., 2006; Lu et al., 2016; Si et al., 2015; Yang et al., 2016), and methanogenic archaea (Avramescu et al., 2011; Correia et al., 2012; Gilmour et al., 2013, 2018; Parks et al., 2013; Podar et al., 2015; Rothenberg et al., 2016) are also capable of equally high rates of methylation. However, only the relatively recent discovery of the hgcA and hgcB gene pair has allowed somewhat better understanding of biochemical mechanisms within the cell (Parks et al., 2013). Direct measurement of hgcAB activity could provide valuable information but is still under development (Bravo & Cosio, 2020).

In contrast to methylation, genes associated with MeHg demethylation were discovered early (Schottel, 1978; Summers & Sugarman, 1974), but for a biotic pathway that is likely not the dominant mode of demethylation (Lu et al., 2017). Although MeHg demethylation may proceed abiotically by photolysis (Fleck et al., 2014) and reaction with sulfide (Deacon, 1978; West et al., 2020), and by at least two microbially mediated pathways (Marvin-DiPasquale et al., 2000), the latter reactions dominate under light-deprived conditions found in soils and sediments. Discovery of genes (mer operon) (Foster et al., 1979) for an active detoxification mechanism—reductive demethylation—provided insight into biochemical mechanisms within the cell. Reductive demethylation results in production of methane and volatile elemental mercury (Barkay et al., 2003; Schaefer et al., 2004), which may evade the local methylation-demethylation cycle in sediments Transcription of the gene merB, which produces an enzyme that breaks the C-Hg bond, was found to be activated by an increase in Hg(II) concentration and suggests that reductive demethylation is activated when a threshold Hg(II) concentration is reached. Another biotic pathway—oxidative demethylation—was found to be a cometabolic process that transforms MeHg to Hg(II), which is again available for methylation (Oremland et al., 1995). Marvin-DiPasquale and Oremland (1998) proposed oxidative demethylation as an overall reaction that is analogous to acetate oxidation by sulfate-reducing bacteria:

$$CH_3Hg^+ + 2H^+ + SO_4^{2-} \rightleftharpoons HS^- + CO_2 + 2H_2O + Hg^{2+} \qquad (2.1)$$

or analogous to monomethylamine degradation by methanogenic archaea:

$$4CH_3Hg^+ + 2H_2O + 4H^+ \rightleftharpoons 3CH_4 + CO_2 + 4H_2 + 4Hg^{2+} \qquad (2.2)$$

Genes involved in oxidative demethylation have not been identified, and biochemical mechanisms are not well understood. However, oxidative demethylation might be more common than reductive demethylation because highly contaminated sites are rare (Lu et al., 2017).

2.4. Review of rate laws for Hg(II) methylation and MeHg demethylation

Currently used rate laws for Hg(II) methylation and MeHg demethylation are empirical and based on knowledge about overall reactions. Microbially mediated processes (i.e., linked to organic-matter degradation) such as methylation and demethylation can be described with empirical rate laws based on overall reactions (Berner, 1964, 1980). A theoretical justification was presented by Boudreau (1997). Rate laws based on elementary reactions are unlikely to be practical for the complex mechanisms involved in Hg(II) methylation and MeHg demethylation, but knowledge about reactions and rate-limiting steps can help to determine the best mathematical forms for empirical rate laws. Efforts to determine rate-limiting steps have been made (Kritee et al., 2009, 2013), but there are still many unknowns.

The use of an irreversible pseudo first-order rate law for empirical fitting of experimental data to determine Hg(II) methylation and MeHg demethylation rates was first presented by Hintelmann et al. (2000), Marvin-Dipasquale et al. (2000), and Marvin-DiPasquale and Agee (2003). This approach has been followed by most subsequent studies (see Suppl. Table S2.1). Among the reviewed studies, rates of methylation and demethylation are typically investigated via isotope-tracer assays using two different mercury isotopes to label Hg(II) and MeHg. This dual isotope method allows separate determination of each rate within the same sample (Ramlal et al., 1986), which enables assessment of the relative magnitude of each process. Radioisotopes of Hg were initially used (Furutani & Rudd, 1980; Ramlal et al., 1986) but were not considered true tracer experiments because the radioisotope, such as ^{203}Hg, had low specific activity (Hintelmann et al., 2000). This problem was solved by preparing ^{203}Hg with high specific activity (Gilmour & Riedel, 1995). With improvements in the sensitivity of mass spectrometers, the use of stable Hg isotopes for rate studies has become common practice since the early study by Hintelmann et al. (1995). In the next sections, we present derivations of first-order rate laws for Hg(II) methylation and MeHg demethylation to clarify differences in application when different assumptions or isotopes were used experimentally.

2.4.1. Irreversible pseudo first-order rate law for Hg(II) methylation

The majority of studies employed the approach proposed by Hintelmann et al. (2000) to calculate the Hg(II) methylation rate and rate constant. They assumed an irreversible pseudo first-order rate law for Hg(II) methylation over the time of the incubation experiment, here shown with the stable isotope ^{199}Hg:

$$^{199}Hg^{2+} \rightarrow CH_3{}^{199}Hg^{+} \qquad (2.3).$$

The differential rate law for an irreversible pseudo first-order rate can be written in terms of the reactant or the product. Hintelmann et al. (2000) described the rate as the change of product concentration over time:

$$\frac{d[CH_3{}^{199}Hg^{+}]}{dt} = k_m[^{199}Hg^{2+}] \qquad (2.4)$$

where $[^{199}Hg^{2+}]$ is the concentration of the isotope tracer $^{199}Hg^{2+}$ (ng/g) added at the start of the experiment, $[CH_3{}^{199}Hg^{+}]$ is the concentration of $CH_3{}^{199}Hg^{+}$ (ng/g) newly generated from the

$^{199}Hg^{2+}$ tracer, k_m is the methylation rate constant (d^{-1}), and t is incubation time (d). The approach assumes that the reaction in Equation (2.3) is irreversible and that the concentration of the product depends only on the concentration of the reactant, and not on other constituents in the system. Hintelmann et al. (2000) also assumed that the concentration of $^{199}Hg^{2+}$ added at the start of the experiment (denoted $[^{199}Hg^{2+}]_{t=0}$ in the following equations) remains approximately constant over the time of the experiment. With these assumptions, Equation (2.4) can be rearranged to:

$$d[CH_3{}^{199}Hg^+] = k_m[^{199}Hg^{2+}]_{t=0}\,dt \tag{2.5}$$

Equation (2.5) can be integrated from $t = 0$ to some later time *(t)*:

$$\int_{CH_3{}^{199}Hg^+_{t=0}}^{CH_3{}^{199}Hg^+_t} d[CH_3{}^{199}Hg^+] = k_m[^{199}Hg^{2+}]_{t=0}\int_{t=0}^{t} dt \tag{2.6}$$

Integrating and applying these limits results in:

$$[CH_3{}^{199}Hg^+]_t - [CH_3{}^{199}Hg^+]_{t=0} = k_m[^{199}Hg^{2+}]_{t=0}\,t \tag{2.7}$$

Assuming that $[CH_3{}^{199}Hg^+]_{t=0} = 0$, Equation (2.7) reduces to:

$$[CH_3{}^{199}Hg^+]_t = k_m[^{199}Hg^{2+}]_{t=0}\,t \tag{2.8}$$

Equation (2.8) can be rearranged to calculate k_m directly:

$$k_m = \left(\frac{[CH_3{}^{199}Hg^+]_t}{[^{199}Hg^{2+}]_{t=0}}\right)t^{-1} \tag{2.9}$$

With Equation (2.9), the methylation rate constant k_m can be determined minimally with only two measurements—the Hg(II) tracer concentration added at the beginning of the experiment and the MeHg generated from methylation at time *t*. Most reviewed studies used two measurements. The disadvantage of only two measurements is that it is not possible to assess whether the assumption of a first-order rate law is valid, resulting in potential over- or under-estimation, which is discussed later.

The differential rate law for Equation (2.3) can be also written in terms of change in concentration of the reactant $^{199}Hg^{2+}$:

$$-\frac{d[^{199}Hg^{2+}]}{dt} = k_m[^{199}Hg^{2+}] \tag{2.10}$$

Integration over time using the reactant concentration is a common approach for evaluating first-order rate laws and was done in several Hg(II) methylation kinetic studies. The approach was first presented by Marvin-DiPasquale and Agee (2003); rearranging Equation (2.10):

$$\frac{d[^{199}Hg^{2+}]}{[^{199}Hg^{2+}]} = -k_m dt \tag{2.11}$$

and then integrating from the initial $[^{199}Hg^{2+}]$ concentration at time $t = 0$ to the concentration of $[^{199}Hg^{2+}]$ at some time *(t)* gives:

$$\int_{^{199}Hg^{2+}_{t=0}}^{^{199}Hg^{2+}_{t}} \frac{d[^{199}Hg^{2+}]}{[^{199}Hg^{2+}]} = -k_m \int_{t=0}^{t} dt \qquad (2.12).$$

Integrating and applying these limits results in:

$$\ln[^{199}Hg^{2+}]_t - \ln[^{199}Hg^{2+}]_{t=0} = -k_m t \qquad (2.13).$$

Considering natural logarithm rules, Equation (2.13) can be written as:

$$\ln\left(\frac{[^{199}Hg^{2+}]_t}{[^{199}Hg^{2+}]_{t=0}}\right) = -k_m t \qquad (2.14).$$

Marvin-DiPasquale and Agee (2003) further adapted Equation (2.14) because the concentration of the product $CH_3{}^{199}Hg^{+}$, rather than reactant $^{199}Hg^{2+}$, was measured. Because all product $CH_3{}^{199}Hg^{+}$ is derived from reactant $^{199}Hg^{2+}$, mass balance requires:

$$[^{199}Hg^{2+}]_{t=0} = [^{199}Hg^{2+}]_t + [CH_3{}^{199}Hg^{+}]_t \qquad (2.15).$$

Solving Equation (2.15) for $[^{199}Hg^{2+}]_t$ and substituting into Equation (2.14) can be written:

$$\ln\left(\frac{[^{199}Hg^{2+}]_{t=0} - [CH_3{}^{199}Hg^{+}]_t}{[^{199}Hg^{2+}]_{t=0}}\right) = -k_m t \qquad (2.16).$$

Simplifying Equation (2.16), Marvin-DiPasquale and Agee (2003) directly calculated k_m:

$$k_m = -\left[\ln\left(1 - \frac{[CH_3{}^{199}Hg^{+}]_t}{[^{199}Hg^{2+}]_{t=0}}\right)\right] t^{-1} \qquad (2.17).$$

Note that Equation (2.17) is an exact solution of the rate law with no assumptions, whereas Equation (2.9) assumed a constant concentration of initial $^{199}Hg^{2+}$. Equation (2.9) approximates Equation (2.17) if a Taylor series expansion is applied:

$$ln(1-x) = -x - \frac{x^2}{2} - \frac{x^3}{3}\ldots \qquad (2.18).$$

Truncating after the first-order term gives:

$$ln(1-x) \cong -x \qquad (2.19).$$

Assuming that $x = \frac{[CH_3{}^{199}Hg^{+}]_t}{[^{199}Hg^{2+}]_{t=0}}$, Equation (2.17) can be rewritten as:

$$k_m = -\left[\ln\left(1-x\right)\right]t^{-1} \tag{2.20}$$

which reduces to Equation (2.9) when the approximation in Equation (2.19) is applied. Hintelmann et al.'s (2000) Equation (2.9) agrees with Marvin-DiPasquale and Agee's (2003) Equation (2.17) only when the amount of Hg(II) that is transformed to MeHg is small (below ~10%; see Suppl. Figure S2.1).

2.4.2. Irreversible pseudo first-order rate law for MeHg demethylation

The approach used by most studies for demethylation of MeHg to Hg(II) assumes an irreversible pseudo first-order rate law over the course of the experiment, shown here with the isotope $CH_3{}^{201}Hg^+$:

$$CH_3{}^{201}Hg^+ \rightarrow {}^{201}Hg^{2+} \tag{2.21}.$$

This approach was first presented by Hintelmann et al. (2000) and Marvin-Dipasquale et al. (2000). Hintelmann et al. (2000) described the differential rate law in terms of the change in reactant concentration:

$$-\frac{d[CH_3{}^{201}Hg^+]}{dt} = k_d[CH_3{}^{201}Hg^+] \tag{2.22}$$

where $[CH_3{}^{201}Hg^+]$is the concentration of isotope tracer $CH_3{}^{201}Hg^+$ (ng/g), k_d is the demethylation rate constant (d^{-1}), and t is incubation time (d). The rate equation can be rearranged and integrated similarly to the Hg(II) methylation equations above:

$$\frac{d[CH_3{}^{201}Hg^+]}{[CH_3{}^{201}Hg^+]} = -k_d dt \tag{2.23}$$

$$\int_{CH_3{}^{201}Hg^+_{t=0}}^{CH_3{}^{201}Hg^+_t} \frac{d[CH_3{}^{201}Hg^+]}{[CH_3{}^{201}Hg^+]} = -k_d\int_{t=0}^{t} dt \tag{2.24}$$

$$\ln[CH_3{}^{201}Hg^+]_t - \ln[CH_3{}^{201}Hg^+]_{t=0} = -k_d t \tag{2.25}.$$

Equation (2.25) can be rearranged to:

$$\ln[CH_3{}^{201}Hg^+]_t = -k_d t + \ln[CH_3{}^{201}Hg^+]_{t=0} \tag{2.26}.$$

Equation (2.26) has the form of an equation for a straight line. Hintelmann et al. (2000) derived k_d from the slope of a plot of $y = \ln[CH_3{}^{201}Hg^+]_t$ over time ($x = t$).

Slightly different equations were used by Marvin-DiPasquale et al. (2000) because they isotopically labeled the carbon (C) atom with ^{14}C instead of Hg in CH_3Hg^+. Marvin-Dipasquale et al. (2000) rearranged Equation (2.25) to:

$$k_d = -\left[\ln\left(\frac{[CH_3Hg^+]_t}{[CH_3Hg^+]_{t=0}}\right)\right]t^{-1} \quad (2.27).$$

They assumed a rate law based on:

$$^{14}CH_3Hg^+ \rightarrow (^{14}CH_4 + ^{14}CO_2) \quad (2.28)$$

and applied mass balance for ^{14}C species, where:

$$[^{14}CH_3Hg^+]_{t=0} = \sum([^{14}CH_4]+[^{14}CO_2]+\ldots)_t + [^{14}CH_3Hg^+]_t \quad (2.29).$$

This approach is based on the assumption that all of the labeled carbon of the methyl group is transformed into $^{14}CH_4$ or $^{14}CO_2$ and all other intermediate carbon species are negligible. Ignoring intermediates, solving Equation (2.29) for $[^{14}CH_3Hg^+]_t$ and substituting into Equation (2.27)gives:

$$k_d = -\left[\ln\left(\frac{[^{14}CH_3Hg^+]_{t=0} - \sum([^{14}CH_4]+[^{14}CO_2])_t}{[^{14}CH_3Hg^+]_{t=0}}\right)\right]t^{-1} \quad (2.30).$$

Simplifying Equation (2.30) yields the final equation used by Marvin-Dipasquale et al. (2000) to calculate k_d:

$$k_d = -\left[\ln\left(1 - \frac{\sum([^{14}CH_4]+[^{14}CO_2])_t}{[^{14}CH_3Hg^+]_{t=0}}\right)\right]t^{-1} \quad (2.31).$$

The approach of Marvin-Dipasquale et al. (2000) (labeling C in CH_3Hg^+) uses a different tracer for MeHg than Hintelmann et al. (2000) (labeling Hg in CH_3Hg^+), but the mathematical approach is the same and the k_d values are equivalent as long as the added tracer is demethylated only to CH_4 and/or CO_2.

2.4.3. Variations on first-order (de)methylation rate laws

A few studies varied the assumed rate laws, mathematical solutions, and/or their experimental set-up to improve precision of the derived rate constants and to quantify under- or over-estimation connected with applying the first-order rate to two time-point measurements. Four of the reviewed studies (Johnson et al., 2015; Jonsson et al., 2012; Olsen et al., 2016; Rodriguez Martin-Doimeadios et al., 2004) combined the first-order rate laws for Hg(II) methylation and MeHg demethylation into one equation and derived rate constants from a time series instead of two time points. Martin-Doimeadios et al. (2004) found higher rate constants when using a time series compared to two time points, whereas Olsen et al. (2016) found lower rate constants. Jonsson et al. (2012) and Johnson et al. (2015) did not compare rate constants from different approaches. Two of the reviewed studies (Lehnherr et al., 2011; Olsen et al., 2018) added additional terms to the rate laws based on measured availability of the Hg(II) and/or MeHg tracers over time. Tracers were added in dissolved form, which is generally more bioavailable for methylation or demethylation than solid tracer (Hintelmann et al., 2000; Jonsson et al., 2012; W. Zhu et al., 2018) because Hg(II)

must be able to pass into bacterial cells. Variation in methylation rate depending on Hg(II) species were observed by Hintelmann et al. (2000), who reasoned that adsorption and dissociation kinetics could be a factor depending on the charge of the tracer species and possible binding to strong adsorption sites. Most Hg methylation studies added the tracer as $HgCl_2$ or $Hg(NO_3)_2$. The tracer for MeHg demethylation studies is typically supplied as CH_3HgCl and sometimes as CH_3HgI. Dissolved species may become less available with time by sorption onto sediment organic matter (Qian et al., 2002; Skyllberg et al., 2003). Both Lehnherr et al. (2011) and Olsen et al. (2018) measured a strong decline of bioavailable Hg(II) over 24 hours. Olsen et al. (2018) compared the approach assuming first-order rates and using two time points with their approach of taking into account the decline of tracer due to sorption and using a time series. They found rate constants in periphyton biofilms that were three times higher for Hg(II) methylation and either lower or higher for MeHg demethylation, depending on the interval between the two time points selected compared with the entire time series over 72 hours.

2.5. Critical evaluation of Hg(II) methylation and MeHg demethylation rate constants

In this review, we considered literature published up until and including 2020. We initially compiled data from 62 studies that reported observed rates and rate constants for Hg(II) methylation and/or MeHg demethylation in various types of samples. Importance was given to retrieving all relevant publications. An initial screening was conducted in which a subset of 28 studies reporting k_m and 17 studies reporting k_d was selected (see Suppl. Tables S2.1 and S2.2) based on the following criteria: 1) experiments used at least one stable Hg isotope or radioactive Hg or C tracer; 2) reported rate constants assumed irreversible first-order reactions and followed the approaches presented above by Hintelmann et al. (2000) and Marvin-Dipasquale et al. (2000); 3) assumptions and incubation conditions were reported in sufficient detail; 4) rate constants were reported. Several studies reported the percentage of Hg tracer converted to product, either MeHg or Hg(II), which is not directly comparable to rate constants. Rate constants could be calculated from the percentage with Equation (2.9) and knowledge of the incubation time. However, reporting of rate constants would make comparison easier. Among the subset were 22 Hg(II) methylation and 17 MeHg demethylation studies that measured product formation once at the end of the incubation time and six Hg(II) methylation studies that measured product formation at multiple time points during incubation. Incubation times varied between 2 and 456 hours. Two studies included separate measurements of the bioavailable Hg(II) tracer in addition to the use of a time series (see previous section). The subset was further narrowed based on assessment of uncertainty. Only studies that measured product formation once were considered for further assessment because this was the most common approach, and the goal was to find trends among studies. Sample type and incubation time were found to add uncertainty and are discussed further below. A summary of compiled rate constants and recommended values for Hg(II) methylation and MeHg demethylation for aquatic sediments are given in Table 2.1 and discussed in detail in the next sections.

2.5.1. Difference due to sample type

Rate constants differed among sample types, which included water samples, pure cell cultures, phytoplankton, marine snow, and sediments (Suppl. Table S2.1). The lowest k_m was found in phytoplankton ($0.00014\ d^{-1}$, Olsen et al., 2016) and was half as large as the lowest k_m in sediment ($0.0003\ d^{-1}$, Kronberg et al., 2012; Marvin-DiPasquale et al., 2003). The highest k_m was found for sediment (1.5 d^{-1}, Marvin-DiPasquale et al., 2014) and was two orders-of-magnitude

higher than the highest value for other types of samples (0.09 d^{-1}, Eckley et al., 2005). The lowest k_d was found in sediment (0.002 d^{-1}, Marvin-DiPasquale & Oremland, 1998) whereas the lowest k_d in other sample types was found in marine snow (0.01 d^{-1}, Ortiz et al., 2015). The highest k_d value was two orders-of-magnitude higher in sediment (63 d^{-1}, Liu et al., 2015) than in other sample types (0.51 d^{-1}, Lehnherr et al., 2011). Differences between sample types can be partially explained in that methylation and demethylation rates are affected by interactions between bacteria (Yu et al., 2018; Xu et al., 2019), organic material, and minerals (Zhang et al., 2019), which differ between sample types. In considering the variability of rate constants among sample types, further assessment was limited to aquatic sediment samples (Table 2.1).

2.5.2. Uncertainty related to incubation time

Methylation and demethylation rate constants tended to be larger with shorter incubation times when an irreversible pseudo first-order reaction was assumed. Because the effect was expected to be most pronounced for larger values, the median of the maximum values reported in all studies of aquatic sediments was calculated (Table 2.1Table 2.). Maximum reported k_m values tended to be more than three times higher for 2–5 hours incubation time than those incubated for 48 hours. The difference was even larger for k_d for which the median for 2–5 hours incubation time was more than 41 times higher than those incubated for 48 hours. This observation points to systematic under- or over-estimation of rate constants as a function of incubation time. Considering the integrated first-order rate law for Hg(II) methylation, Equation (2.17) can be rearranged to an equation with the form of a straight line:

$$\ln\left(1-\frac{[CH_3{}^{199}Hg^+]_t}{[{}^{199}Hg^{2+}]_{t=0}}\right)=-k_m t \qquad (2.32).$$

A plot of the left side of Equation (2.32) versus time t can be used to assess if experimental data support the use of a first-order rate; if so, the rate constant can be determined from the slope. Data from three studies that published raw data for time series experiments (Hintelmann et al., 2000; Jonsson et al., 2012; Martin-Doimeadios et al., 2004) do not fit a straight line (Figure 2.1). As pointed out and discussed by Olsen et al. (2016, 2018), deviation from linear behavior can be attributed to reactions other than Hg(II) methylation that influence MeHg concentration during longer incubation times. Possible reactions besides Hg(II) methylation are: 1) MeHg demethylation; and 2) adsorption and precipitation of dissolved Hg(II) tracer that make the tracer less bioavailable. Occurrence of one or both processes will result in underestimation of k_m by Equation (2.32). Therefore, the shorter the incubation time, the smaller the uncertainty that is associated with k_m when assuming a first-order rate. We did not find published time-series data for MeHg demethylation. However, it is likely that the occurrence of the back reaction and reduction of tracer bioavailability adds uncertainty to MeHg demethylation rate constants as well during longer measurement periods.

2.5.3. Hg(II) methylation rate constants

A linear least-squares fit of k_m from selected 2-hour incubation experiments (Hollweg et al., 2010; Kim et al., 2006; Marvin-DiPasquale et al., 2014; Mitchell & Gilmour, 2008) with sediment total Hg (THg) indicated that k_m values were almost constant at around $k_m = 0.042\ d^{-1}$ (95% confidence interval of $\pm 0.03\ d^{-1}$) over the considered range of sediment THg (Figure 2.2). Studies with a 2-hour incubation time were selected because they were found to be associated with the lowest uncertainty when assuming a pseudo first-order rate law. However, k_m values had

considerable scatter at higher sediment THg concentrations, resulting in a low coefficient of determination. When separated by study, the coefficient of determination was still low (0.06 for Hollweg et al. (2010), 0.17 for Kim et al. (2006), 0.1 for Mitchell and Gilmour (2008), 0.0003 for Marvin-DiPasquale et al. (2014)). The range of k_m was largest for data from Marvin-DiPasquale et al. (2014)—small values were one order of magnitude smaller and large values were one order of magnitude larger than in the other three studies. Among the studies compared in Figure 2.2, a significant difference is that Marvin-DiPasquale et al. (2014) examined agricultural and non-agricultural wetlands in the San Francisco Bay-Delta, whereas the three other studies assessed estuarine and marine sediments, or salt marshes, in Chesapeake Bay. Agricultural wetlands and estuaries both have high potentials for environmental fluctuations (Singer et al., 2016; Windham-Myers et al., 2013) due to cultivation/irrigation and tidal variation, respectively. However, both environments are different in terms of redox cycling (complete drying once a year in seasonal wetlands), organic carbon input (plant residues in agricultural wetlands), and sulfur concentrations. A number of factors such as hydrology, bioavailable organic matter concentration, temperature, and electron-acceptor supply (SO_4^{2-}, $Fe(III)$) are thought to affect Hg(II) methylation, probably by influencing the activity of bacteria that promote methylation (Marvin-DiPasquale et al., 2014; Olsen et al., 2016). The effect of environmental conditions on Hg methylation are discussed further in Supplementary Information (Sec. S4.3). Correlation analysis with data from all four studies were conducted to identify trends in k_m due to environmental conditions (Suppl. Table S2.3, Suppl. Figures S2.2–S2.6). Data from Marvin-DiPasquale et al. (2014), for which the range of incubation temperature was largest from the four assessed studies, support the idea that there is a weak dependence of k_m on temperature, which partially explains the scatter in Figure 2.2. Rate data compiled for temperature and other parameters did not show sufficiently strong trends to justify a statistical dependence (Suppl. Figures S2.2–S2.6). Quantifying the effect of temperature based on published rate constants is particularly difficult because many studies perform tracer incubations at room temperature. Tracer assays that systematically vary one parameter while holding all other parameters constant would be better suited to quantify the effect of environmental conditions on rates. No further statistical analysis was applied because an integral aspect of this study was to assess the utility of literature rate constants to reproduce experimental data using biogeochemical reaction simulations (Section 5). As discussed later, simulations supported a value of $k_m = 0.04 \pm 0.03\ d^{-1}$ as a good estimate for wetland sediments with low levels of Hg contamination.

2.5.4. Methylmercury demethylation rate constants

Published MeHg demethylation rate constants were associated with more variability and more uncertainty than Hg(II) methylation rate constants. The difference between the calculated median of maximum observed rate constants from 2–5 hours and 48 hours incubation time was significantly larger for demethylation than for methylation (reported median in Table 2.1), which supports the notion of additional uncertainties in k_d. As was shown for Hg(II) methylation, uncertainties associated with assuming a first-order rate law can be decreased by using short incubation times. However, MeHg analytical limitations and the existence of multiple pathways limit the usefulness of this approach for estimating demethylation rates. Studies with short, 2-hour incubations (Hollweg et al., 2010; Kim et al., 2006; Bian Liu et al., 2015) required spiking isotopically labeled MeHg tracer at concentrations of 2 to 97 times the ambient MeHg concentration to produce measurable demethylation rates. The use of tracer concentrations that are very different from ambient concentrations could lead to over- or under-estimation of rates, as discussed by Olsen et al. (2018). Drott et al. (2008b) found positive or negative correlations between k_d and MeHg tracer concentration depending on ambient MeHg concentration, but only when the tracer concentration was higher than ambient MeHg. Marvin-DiPasquale and Oremland

(1998) found a negative correlation between k_d and MeHg tracer in uncontaminated wetlands for tracer concentrations that were 4 to 100 times larger than ambient concentrations. Studies with 6–48 hours incubation time (Figure 2.3) have been shown to be long enough to allow MeHg tracer concentrations at ambient levels (Hintelmann et al., 2000; Kronberg et al., 2012, 2018; Tjerngren et al., 2012). Moreover, incubation times of many days generally added uncertainty to rate estimates due to depletion of electron acceptors and nutrients (Levenspiel, 1980). As discussed later, biogeochemical reaction simulations indicate that studies with 6–48 hours incubation time are best suited to estimate k_d.

Maximum demethylation rate constants differed with proximity to a Hg contamination source regardless of other environmental conditions. Figure 2.3 shows that maximum k_d values (6–48 hours incubation time) tended to be considerably larger when an identified industrial or mining-related Hg source was present within approximately 70 km. In the absence of an identified Hg source, lower k_d values were found for an array of environments (Figure 2.3), a trend previously highlighted by Marvin-Dipasquale et al. (2000). Although the number of sites with an identified Hg source is limited, the consistently smaller rate constants among the ten sites with no identified Hg source is striking. The question arises whether the observed rate constants may reflect different biotic demethylation pathways. Schaefer et al. (2004) found that reductive demethylation tends to be faster than oxidative demethylation and that microbial communities at highly contaminated sites might be enriched in Hg-resistant strains. Early on it was found that reductive demethylation is activated by an increasing Hg(II) concentration (Schaefer et al., 2004; Silver & Phung, 1996; Yu et al., 1996). Schaefer et al. (2002) hypothesized that redox conditions indirectly decrease activation of reductive demethylation by decreasing transport of Hg(II) into the cell due to changes in cell-wall composition. Sediment oxidation potential might be a reason for the poor correlation between demethylation rate constants and Hg(II) concentrations observed in the field, perhaps due to the extent of complexation of MeHg with either organic matter or dissolved sulfide (Drott et al., 2008b). The poor correlation and the limited knowledge about biochemical mechanisms of oxidative demethylation make it difficult to determine the dominant biotic demethylation pathway under specific environmental conditions.

2.6. Assessment of selected literature values with biogeochemical reaction simulations

Constrained values for k_m and k_d in aquatic sediments are useful if they can be applied generally in laboratory or field settings where rates are dependent on many environmental and biogeochemical factors. Due to the complex nature of Hg cycling, a statistical analysis of field and laboratory data for rates of Hg(II) methylation and MeHg demethylation does not always yield conclusive results. Computational simulations can be useful in interpreting field and laboratory data, improving our general understanding, and quantifying Hg cycling. Biogeochemical Hg reaction simulations to date have focused on speciation and transport of Hg (Johannesson & Neumann, 2013; Leterme et al., 2014; Leterme & Jacques, 2015; V. Liem-Nguyen, Skyllberg, & Björn, 2017; Richard et al., 2016), but less on transformation of Hg (Bessinger et al., 2012; Blanc et al., 2018). In this section, we expand on the thermodynamic-kinetic model presented by Bessinger et al. (2012) by coupling microbially mediated Hg(II) methylation to degradation of organic matter (OM) and comparing model results to experimental data. The model used here was developed using PHREEQC (Parkhurst & Appelo, 2013) and runs as a batch reactor. The goals of the simulations were to: 1) test the sensitivity of the model results to variation in the absolute values of k_m and k_d; 2) assess the ability of k_m and k_d values derived from literature review to reproduce experimental data from incubation experiments by Schwartz and Gilmour (2017); and 3) compare

the performance of literature-derived k_m and k_d values with k_m and k_d values calculated by Schwartz and Gilmour (2017).

2.6.1. Model formulation

The model presented by Bessinger et al. (2012) and used in this study applied Berner's (1964) early diagenesis model with adaptations made by Van Cappellen and Wang (1996) and Hunter et al. (1998). See Supplemental Information (Sec. S5.1) for details of this general approach in which kinetic rates for electron-acceptor reactions are linked to the degradation of OM. Linearized rate expressions for primary redox reactions, second-order (bimolecular) rate laws for secondary reactions, and rate laws for mineral dissolution or precipitation are included in the model (see Suppl. Table S2.4) and form a network of kinetic reactions (Hunter et al., 1998) in which the methylation and demethylation rates were integrated as two separate reactions. The overall reaction for methylation is assumed to be:

$$CH_4 + Hg^{2+} \rightarrow CH_3Hg^+ + H^+ \quad (2.33).$$

The overall reaction assumed for demethylation is:

$$CH_3Hg^+ + H^+ \rightarrow CH_4 + Hg^{2+} \quad (2.34).$$

The methylation rate is coupled to OM degradation via the fraction of sulfate reduction $f_{SO_4^{2-}}$:

$$R_{meth} = k_m[Hg_{I,TOT}]f_{SO_4^{2-}} \quad (2.35)$$

where k_m is the methylation rate constant and $[Hg_{I,TOT}]$ is the concentration of total aqueous Hg(II) (see SI Sec. S5.2). The simplified approach that all aqueous Hg(II) is assumed to be available for methylation was supported by the finding that simulated aqueous Hg(II) concentrations matched filtered THg (FTHg) concentrations observed by Schwartz and Gilmour (2017) for the study site. However, FTHg is an operational definition dependent on filter size and may consist of dissolved Hg(II) and Hg(II) adsorbed to particulate OM or associated with colloidal or nanoscale $HgS_{(s)}$ (V. Liem-Nguyen, Skyllberg, & Björn, 2017), the latter of which was found in some studies to be available for methylation (Pham et al., 2014; T. Zhang et al., 2012). The fraction of Hg(II) that is potentially bioavailable from sediment is sometimes estimated based on extraction with stannous chloride and referred to as "reactive" Hg ($Hg(II)_R$) (Marvin-DiPasquale et al., 2008; Marvin-DiPasquale et al., 2014; Johnson et al., 2015). $Hg(II)_R$ is typically a small percentage of THg in sediment. Similarly, a thiol-based extraction suggested that the bioavailable Hg(II) fraction is often less than half a percent of THg (Ticknor et al., 2015). A simplified approach of making all dissolved Hg(II) available for methylation was chosen here because quantifying the bioavailability of different Hg(II) species and fractions for model simulations is difficult, as discussed in detail by Hsu-Kim et al. (2013), but could be tested in simulations if data are available.

Coupling of methylation to iron reduction and methanogenesis will be included in future model simulations but was not considered necessary for the current simulations because sulfate reduction was dominant at the modeled site, as discussed in Supplementary Information (Sec. S5.2). The demethylation rate is given by:

$$R_{demeth} = k_d[MeHg_{TOT}] \quad (2.36)$$

where k_d is the demethylation rate constant and $[MeHg_{TOT}]$ is the total aqueous MeHg concentration. Model parameters for kinetic reactions are listed in Suppl. Table S2.5. Thermodynamic constants for Hg(II) species that were added to the default LLNL database are listed in Suppl. Table S2.6.

2.6.2. Application and assessment of rate constants

Published data from incubation experiments with salt marsh sediments from Chesapeake Bay (NJ, USA) conducted by Schwartz and Gilmour (2017) were used to set initial conditions, evaluate model performance, and test the sensitivity of model results to variation in k_m and k_d. Schwartz and Gilmour (2017) performed comprehensive measurements of geochemical parameters and measured THg and MeHg concentrations in soil and porewater at five time points over 28 days. Rate constants were calculated from isotope tracer additions. Simulation output from our PHREEQC model was compared to experimental incubation data up to day 20 (see SI Sec. S5.2 for details of the incubation experiments and model simulations).

In model simulations, the initial aqueous solution and solid phase composition (Suppl. Table S2.7) were based on conditions measured at the beginning of the incubation experiment. One model parameter—the OM degradation rate constant (k_{OM})—was determined by fitting to the change in measured sulfate concentration (see Figure 2.4B), assuming that OM degradation proceeded primarily via sulfate reduction. The simplified approach to estimate k_{OM} based on sulfate reduction was considered sufficient to assess k_m and k_d selected from the literature because no quantifiable trends associated with specific redox conditions emerged from the literature review, and no major changes in redox conditions were observed during the simulations. All other model parameters were estimated based on independent studies (see Suppl. Table S2.5 and S2.6). Adsorption of Hg(II) and MeHg on dissolved and particulate OM was not included in the model simulation because it was assumed that sorbed species reached steady state rapidly (<24 hours) and did not significantly change the availability of Hg(II) and MeHg over the incubation time. Adsorption will be included in future studies and is important for model simulations that aim to determine drivers of net MeHg production at a specific site or to assess management options for decreasing bioavailable Hg(II).

2.6.3. Simulation results and discussion

Concentrations of simulated Hg and non-Hg species agreed well with measured concentrations (Schwartz & Gilmour, 2017). The observed pH was replicated in the model simulations and did not vary significantly over the incubation time (Figure 2.4A). The OM degradation rate constant was adjusted such that the simulated and observed decrease in sulfate concentration matched each other (Figure 2.4B). The simulation slightly overpredicted sulfide concentrations by $3 \cdot 10^{-6}\, mol/l$ to $1 \cdot 10^{-5} mol/l$ (Figure 2.4C). Simulated dissolved THg matched observed FTHg well when assuming supersaturation of nano-HgS and setting the maximum initial amount that can dissolve to zero. Some of the observed FTHg might have been colloidal Hg(II) and is likely associated with OM. It is unlikely that observed and simulated data fit accidentally because the degrees of freedom in the model are reduced by the strong dependence of kinetic reactions on each other, as described by Van Cappellen and Wang (1996). Therefore, the good match for multiple species supports the validity of both the underlying reaction network and the choice of model parameter values.

A sensitivity analysis showed that the average Hg(II) methylation rate constant ($k_m = 0.042\, d^{-1}$) selected from 2-hour incubations (see Figure 2.5) reproduced MeHg/FTHg ratios observed in marsh soils by Schwartz and Gilmour (2017) between 6 and 20 days (Figure 2.5A). At

the initial time step, the experimental MeHg/FTHg ratio was ~25%, then decreased to ~10% at day 6, and remained at this ratio until day 20. Values of k_m were varied to cover a representative range. The demethylation rate constant was fixed to $0.5\ d^{-1}$, based on assessment of reported values (Figure 2.3) and a sensitivity analysis of k_d (see below). Simulated dissolved MeHg/THg matched experimental MeHg/FTHg in porewater well. The smallest value of $k_m = 0.0084\ d^{-1}$ tested in the simulation resulted in underestimation of MeHg/THg and a small absolute deviation of simulated MeHg from observed MeHg concentrations (Suppl. Figure S2.7). The small deviation illustrates that variations of $k_m < 0.01\ d^{-1}$ have a negligible effect on simulated MeHg concentrations. Simulations with $k_m = 0.042\ d^{-1}$ resulted in a close match of simulated and measured MeHg/THg. Simulations with $k_m = 0.084\ d^{-1}$ and $k_m = 0.168\ d^{-1}$ resulted in overestimation of MeHg/THg, with the first value approximately marking the upper limit of the 95% confidence interval from Figure 2.2 and the latter value being larger than the majority of k_m values reported in the literature and considered to be an upper limit. Reconciling observations from the sensitivity analysis leads to $k_m = 0.04 \pm 0.03\ d^{-1}$ as a good literature-based estimate for the simulated site, and potentially for sites with similar characteristics. Environmental conditions will likely affect the value of k_m, although quantification of those effects was not possible based on the reviewed literature.

Simulations showed that demethylation rate constants estimated from studies with 6–48 hours incubation time resulted in a good match between simulated and observed MeHg/THg (Figure 2.5B). For a sensitivity analysis of k_d, the methylation rate constant was fixed to $k_m = 0.042\ d^{-1}$from above. The maximum value from studies with 6–48 hours incubation time without an identified Hg point source, $k_d = 0.5\ d^{-1}$, resulted in the best match of simulated and measured MeHg/Hg ratios. Other values for k_d, including an average of 2-hour incubations ($k_d = 3.3\ d^{-1}$, Suppl. Figure S2.8) and the maximum k_d for sites with an identified Hg point source ($k_d = 1.8\ d^{-1}$, Figure 2.3), resulted in underestimation of MeHg/THg. The value $k_d = 0.05\ d^{-1}$, chosen to examine a lower limit, resulted in a large overestimation of MeHg/THg ratios and absolute MeHg concentrations. Due to lack of data, we were not able to determine numerical values for uncertainty of k_d.

The ratio of k_m/k_d and aqueous (porewater) MeHg/THg at approximately steady-state concentrations was used to estimate a lower boundary for k_d. Hg(II) methylation would be strongly favored when k_m/k_d exceeds one considering that the first-order rate is calculated by multiplying the rate constant with the reactant concentration (Hg(II) or MeHg) and that $MeHg/Hg(II) = k_m/k_d$ at steady-state conditions. Porewater MeHg/THg is often less than 0.01, but considerably higher values have been observed (e.g., 0.16 in Mitchell et al., 2008; 0.7 in Bailey et al., 2017). Based on the optimum k_m determined in our simulations, we estimated a lower boundary at $k_d = 0.05\ d^{-1}$. However, it should be noted that total bioavailable concentrations of MeHg and Hg(II) in sediments, not just MeHg/Hg(II) in porewater, need to be considered when assessing net MeHg production for a particular site (Skyllberg, 2008), and that Hg(II) speciation at non-equilibrium conditions might differ from speciation at equilibrium (steady-state) conditions (Hsu-Kim et al., 2013).

The rate constants $k_m = 0.042\ d^{-1}$ and $k_d = 0.5\ d^{-1}$ determined from literature values and rate constants $k_m = 0.018\ d^{-1}$ and $k_d = 0.2\ d^{-1}$ determined experimentally by Schwartz and Gilmour (2017) using Hg(II) isotope tracers result in similar MeHg/THg under steady state conditions because the ratio of k_m/k_d is similar (Suppl. Figure S2.9). The data illustrate that steady state conditions are reached faster when the absolute values are larger. It is important to note that the rate laws and assumptions were the same for measured and literature-based values and that incubation times for k_m were short (2 hours for literature-derived, 24 hours for k_m calculated by Schwartz and Gilmour (2017)). There was a larger difference in incubation times for k_d, but its

effect is difficult to assess because there is generally more variability and uncertainty in k_d values. The simulations suggest that the rate constants chosen from the literature can be applied generally to aquatic sediments, although simulations with more sites should be conducted to confirm results.

2.7. Summary and recommendations for application

This study assessed published Hg(II) methylation rate constants (k_m) and MeHg demethylation rate constants (k_d) with the goal of providing general estimates for k_m and k_d in aquatic sediments. Similar rate constants were reported for Hg(II) methylation within the water column (Eckley et al., 2005), but MeHg produced within the water column might be significant only in systems with a high water/sediment ratio such as reservoirs, lakes, and coastal waters (Eckley et al., 2005; He et al., 2008; Monperrus et al., 2007). Rate laws for Hg(II) methylation and MeHg demethylation were reviewed, published rate constants were compiled and critically evaluated, and biogeochemical reaction simulations based on published data from an incubation experiment (Schwartz & Gilmour, 2017) were conducted. This critical review has the following uses and benefits:

1) Guiding the design of future isotope tracer studies: This review highlights some factors to consider when choosing incubation conditions and experimental variables (Hintelmann et al., 2000; Marvin-Dipasquale et al., 2000; Marvin-DiPasquale & Agee, 2003) for isotope-tracer studies, thereby expanding on previous research (Johnson et al., 2015; Jonsson et al., 2012; Lehnherr et al., 2011; Olsen et al., 2016, 2018; Regnell & Watras, 2019; Rodriguez Martin-Doimeadios et al., 2004). Longer incubation times can lead to underestimation of k_m and k_d when assuming a pseudo first-order rate law because the overall rate depends only on the concentration of bioavailable Hg or MeHg, which, in applying this rate law, is assumed to decrease by methylation or demethylation and not by any other processes. Alternatively, rate laws could include additional terms to account for sorption or other rate-controlled reactions that reduce Hg or MeHg concentration (Lehnherr et al., 2011; Olsen et al., 2018), but this approach requires knowledge of specific reaction rates for a particular system. Incubation times must be long enough to add tracer concentrations that mimic ambient concentrations. For k_m, the shortest incubation time used in all reviewed studies was 2 hours and resulted in k_m values that were a good estimate in model simulations. Analytical limitations prevent such short incubation times for k_d. Reaction simulations suggested that studies with incubation times of 6 to 48 hours provided the best estimates for k_d. To obtain multiple rate determinations, measuring the same sample over different incubation times could be achieved by taking subsamples from homogenized sediment (Drott et al., 2007b, 2008a; Hintelmann et al., 2000; Jonsson et al., 2012; Kronberg et al., 2018; Marvin-DiPasquale et al., 2000) or sediment cores (Jonsson et al., 2014).

2) Comparing rate constants from new studies with existing literature: In this review, we showed that rate constants calculated with the same rate law and based on experiments with similar incubation conditions can be compared to each other. Sensitivity of simulated MeHg and MeHg/Hg(II) was low for $k_m < 0.01\ d^{-1}$, suggesting that variations smaller than this value are probably negligible for sediments. Simulations indicated that $k_m = 0.04 \pm 0.03\ d^{-1}$ was a reasonable estimate for Hg(II) methylation in salt marsh soils and wetland sediments. MeHg demethylation rate constants were found to be associated with more variability and uncertainty than k_m, but some general patterns related to the level of Hg contamination emerged (Marvin-Dipasquale et al., 2000; Silver & Phung, 1996; Yu et al., 1996). Maximum k_d values tended to be about three times smaller at sites where no identified Hg sources was present ($k_d = 0.5\ d^{-1}$) than at sites with identified Hg source ($k_d = 1.8\ d^{-1}$).

3) Implementation and testing of experimentally determined rate constants with a biogeochemical model: Reaction simulations are a valuable tool to assess k_m and k_d. Model simulations relate independently observed rate constants to each other, to bioavailable Hg(II) and MeHg, and to cycling of major elements such as carbon, sulfur, and iron as their speciation changes in response to changes in system pH and redox potential. The relative importance of methylation versus demethylation rate can be assessed this way. Moreover, modeling can be used to determine k_d when all other parameters are constrained because of the model's sensitivity to k_d.

4) Provide estimates of k_m and k_d values for simulations and site applications: Generalized rate constants are useful for simulations to test newly developed models but could also aid in the assessment of specific sites. Estimated values can be applied in any computational program where the Hg(II) methylation and MeHg demethylation rates can be implemented as first-order rates and where the concentration of bioavailable Hg(II) and MeHg can be simulated. Programs can be reaction-transport model codes (e.g., PHREEQC, CrunchFlow, TOUGHREACT, The Geochemist's Workbench), water quality models (e.g., WASP), or small- to watershed-scale hydrological and hydrodynamic models with the capability to simulate water quality (e.g., SWAT, CE-QUAL-W2). When exemplary simulations for newly developed models are conducted, k_m and k_d are often chosen from literature. This review provides guidance on which values to choose. Examples are the enhancement of CapSim (Shen et al., 2018), CE-QUAL-W2 (S. Zhu et al., 2017), and WARMF (Chen et al., 2006) to simulate mercury cycling.

Our recommended values $k_m = 0.04 \pm 0.03\ d^{-1}$ and $k_d = 0.5\ d^{-1}$ can be useful for simulations of a specific site for which rate constants were not measured. One should note that a pseudo first-order rate law to describe Hg(II) methylation and MeHg demethylation is a simplification that has been employed because it is practical and commonly used, and because detailed Hg(II) methylation and MeHg demethylation mechanism are not known (Du et al., 2019; Hsu-Kim et al., 2013; Ma et al., 2019). However, environmental conditions such as temperature, pH, electron acceptor supply, and organic matter supply (Avramescu et al., 2011; J.M. Benoit et al., 2003; Ullrich et al., 2001) should be considered when selecting k_m and k_d values to perform simulations for a specific site. Notably these rate constants are best applied to simulations describing dynamic or transient conditions because they were measured in short-term experiments after tracer addition and likely before new a steady state prevailed.

The difficulty in quantifying the effects of environmental conditions, the high variability of k_d, and the high uncertainty when deriving k_d from measurements pose limitations on predicting net MeHg production. More research is needed on MeHg demethylation rates in particular and in differentiating and quantifying rates of demethylation pathways under different biogeochemical conditions. Whether relatively fast methylation or slow demethylation causes high net MeHg production under a particular set of conditions is important for informing best management practices or mitigation measures to reduce the potential for MeHg biomagnification. This review provides observations and tools that bring us closer to achieving this goal.

2.8. Acknowledgements

This material is based upon work supported by the Delta Stewardship Council Delta Science Fellows Program and the Delta Science Program in partnership with the California Department of Fish and Wildlife (Contract #18208). Any opinions, findings, and conclusions or recommendations expressed in this material are those of the authors and do not necessarily reflect the views of the Delta Stewardship Council. This journal article has been peer reviewed and approved for publication consistent with USGS Fundamental Science Practices (https://pubs.usgs.gov/circ/1367/). We thank C. Gilmour and G. Schwartz for providing

experimental data. We thank C. Gilmour, M. Marvin-DiPasquale, and three anonymous reviewers for their helpful reviews of this manuscript. Any use of trade, firm, or product names is for descriptive purposes only and does not imply endorsement by the U.S. government.

2.9. References

Adediran, G. A., Liem-Nguyen, V., Song, Y., Schaefer, J. K., Skyllberg, U., & Björn, E. (2019). Microbial biosynthesis of thiol compounds: Implications for speciation, cellular uptake, and methylation of Hg(II). Environmental Science & Technology, 53, 8187–8196. https://doi.org/10.1021/acs.est.9b01502

Avramescu, M. L., Yumvihoze, E., Hintelmann, H., Ridal, J., Fortin, D., & R.S. Lean, D. (2011). Biogeochemical factors influencing net mercury methylation in contaminated freshwater sediments from the St. Lawrence River in Cornwall, Ontario, Canada. Science of the Total Environment, 409(5), 968–978. https://doi.org/10.1016/j.scitotenv.2010.11.016

Bailey, L. T., Mitchell, C. P. J., Engstrom, D. R., Berndt, M. E., Coleman Wasik, J. K., & Johnson, N. W. (2017). Influence of porewater sulfide on methylmercury production and partitioning in sulfate-impacted lake sediments. Science of the Total Environment, 580, 1197–1204. https://doi.org/10.1016/j.scitotenv.2016.12.078

Barkay, T., Miller, S. M., & Summers, A. O. (2003). Bacterial mercury resistance from atoms to ecosystems. FEMS Microbiology Reviews, 27(2–3), 355–384. https://doi.org/10.1016/S0168-6445(03)00046-9

Beckers, F., Mothes, S., Abrigata, J., Zhao, J., Gao, Y., & Rinklebe, J. (2019). Mobilization of mercury species under dynamic laboratory redox conditions in a contaminated floodplain soil as affected by biochar and sugar beet factory lime. Science of the Total Environment, 672, 604–617. https://doi.org/10.1016/j.scitotenv.2019.03.401

Beckers, F., & Rinklebe, J. (2017). Cycling of mercury in the environment: Sources, fate, and human health implications: A review. Critical Reviews in Environmental Science and Technology, 47(9), 693–794. https://doi.org/10.1080/10643389.2017.1326277

Benoit, J. M. J., Gilmour, C. C., Heyes, A., Mason, R., & Miller, C. (2003). Geochemical and biological controls over methylmercury production and degradation in aquatic ecosystems. ACS Symposium, 835, 1–33. https://doi.org/10.1021/bk-2003-0835.ch019

Berner, R. A. (1964). An idealized model of dissolved sulfate distribution in recent sediments. Geochimica et Cosmochimica Acta, 28(9), 1497–1503. https://doi.org/10.1016/0016-7037(64)90164-4

Berner, R. A. (1980). Early Diagenesis: A theoretical approach. Princeton University Press.

Bessinger, B. A., Vlassopoulos, D., Serrano, S., & O'Day, P. A. (2012). Reactive transport modeling of subaqueous sediment caps and implications for the long-term fate of arsenic, mercury, and methylmercury. Aquatic Geochemistry, 18(4), 297–326. https://doi.org/10.1007/s10498-012-9165-4

Bigham, G. N., Murray, K. J., Masue-slowey, Y., & Henry, E. A. (2016). Biogeochemical controls on methylmercury in soils and sediments: Implications for site management. Integrated Environmental Assessment and Management, 13(2), 1–14. https://doi.org/10.1002/ieam.1822

Blanc, P., Burnol, A., Marty, N., Hellal, J., Guérin, V., & Laperche, V. (2018). Methylmercury complexes: Selection of thermodynamic properties and application to the modelling of a column experiment. Science of the Total Environment, 621, 368–375. https://doi.org/10.1016/j.scitotenv.2017.11.259

Boudreau, B. P. (1997). Diagenetic models and their implementation. Springer, Berlin, Germany. http://linkinghub.elsevier.com/retrieve/pii/S0264817298800056

Bravo, A. G., & Cosio, C. (2020). Biotic formation of methylmercury: A bio–physico–chemical conundrum. Limnology and Oceanography, 65(5), 1010–1027. https://doi.org/10.1002/lno.11366

Chen, C., Herr, J. W., & Tsai, W. (2006). Enhancement of Watershed Analysis Risk Management Framework (WARMF) for mercury watershed management and total maximum daily loads (TMDLs). Electric Power Research Institute.

Clarkson, T. W. (1997). The toxicology of mercury. Critical Reviews in Clinical Laboratory Sciences, 34(4), 369–403. https://doi.org/10.3109/10408369708998098

Compeau, G. C., & Bartha, R. (1985). Sulfate-reducing bacteria: Principal methylators of mercury in anoxic estuarine sediment. Applied and Environmental Microbiology, 50(2), 498–502. https://doi.org/10.1128/AEM.50.2.498-502.1985

Correia, R. R. S., Miranda, M. R., & Guimarães, J. R. D. (2012). Mercury methylation and the microbial consortium in periphyton of tropical macrophytes: Effect of different inhibitors. Environmental Research, 112, 86–91. https://doi.org/10.1016/j.envres.2011.11.002

Deacon, G. (1978). Volatilisation of methyl-mercuric chloride by hydrogen sulphide. Nature, 275, 344. https://doi.org/10.1038/275344a0

Drott, A., Lambertsson, L., Björn, E., & Skyllberg, U. (2007a). Effects of oxic and anoxic filtration on determined methyl mercury concentrations in sediment pore waters. Marine Chemistry, 103(1–2), 76–83. https://doi.org/10.1016/j.marchem.2006.06.004

Drott, A., Lambertsson, L., Björn, E., & Skyllberg, U. (2007b). Importance of Dissolved Neutral Mercury Sulfides for Methyl Mercury Production in Contaminated Sediments. Environmental Science & Technology, 41(7), 2270–2276.

Drott, A., Lambertsson, L., Björn, E., & Skyllberg, U. (2008a). Do potential methylation rates reflect accumulated methyl mercury in contaminated sediments? Environmental Science and Technology, 42(1), 153–158. https://doi.org/10.1021/es0715851

Drott, A., Lambertsson, L., Björn, E., & Skyllberg, U. (2008b). Potential demethylation rate determinations in relation to concentrations of MeHg, Hg and pore water speciation of MeHg in contaminated sediments. Marine Chemistry, 112(1–2), 93–101. https://doi.org/10.1016/j.marchem.2008.07.002

Du, H., Ma, M., Igarashi, Y., & Wang, D. (2019). Biotic and abiotic degradation of methylmercury in aquatic ecosystems: A review. Bulletin of Environmental Contamination and Toxicology, 102(5), 605–611. https://doi.org/10.1007/s00128-018-2530-2

Eckley, C. S., Gilmour, C. C., Janssen, S., Luxton, T. P., Randall, P. M., Whalin, L., & Austin, C. (2020). The assessment and remediation of mercury contaminated sites: A review of current approaches. Science of the Total Environment, 707(December). https://doi.org/10.1016/j.scitotenv.2019.136031

Eckley, C. S., Luxton, T. P., Goetz, J., & McKernan, J. (2017). Water-level fluctuations influence sediment porewater chemistry and methylmercury production in a flood-control reservoir. Environmental Pollution, 222, 32–41. https://doi.org/10.1016/j.envpol.2017.01.010

Eckley, C. S., Watras, C. J., Hintelmann, H., Morrison, K., Kent, A. D., & Regnell, O. (2005). Mercury methylation in the hypolimnetic waters of lakes with and without connection to wetlands in northern Wisconsin. Canadian Journal of Fisheries and Aquatic Science, 411, 400–411. https://doi.org/10.1139/F04-205

Feng, X., Li, P., Qiu, G., Wang, S., Li, G., Shang, L., Meng, B., Jiang, H., Bai, W., Li, Z., & Fu, X. (2008). Human exposure to methylmercury through rice intake in mercury mining areas, Guizhou province, China. Environmental Science and Technology, 42(1), 326–332. https://doi.org/10.1021/es071948x

Fleck, J. A., Gill, G., Bergamaschi, B. A., Kraus, T. E. C., Downing, B. D., & Alpers, C. N. (2014). Concurrent photolytic degradation of aqueous methylmercury and dissolved organic matter. Science of the Total Environment, 484(1), 263–275. https://doi.org/10.1016/j.scitotenv.2013.03.107

Fleck, J. A., Marvin-DiPasquale, M., Eagles-Smith, C. A., Ackerman, J. T., Lutz, M. A., Tate, M., Alpers, C. N., Hall, B. D., Krabbenhoft, D. P., & Eckley, C. S. (2016). Mercury and methylmercury in aquatic sediment across western North America. The Science of the Total Environment, 568, 727–738. https://doi.org/10.1016/j.scitotenv.2016.03.044

Fleming, E. J., Mack, E. E., Green, P. G., & Nelson, D. C. (2006). Mercury methylation from unexpected sources: Molybdate-inhibited freshwater sediments and an iron-reducing bacterium. Applied and Environmental Microbiology, 72(1), 457–464. https://doi.org/10.1128/AEM.72.1.457-464.2006

Foster, T. J., Nakahara, H., Weiss, A. A., & Silver, S. (1979). Transposon A-generated mutations in the mercuric resistance genes of plasmid R100-1. Journal of Bacteriology, 140(1), 167–181. https://doi.org/10.1128/jb.140.1.167-181.1979

Frohne, T., Rinklebe, J., Langer, U., Du Laing, G., Mothes, S., & Wennrich, R. (2012). Biogeochemical factors affecting mercury methylation rate in two contaminated floodplain soils. Biogeosciences, 9(1), 493–507. https://doi.org/10.5194/bg-9-493-2012

Fuhrmann, B. C., Beutel, M. W., O'Day, P. A., Tran, C., Funk, A., Brower, S., Pasek, J., & Seelos, M. (2021). Effects of mercury, organic carbon, and microbial inhibition on methylmercury cycling at the profundal sediment-water interface of a sulfate-rich hypereutrophic reservoir. Environmental Pollution, 268. https://doi.org/10.1016/j.envpol.2020.115853

Furutani, A., & Rudd, J. W. M. (1980). Measurement of mercury methylation in lake water and sediment samples. Applied and Environmental Microbiology, 40(4), 770–776. https://aem.asm.org/content/40/4/770

Gilmour, C. C., Bullock, A. L., Mcburney, A., & Podar, M. (2018). Robust mercury methylation across diverse methanogenic archaea. American Society for Microbiology, 9(2), 1–13. https://mbio.asm.org/content/9/2/e02403-17.full.pdf

Gilmour, C. C., Henry, E. a, & Mitchell, R. (1992). Sulfate stimulation of mercury methylation in freshwater sediments. Environmental Science & Technology, 26(3), 2281–2287. https://doi.org/10.1021/es00035a029

Gilmour, C. C., Podar, M., Bullock, A. L., Graham, A. M., Brown, S. D., Somenahally, A. C., Johs, A., Hurt, R. A., Bailey, K. L., & Elias, D. A. (2013). Mercury methylation by novel

microorganisms from new environments. Environmental Science and Technology, 47(20), 11810–11820. https://doi.org/10.1021/es403075t

Gilmour, C., & Riedel, G. (1995). Measurement of Hg methylation in sediments using high specific-activity 203 Hg and ambient incubation. Water, Air, and Soil Pollution, 80(1), 747–756. http://www.springerlink.com/index/G301128043174570.pdf

Graham, A. M., Aiken, G. R., & Gilmour, C. C. (2012). Dissolved organic matter enhances microbial mercury methylation under sulfidic conditions. Environmental Science and Technology, 46(5), 2715–2723. https://doi.org/10.1021/es203658f

He, T., Feng, X., Guo, Y., Qiu, G., Li, Z., Liang, L., & Lu, J. (2008). The impact of eutrophication on the biogeochemical cycling of mercury species in a reservoir: A case study from Hongfeng Reservoir, Guizhou, China. Environmental Pollution, 154(1), 56–67. https://doi.org/10.1016/j.envpol.2007.11.013

Hintelmann, H., Evans, D., & Villeneuve, J. Y. (1995). Measurement of mercury methylation in sediments by using enriched stable mercury isotopes combined with methylmercury determination by gas chromatography-inductively coupled plasma mass spectrometry. Journal of Analytical Atomic Spectrometry, 10(September), 619–624. http://dx.doi.org/10.1039/JA9951000619

Hintelmann, H., Keppel-Jones, K., & Evans, D. (2000). Constants of mercury methylation and demethylation rates in sediments and comparison of tracer and ambient mercury availability. Environmental Toxicology and Chemistry, 19(9), 2204–2211. https://doi.org/10.1002/etc.5620190909

Hoggarth, C. G. J., Hall, B. D., & Mitchell, C. P. J. (2015). Mercury methylation in high and low-sulphate impacted wetland ponds within the prairie pothole region of North America. Environmental Pollution, 205, 269–277. https://doi.org/10.1016/j.envpol.2015.05.046

Hollweg, T. A., Gilmour, C. C., & Mason, R. P. (2009). Methylmercury production in sediments of Chesapeake Bay and the mid-Atlantic continental margin. Marine Chemistry, 114(3–4), 86–101. https://doi.org/10.1016/j.marchem.2009.04.004

Hollweg, T. A., Gilmour, C. C., & Mason, R. P. (2010). Mercury and methylmercury cycling in sediments of the mid-Atlantic continental shelf and slope. Limnology and Oceanography, 55(6), 2703–2722. https://doi.org/10.4319/lo.2010.55.6.2703

Hsu-Kim, H., Eckley, C. S., Acha, D., Gilmour, C. C., Jonsson, S., & Mitchell, C. P. J. (2018). Challenges and opportunities for managing aquatic mercury pollution in altered landscapes. Ambio, 47, 141–169. https://doi.org/10.1007/s13280-017-1006-7

Hsu-Kim, H., Kucharzyk, K. H., Zhang, T., & Deshusses, M. A. (2013). Mechanisms regulating mercury bioavailability for methylating microorganisms in the aquatic environment: A critical review. Environmental Science and Technology, 47(6), 2441–2456. https://doi.org/10.1021/es304370g

Hunter, K. S., Wang, Y., & Van Cappellen, P. (1998). Kinetic modeling of microbially-driven redox chemistry of subsurface environments: Coupling transport, microbial metabolism and geochemistry. Journal of Hydrology, 209, 53–80. https://doi.org/10.1016/S0022-1694(00)00219-5

Jensen, S., & Jerneloev, A. (1969). Biological methylation of mercury in aquatic organisms. Nature, 223, 753–754. https://doi.org/10.1038/223753a0

Johannesson, K. H., & Neumann, K. (2013). Geochemical cycling of mercury in a deep, confined aquifer: Insights from biogeochemical reactive transport modeling. Geochimica et Cosmochimica Acta, 106, 25–43. https://doi.org/10.1016/j.gca.2012.12.010

Johnson, W. P., Swanson, N., Black, B., Rudd, A., Carling, G., Fernandez, D. P., Luft, J., Van Leeuwen, J., & Marvin-DiPasquale, M. (2015). Total- and methyl-mercury concentrations and methylation rates across the freshwater to hypersaline continuum of the Great Salt Lake, Utah, USA. Science of the Total Environment, 511, 489–500. https://doi.org/10.1016/j.scitotenv.2014.12.092

Jonsson, S., Skyllberg, U., Nilsson, M. B., Lundberg, E., Andersson, A., & Björn, E. (2014). Differentiated availability of geochemical mercury pools controls methylmercury levels in estuarine sediment and biota. Nature Communications, 5. https://doi.org/10.1038/ncomms5624

Jonsson, S., Skyllberg, U., Nilsson, M. B., Westlund, P., Shchukarev, A., Lundberg, E., & Bjo, E. (2012). Mercury methylation rates for geochemically relevant Hg(II) species in sediments. Environmental Science & Technology, 46(21), 11653–11659. https://doi.org/10.1021/es3015327%0A

Kerin, E. J., Gilmour, C. C., Roden, E., Suzuki, M. T., Coates, J. D., & Mason, R. P. (2006). Mercury methylation by dissimilatory iron-reducing bacteria. Applied and Environmental Microbiology, 72(12), 7919–7921. https://doi.org/10.1128/AEM.01602-06

Kim, E. H., Mason, R. P., Porter, E. T., & Soulen, H. L. (2006). The impact of resuspension on sediment mercury dynamics, and methylmercury production and fate: A mesocosm study. Marine Chemistry, 102(3–4), 300–315. https://doi.org/10.1016/j.marchem.2006.05.006

Kritee, K., Barkay, T., & Blum, J. D. (2009). Mass dependent stable isotope fractionation of mercury during mer mediated microbial degradation of monomethylmercury. Geochimica et Cosmochimica Acta, 73, 1285–1296. https://doi.org/10.1016/j.gca.2008.11.038

Kritee, K., Blum, J. D., Reinfelder, J. R., & Barkay, T. (2013). Microbial stable isotope fractionation of mercury: A synthesis of present understanding and future directions. Chemical Geology, 336, 13–25. https://doi.org/10.1016/j.chemgeo.2012.08.017

Kronberg, R. M., Tjerngren, I., Drott, A., Björn, E., & Skyllberg, U. (2012). Net degradation of methyl mercury in alder swamps. Environmental Science and Technology, 46(24), 13144–13151. https://doi.org/10.1021/es303543k

Kronberg, R., Schaefer, J. K., Björn, E., & Skyllberg, U. (2018). Mechanisms of methyl mercury net degradation in Alder Swamps: The role of methanogens and abiotic processes. Environmental Science & Technology Letters, 5, 220–225. https://doi.org/10.1021/acs.estlett.8b00081

Lehnherr, I., Louis, V. L. S., Hintelmann, H., & Kirk, J. L. (2011). Methylation of inorganic mercury in polar marine waters. Nature Geoscience, 4(5), 298–302. https://doi.org/10.1038/ngeo1134

Leterme, B., Blanc, P., & Jacques, D. (2014). A reactive transport model for mercury fate in soil—application to different anthropogenic pollution sources. Environmental Science and Pollution Research, 21(21), 12279–12293. https://doi.org/10.1007/s11356-014-3135-x

Leterme, B., & Jacques, D. (2015). A reactive transport model for mercury fate in contaminated soil—sensitivity analysis. Environmental Science and Pollution Research, 22(21), 16830–16842. https://doi.org/10.1007/s11356-015-4876-x

Levenspiel, O. (1980). The Monod Equation: A Revisit and a Generalization to Product Inhibition Situations. Biotechnology and Bioengineering, 22(8), 1671–1687. https://doi.org/10.1002/bit.260220810

Liem-Nguyen, V., Skyllberg, U., & Björn, E. (2017). Thermodynamic modelling of the solubility and chemical speciation of mercury and methylmercury driven by organic thiols and micromolar sulfide concentrations in boreal wetlands. Environmental Science & Technology, 51, 3678–3686. https://doi.org/10.1021/acs.est.6b04622

Lim, L., Brodberg, R., Gassel, M., & KLasing, S. (2013). Statewide health advisory and guidelines for eating fish from California's lakes and reservoirs without site-specific advice. California Environmental Protection Agency.

Liu, B., Schaider, L. A., Mason, R. P., Shine, J. P., Rabalais, N. N., & Senn, D. B. (2015). Controls on methylmercury accumulation in northern Gulf of Mexico sediments. Estuarine, Coastal and Shelf Science, 159, 50–59. https://doi.org/10.1016/j.ecss.2015.03.030

Loux, N. T. (2007). An assessment of thermodynamic reaction constants for simulating aqueous environmental monomethylmercury speciation. Chemical Speciation and Bioavailability, 19(4), 183–196. https://doi.org/10.3184/095422907X255947

Lu, X., Gu, W., Zhao, L., Ul Haque, M. F., DiSpirito, A. A., Semrau, J. D., & Gu, B. (2017). Methylmercury uptake and degradation by methanotrophs. Science Advances, 3(5), 1–6. https://doi.org/10.1126/sciadv.1700041

Lu, X., Liu, Y., Johs, A., Zhao, L., Wang, T., Yang, Z., Lin, H., Elias, D. A., Pierce, E. M., Liang, L., Barkay, T., & Gu, B. (2016). Anaerobic mercury methylation and demethylation by Geobacter bemidjiensis Bem. Environmental Science and Technology, 50(8), 4366–4373. https://doi.org/10.1021/acs.est.6b00401

Ma, M., Du, H., & Wang, D. (2019). Mercury methylation by anaerobic microorganisms: A review. Critical Reviews in Environmental Science and Technology, 49(20), 1893–1936. https://doi.org/10.1080/10643389.2019.1594517

Malm, O., Branches, J. F., Akagi, H., Castro, M. B., Pfeiffer, W. C., Harada, M., Bastos, W. R., & Kato, H. (1995). Mercury and methylmercury in fish and human hair from the Tapajós river basin, Brazil. The Science of the Total Environment, 175, 141–150. https://doi.org/10.1016/0048-9697(95)04910-X.

Martin-Doimeadios, R., Tessier, E., Amouroux, D., Guyoneaud, R., Duran, R., Caumette, P., & Donard, O. F. X. (2004). Mercury methylation/demethylation and volatilization pathways in estuarine sediment slurries using species-specific enriched stable isotopes. Marine Chemistry, 90, 107–123. https://doi.org/10.1016/j.marchem.2004.02.022

Marvin-DiPasquale, M., & Agee, J. L. (2003). Microbial mercury cycling in sediments of the San Francisco Bay-Delta. Estuaries, 26(6), 1517–1528. https://doi.org/10.1007/bf02803660

Marvin-DiPasquale, M., & Oremland, R. S. (1998). Bacterial methylmercury degradation in Florida everglades peat sediment. Environmental Science & Technology, 32(17), 2556–2563. https://doi.org/10.1021/es971099l

Marvin-DiPasquale, Mark, Agee, J. L., Bouse, R. M., & Jaffe, B. E. (2003). Microbial cycling of mercury in contaminated pelagic and wetland sediments of San Pablo Bay, California. Environmental Geology, 43(3), 260–267. https://doi.org/10.1007/s00254-002-0623-y

Marvin-DiPasquale, Mark, Agee, J., Mcgowan, C., Oremland, R. S., Thomas, M., Krabbenhoft, D., & Gilmour, C. C. (2000). Methyl-mercury degradation pathways: A comparison among three mercury impacted ecosystems. Environmental Science and Technology, 34(23), 4908–4916. https://doi.org/10.1021/es0013125

Marvin-DiPasquale, Mark, Windham-Myers, L., Agee, J. L., Kakouros, E., Kieu, L. H., Fleck, J. A., Alpers, C. N., & Stricker, C. A. (2014). Methylmercury production in sediment from agricultural and non-agricultural wetlands in the Yolo Bypass, California, USA. Science of the Total Environment, 484(1), 288–299. https://doi.org/10.1016/j.scitotenv.2013.09.098

Mason, R. P., Abbott, M. L., Bodaly, R. A., Bullock, O. R., Driscoll, C. T., Evers, D., Lindberg, S. E., & Swain, E. B. (2005). Monitoring the response to changing mercury deposition. Environmental Science & Technology, 39, 14A-22A. https://www.osti.gov/biblio/912319

Mergler, D., Anderson, H. A., Chan, L. H. M., Mahaffey, K. R., Murray, M., Sakamoto, M., & Stern, A. H. (2007). Methylmercury exposure and health effects in humans: A worldwide concern. Ambio, 36(1), 3–11. https://doi.org/10.1579/0044-7447(2007)36[3:MEAHEI]2.0.CO;2

Merritt, K. A., & Amirbahman, A. (2009). Mercury methylation dynamics in estuarine and coastal marine environments - A critical review. Earth-Science Reviews, 96(1–2), 54–66. https://doi.org/10.1016/j.earscirev.2009.06.002

Mitchell, C. P. J., Branfireun, B. A., & Kolka, R. K. (2008). Assessing sulfate and carbon controls on net methylmercury production in peatlands: An in situ mesocosm approach. Applied Geochemistry, 23(3), 503–518. https://doi.org/10.1016/j.apgeochem.2007.12.020

Mitchell, C. P. J., & Gilmour, C. C. (2008). Methylmercury production in a Chesapeake Bay salt marsh. Journal of Geophysical Research, 113(April), 1–14. https://doi.org/10.1029/2008JG000765

Monperrus, M., Tessier, E., Amouroux, D., Leynaert, A., Huonnic, P., & Donard, O. F. X. (2007). Mercury methylation, demethylation and reduction rates in coastal and marine surface waters of the Mediterranean Sea. Marine Chemistry, 107(1), 49–63. https://doi.org/10.1016/j.marchem.2007.01.018

Morel, F. M. M., Kraepiel, A. M. L., & Amyot, M. (1998). The chemical cycle and bioaccumulation of mercury. Annual Review of Ecology and Systematics, 29(1), 543–566. https://doi.org/10.1146/annurev.ecolsys.29.1.543

Olsen, T. A., Brandt, C. C., & Brooks, S. C. (2016). Periphyton biofilms influence net methylmercury production in an industrially contaminated system. Environmental Science & Technology, 50, 10843–10850. https://doi.org/10.1021/acs.est.6b01538

Olsen, T. A., Muller, K. A., Painter, S. L., & Brooks, S. C. (2018). Kinetics of methylmercury production revisited. Environmental Science & Technology, 52, 2063–2070. https://doi.org/10.1021/acs.est.7b05152

Oremland, R. S., Miller, L. G., Dowdle, P., Connell, T., & Barkay, T. (1995). Methylmercury oxidative degradation potentials in contaminated and pristine sediments of the Carson River, Nevada. Applied and Environmental Microbiology, 61(7), 2745–2753. https://aem.asm.org/content/61/7/2745

Ortiz, V. L., Mason, R. P., & Evan Ward, J. (2015). An examination of the factors influencing mercury and methylmercury particulate distributions, methylation and demethylation rates in laboratory-generated marine snow. Marine Chemistry, 177, 753–762. https://doi.org/10.1016/j.marchem.2015.07.006

Pak, K.-R., & Bartha, R. (1998). Mercury methylation and demethylation in anoxic lake sediments and by strictly anaerobic bacteria. Applied and Environmental Microbiology, 64(3), 1013–1017. https://aem.asm.org/content/64/3/1013

Parkhurst, D. L., & Appelo, C. A. J. (2013). Description of input and examples for PHREEQC Version 3 — A computer program for speciation, batch-reaction, one-dimensional transport, and inverse geochemical calculations. In U.S. Geological Survey Techniques and Methods, book 6, chapter A43. https://doi.org/10.1016/0029-6554(94)90020-5

Parks, J. M., Johs, A., Podar, M., Bridou, R., Hurt, R. a., Smith, S. D., Tomanicek, S. J., Qian, Y., Brown, S. D., Brandt, C. C., Palumbo, A. V, Smith, J. C., Wall, J. D., Elias, D. a., & Liang, L. (2013). The genetic basis for bacterial mercury methylation. Science, 339(6125), 1332–1335. https://doi.org/10.1126/science.1230667

Pham, A. L. T., Morris, A., Zhang, T., Ticknor, J., Levard, C., & Hsu-Kim, H. (2014). Precipitation of nanoscale mercuric sulfides in the presence of natural organic matter: Structural properties, aggregation, and biotransformation. Geochimica et Cosmochimica Acta, 133, 204–215. https://doi.org/10.1016/j.gca.2014.02.027

Podar, M., Gilmour, C. C., Brandt, C. C., Soren, A., Brown, S. D., Crable, B. R., Palumbo, A. V., Somenahally, A. C., & Elias, D. A. (2015). Global prevalence and distribution of genes and microorganisms involved in mercury methylation. Science Advances, 1(9), 1–13. https://doi.org/10.1126/sciadv.1500675

Qian, J., Skyllberg, U., Frech, W., Bleam, W. F., Bloom, P. R., & Petit, P. E. (2002). Bonding of methyl mercury to reduced sulfur groups in soil and stream organic matter as determined by X-ray absorption spectroscopy and binding affinity studies. Geochimica et Cosmochimica Acta, 66(22), 3873–3885. https://doi.org/10.1016/S0016-7037(02)00974-2

Ramlal, P. S., Rudd, J. W. M., & Hecky, R. E. (1986). Methods for measuring specific rates of mercury methylation and degradation and their use in determining factors controlling net rates of mercury methylation. Applied and Environmental Microbiology, 51(1), 110–114. https://aem.asm.org/content/51/1/110

Ravichandran, M. (2004). Interactions between mercury and dissolved organic matter - A review. Chemosphere, 55(3), 319–331. https://doi.org/10.1016/j.chemosphere.2003.11.011

Regnell, O., & Watras, C. J. (2019). Microbial mercury methylation in aquatic environments: A critical review of published field and laboratory studies. Environmental Science and Technology, 53(1), 4–19. https://doi.org/10.1021/acs.est.8b02709

Richard, J.-H., Bischoff, C., & Biester, H. (2016). Comparing modeled and measured mercury speciation in contaminated groundwater: Importance of dissolved organic matter composition. Environmental Science & Technology, 50, 7508–7516. https://doi.org/10.1021/acs.est.6b00500

Rothenberg, S. E., Anders, M., Ajami, N. J., Petrosino, J. F., & Balogh, E. (2016). Water management impacts rice methylmercury and the soil microbiome. Science of the Total Environment, 572, 608–617. https://doi.org/10.1016/j.scitotenv.2016.07.017

Schaefer, J. K., Letowski, J., & Barkay, T. (2002). Mer -mediated resistance and volatilization of Hg (II) under anaerobic conditions. Geomicrobiology Journal, 19, 87–102. https://doi.org/10.1080/014904502317246192

Schaefer, J. K., & Morel, F. M. M. (2009). High methylation rates of mercury bound to cysteine by Geobacter sulfurreducens. Nature Geoscience, 2(2), 123–126. https://doi.org/10.1038/ngeo412

Schaefer, J. K., Yagi, J., Reinfelder, J. R., Cardona, T., Ellickson, K. M., Tel-Or, S., & Barkay, T. (2004). Role of the bacterial organomercury lyase (MerB) in controlling methylmercury accumulation in mercury-contaminated natural waters. Environmental Science and Technology, 38(16), 4304–4311. https://doi.org/10.1021/es049895w

Schartup, A. T., Mason, R. P., Balcom, P. H., Hollweg, T. A., & Chen, C. Y. (2013). Methylmercury production in estuarine sediments: Role of organic matter. Environmental Science and Technology, 47(2), 695–700. https://doi.org/10.1021/es302566w

Schottel, J. L. (1978). The mercuric and organomercurial detoxifying enzymes from a plasmid-bearing strain of Escherichia coli. Journal of Biological Chemistry, 253(12), 4341–4349.

Schwartz, G. E., Sanders, J. P., McBurney, A. M., Brown, S. S., Ghosh, U., & Gilmour, C. C. (2019). Impact of dissolved organic matter on mercury and methylmercury sorption to activated carbon in soils: Implications for remediation. Environmental Science: Processes and Impacts, 21(3), 485–496. https://doi.org/10.1039/c8em00469b

Schwartz, G., & Gilmour, C. (2017). Geochemical controls on activated carbon effectiveness in remediating mercury and methylmercury-contaminated soils. Ninth International Conference on the Remediation and Management of Contaminated Sediment.

Shen, X., Lampert, D., Ogle, S., & Reible, D. (2018). A software tool for simulating contaminant transport and remedial effectiveness in sediment environments. Environmental Modelling and Software, 109(August), 104–113. https://doi.org/10.1016/j.envsoft.2018.08.014

Si, Y., Zou, Y., Liu, X., Si, X., & Mao, J. (2015). Mercury methylation coupled to iron reduction by dissimilatory iron-reducing bacteria. Chemosphere, 122, 206–212. https://doi.org/10.1016/j.chemosphere.2014.11.054

Silver, S., & Phung, L. T. (1996). Bacterial heavy metal resistance: New surprises. Annual Review of Microbiology, 50(1), 753–789. https://doi.org/10.1146/annurev.micro.50.1.753

Singer, M. B., Harrison, L. R., Donovan, P. M., Blum, J. D., & Marvin-DiPasquale, M. (2016). Hydrologic indicators of hot spots and hot moments of mercury methylation along river corridors. Science of the Total Environment, 568, 697–711. https://doi.org/10.1016/j.scitotenv.2016.03.005

Skyllberg, U. (2008). Competition among thiols and inorganic sulfides and polysulfides for Hg and MeHg in wetland soils and sediments under suboxic conditions: Illumination of controversies and implications for MeHg net production. Journal of Geophysical Research, 113, 1–14. https://doi.org/10.1029/2008JG000745

Skyllberg, U., Qian, J., Frech, W., Xia, K., & Bleam, W. F. (2003). Distribution of mercury, methyl mercury and organic sulphur species in soil, soil solution and stream of a boreal forest catchment. Biogeochemistry, 64, 53–76. https://doi.org/10.1023/A:1024904502633

Summers, A. O., & Sugarman, L. I. (1974). Cell-free mercury (II)-reducing activity in a plasmid-bearing strain of Escherichia coli. Journal of Bacteriology, 119(1), 242–249. https://doi.org/10.1128/JB.119.1.242-249.1974

Ticknor, J. L., Kucharzyk, K. H., Porter, K. a., Deshusses, M. a., & Hsu-Kim, H. (2015). Thiol-based selective extraction assay to comparatively assess bioavailable mercury in sediments.

Environmental Engineering Science, 32(7), 150505074752008. https://doi.org/10.1089/ees.2014.0526

Tjerngren, I., Karlsson, T., Björn, E., & Skyllberg, U. (2012). Potential Hg methylation and MeHg demethylation rates related to the nutrient status of different boreal wetlands. Biogeochemistry, 108(1–3), 335–350. https://doi.org/10.1007/s10533-011-9603-1

Ullrich, S. M., Tanton, T. W., & Abdrashitova, S. A. (2001). Mercury in the aquatic environment: a review of factors affecting methylation. Critical Reviews in Environmental Science and Technology, 31(3), 241–293. https://doi.org/10.1080/20016491089226

Van Cappellen, P., & Wang, Y. (1996). Cycling of iron and manganese in surface and sediments: A general theory for the coupled transport and reaction of carbon, oxygen, nitrogen, sulfur, iron, and manganese. American Journal of Science, 296, 197–243. https://doi.org/10.1126/science.3.53.32

Vlassopoulos, D., Kanematsu, M., Henry, E. A., Goin, J., Leven, A., Glaser, D., Brown, S. S., & O'Day, P. A. (2018). Manganese(IV) oxide amendments reduce methylmercury concentrations in sediment porewater. Environmental Science: Processes & Impacts, 20(12), 1746–1760. https://doi.org/10.1039/C7EM00583K

West, J., Graham, A. M., Liem-Nguyen, V., & Jonsson, S. (2020). Dimethylmercury degradation by dissolved sulfide and mackinawite. Environmental Science and Technology, 54(21), 13731–13738. https://doi.org/10.1021/acs.est.0c04134

Windham-Myers, L., Marvin-DiPasquale, M., A. Stricker, C., Agee, J. L., H. Kieu, L., & Kakouros, E. (2013). Mercury cycling in agricultural and managed wetlands of California, USA: Experimental evidence of vegetation-driven changes in sediment biogeochemistry and methylmercury production. Science of the Total Environment, 484, 300–307. https://doi.org/10.1016/j.scitotenv.2013.05.028

Windham-Myers, L., Marvin-Dipasquale, M., Krabbenhoft, D. P., Agee, J. L., Cox, M. H., Heredia-Middleton, P., Coates, C., & Kakouros, E. (2009). Experimental removal of wetland emergent vegetation leads to decreased methylmercury production in surface sediment. Journal of Geophysical Research: Biogeosciences, 114(3), 1–14. https://doi.org/10.1029/2008JG000815

Wood, J. M., Kennedy, F. S., & Rosen, C. G. (1968). Synthesis of Methyl-mercury compounds by extracts of a methanogenic bacterium. Nature, 220, 173–174. https://doi.org/10.1038/220173a0

Xu, J., Buck, M., Eklöf, K., Ahmed, O. O., Schaefer, J. K., Bishop, K., Skyllberg, U., Björn, E., Bertilsson, S., & Bravo, A. G. (2019). Mercury methylating microbial communities of boreal forest soils. Scientific Reports, 9, 518. https://doi.org/10.1038/s41598-018-37383-z

Yang, Z., Fang, W., Lu, X., Sheng, G. P., Graham, D. E., Liang, L., Wullschleger, S. D., & Gu, B. (2016). Warming increases methylmercury production in an Arctic soil. Environmental Pollution, 214, 504–509. https://doi.org/10.1016/j.envpol.2016.04.069

Yu, H., Chu, L., & Misra, T. K. (1996). Intracellular inducer Hg2+ concentration is rate determining for the expression of the mercury-resistance operon in cells. Journal of Bacteriology, 178(9), 2712–2714. https://doi.org/10.1128/jb.178.9.2712-2714.1996

Yu, R. Q., Reinfelder, J. R., Hines, M. E., & Barkay, T. (2018). Syntrophic pathways for microbial mercury methylation. ISME Journal, 1–10. https://doi.org/10.1038/s41396-018-0106-0

Zhang, L., Liang, X., Wang, Q., Zhang, Y., Yin, X., Lu, X., Pierce, E. M., & Gu, B. (2021). Isotope exchange between mercuric [Hg(II)] chloride and Hg(II) bound to minerals and thiolate ligands: Implications for enriched isotope tracer studies. Geochimica et Cosmochimica Acta, 292, 468–481. https://doi.org/10.1016/j.gca.2020.10.013

Zhang, L., Wu, S., Zhao, L., Lu, X., Pierce, E. M., Gu, B., Wu, S., Zhao, L., Lu, X., Pierce, E. M., & Gu, B. (2019). Mercury sorption and desorption on organo-mineral particulates as a source for microbial methylation [Research-article]. Environmental Science & Technology, 53(5), 2426–2433. https://doi.org/10.1021/acs.est.8b06020

Zhang, T., Kim, B., Levard, C., Reinsch, B. C., Lowry, G. V, Deshusses, M. A., & Hsu-Kim, H. (2012). Methylation of mercury by bacteria exposed to dissolved, nanoparticulate, and microparticulate mercuric sulfides. Environmental Science & Technology, 46(13), 6950–6958. https://doi.org/10.1021/es203181m

Zhu, S., Zhang, Z., & Liu, X. (2017). Enhanced two dimensional hydrodynamic and water quality model (CE-QUAL-W2) for simulating mercury transport and cycling in water bodies. Water (Switzerland), 9(9). https://doi.org/10.3390/w9090643

Zhu, S., Zhang, Z., & Žagar, D. (2018). Mercury transport and fate models in aquatic systems: A review and synthesis. Science of the Total Environment, 639, 538–549. https://doi.org/10.1016/j.scitotenv.2018.04.397

Zhu, W., Song, Y., Adediran, G. A., Jiang, T., Reis, A. T., Pereira, E., Skyllberg, U., & Björn, E. (2018). Mercury transformations in resuspended contaminated sediment controlled by redox conditions, chemical speciation and sources of organic matter. Geochimica et Cosmochimica Acta, 220, 158–179. https://doi.org/10.1016/j.gca.2017.09.045

2.10. Figures and Tables

Table 2.1. Reported and recommended rate constants for mercury methylation (k_m) and methylmercury demethylation (k_d) for aquatic sediments.

	Incubation time (hours)	Hg methylation rate constant $k_m(d^{-1})$	Refer-ence	MeHg demethylation rate constant $k_d(d^{-1})$	Refer-ence
			Reported		
Range	2–456	0.0003–1.5		0.001–63	
Median upper limit*	2–5	0.13	a, b, c, d, e, f, g, h	21.80	b, c, d, m
	48	0.04	i, j, k, l	0.53	i, l, n, o, p
			Recommended		
With identified Hg source†					
Methylation	2	0.04 ± 0.03‡		-	
Demethylation	6 - 48	-		1.8–0.05	
No identified Hg source†					
Methylation	2	0.04 ± 0.03‡		-	
Demethylation	6 - 48	-		0.5–0.05	

Sources: a (Hollweg et al., 2009), b (Hollweg et al., 2010), c (Kim et al., 2006), d (Liu et al., 2015), e (Mitchell & Gilmour, 2008), f (Hoggarth et al., 2015), g (Marvin-DiPasquale et al., 2014), h (Windham-Myers et al., 2009), i (Hintelmann et al., 2000), j (Tjerngren et al., 2012), k (Drott et al., 2007a), l (Drott et al., 2008a), m (Marvin-DiPasquale et al., 2000), n (Drott et al., 2008b), o (Kronberg et al., 2012), p (Kronberg et al., 2018)

* Median for upper limit of reported range grouped by incubation time was calculated using only studies assuming an irreversible pseudo first-order reaction. Studies reporting averages were not considered.

† With identified Hg source means that Hg-emitting mine or industry lies within 70 km upstream of site. No identified Hg source means that no Hg-emitting mine or industry is present within the watershed or the source lies more than 70 km upstream (see Figure 2.2).

‡ Value and 95% confidence interval based on Figure 2.2 and a sensitivity analysis (see Figure 2.).

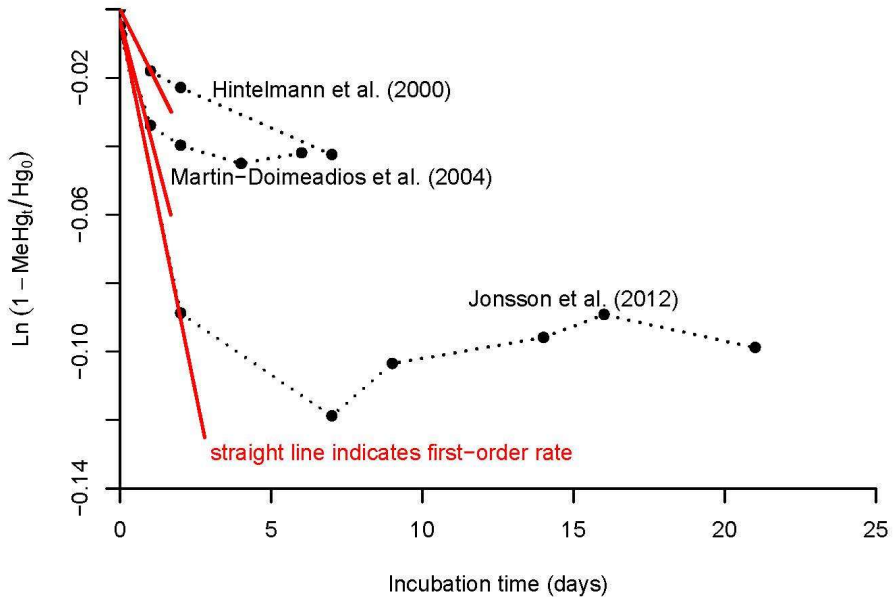

Figure 2.2. Experimental data from Hintelmann et al. (2000), Martin-Doimeadios et al. (2004), and Jonsson et al. (2012) for Hg measured at time = 0 and MeHg measured at time = t (black circles) superimposed with integrated first-order rate law for Hg methylation shown as the equation for a straight line y = mx + b: $ln\left(1-\frac{MeHg_t}{Hg_{t=0}}\right)=-k_m t$, where m = -$k_m$ and b = 0.

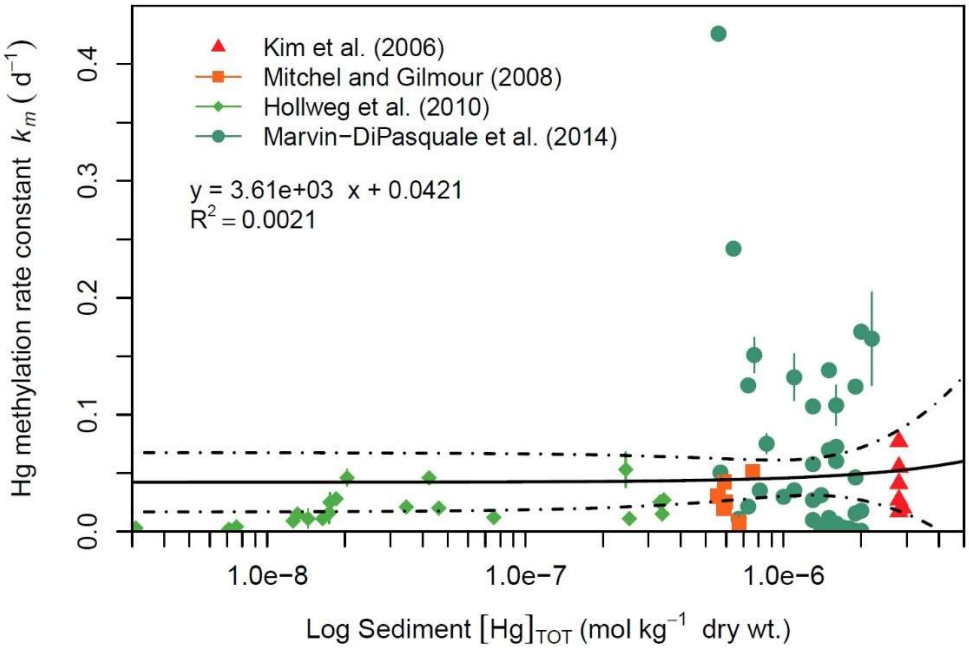

Figure 2.3. Mercury methylation rate constant (k_m) as a function of total sediment mercury concentration $[Hg]_{tot}$ reported by Kim et al., 2006; Mitchell and Gilmour, 2008; Hollweg et al., 2010; Marvin-DiPasquale et al., 2014. Error bars on data are uncertainties reported in studies. All studies assumed a pseudo first-order rate and used single time point measurements after a 2-hour incubation time to calculate k_m. The solid line represents the linear least-squares best fit for all data points, and the dashed line represents the 95% confidence interval.

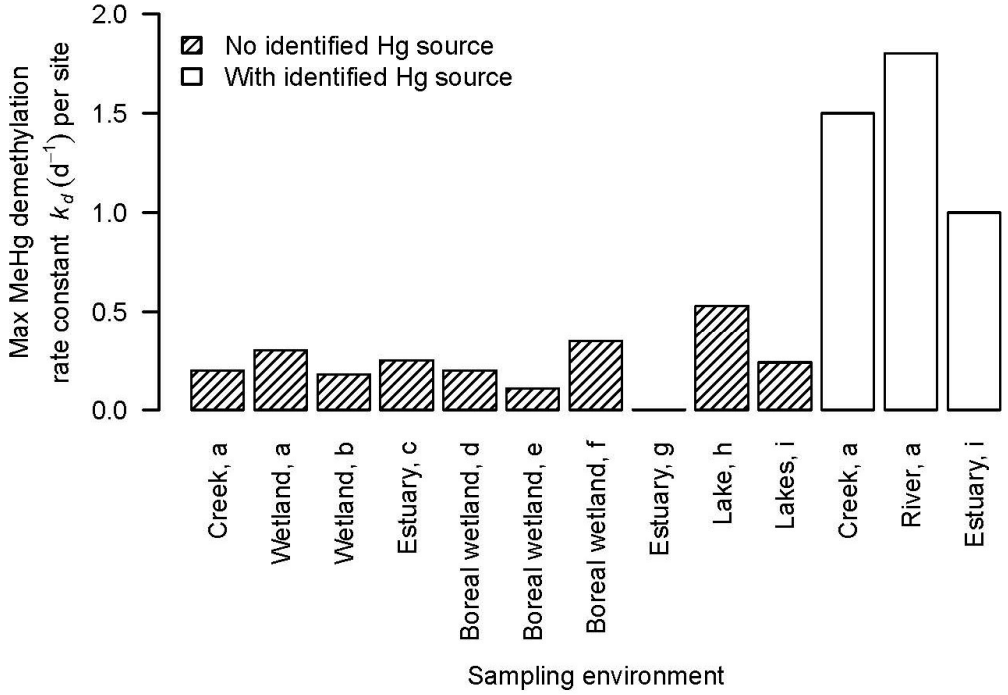

Figure 2.4. Maximum observed methylmercury demethylation rate constants (k_d) per site (one or more samples per site) from selected publications. Studies assumed a pseudo first-order rate and used 6–48 hours incubation times. With identified Hg source means that a Hg-emitting mine or industry lies within approximately 70 km upstream of the site, and no identified Hg source means that no source is present or lies more than 70 km upstream. Sources: a (Marvin-DiPasquale et al., 2000), b (Marvin-DiPasquale and Oremland, 1998), c (Marvin-DiPasquale et al., 2003), d (Tjerngren et al., 2012), e (Kronberg et al., 2012), f (Kronberg et al., 2018), g (Rodriguez Martin-Doimeadios et al., 2004), h (Hintelmann et al., 2000), i (Drott et al., 2008b)

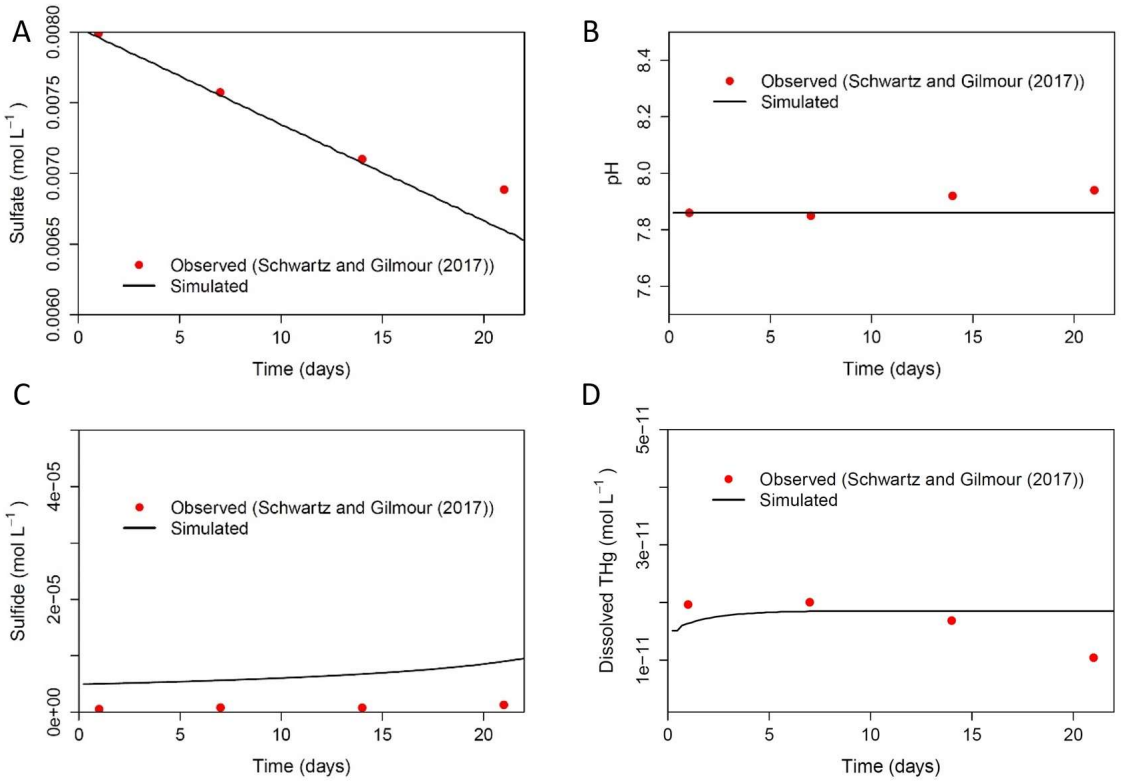

Figure 2.5. Parameters pH (A), sulfate (B), sulfide (C), and dissolved THg (D) measured (red dots) by Schwartz and Gilmour (2017) during incubation experiments with controlled conditions in comparison to PHREEQC simulation performed in this study (solid lines). Initial conditions of the simulation (Suppl. Table S2.7) were based on initial conditions of the incubation.

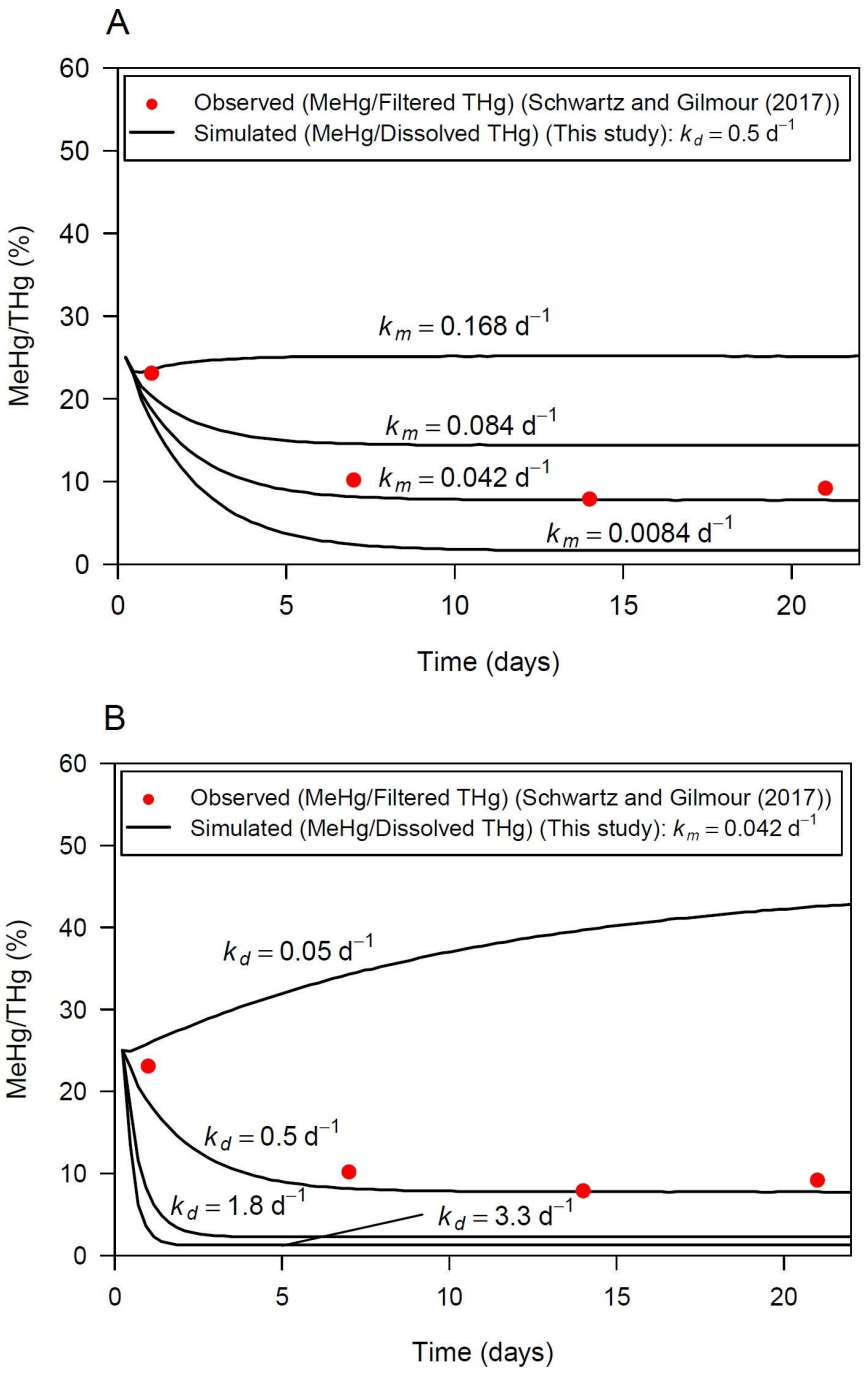

Figure 2.6. Sensitivity of simulated MeHg/Dissolved THg ratio (black line) to Hg methylation rate constant (k_m) (A) and MeHg demethylation rate constant (k_d) (B). MeHg/Filtered THg ratios observed in porewater in incubation experiments by Schwartz and Gilmour (2017) shown by red dots.

3. Assessment of mercury methylation and demethylation in a mercury mine-impacted floodplain using a biogeochemical model

3.1. Abstract

Quantifying the effect of environmental conditions on mercury (Hg) methylation and demethylation remains a challenge. Reaction-transport models combine numerous thermodynamic and kinetic processes in a mechanistic way, which makes them ideal to assess hypotheses and interpret observed data. Here we apply a thermodynamic-kinetic model that simulates aqueous speciation, ion exchange, mineral precipitation and dissolution, primary and secondary redox reactions, and mercury methylation and demethylation to field data from a mercury mine-impacted floodplain area that represents a range of environmental conditions. Data describing evolving conditions of porewater, and dry and wet bulk sediment were used to estimate initial conditions and to assess simulation results. The model successfully predicted iron- and sulfur-related parameters, but simulated dissolved inorganic mercury (Hg(II)) showed stronger variability with aqueous sulfide concentration than was observed in the field data. The poor simulation of Hg(II) resulted in poor simulation of dissolved MeHg. A rate formulation was developed to simulate kinetic precipitation of metacinnabar as a function of aqueous sulfide concentration and the number of thiol groups on dissolved organic matter. The addition of the variable precipitation rate for HgS(s) improved simulation of porewater Hg(II) and MeHg concentrations.

3.2. Introduction

Contamination with the neurotoxin mercury (Hg) is a worldwide human health concern (Chumney et al., 2021; Clarkson, 1997; Lim et al., 2013; Mergler et al., 2007) Mercury occurs in multiple chemical forms in the environment, including – elemental Hg^0, inorganic mercury (Hg(II)), and methylmercury (MeHg, monomethylmercury CH_3Hg^+). Methylmercury biomagnifies along the food chain and can reach dangerous concentrations in fish (Lim et al., 2013; Malm et al., 1995). Microorganisms with the hgcAB gene cluster convert Hg(II) to MeHg in anoxic sediments (Parks et al., 2013). Methylmercury is abiotically and biotically degraded (demethylated) to Hg(II) and Hg^0 (Barkay & Gu, 2021). Although Hg is naturally occurring, elevated concentrations are present in areas affected by mining of mercury and precious metals (Alpers et al., 2005). Anthropogenic activity has caused mobilization of Hg(II) and therefore affected net MeHg production (Driscoll et al., 2013), resulting in a need to manage Hg(II) and MeHg.

Quantifying the effect of varying environmental conditions on MeHg production is still lacking, which is reflected in poor simulation of Hg(II) and MeHg concentrations by thermodynamic and kinetic models. Mercury speciation and microbial activity depend on hydrology, pH, salinity, organic matter (OM), and cycling of redox sensitive elements iron and sulfur (Bigham et al., 2016; O'Connor et al., 2019). Complexation with inorganic sulfide and organic thiol groups (RSH) is a key factor in controlling Hg(II) speciation and bioavailability (Liem-Nguyen et al., 2021). Recent work indicates that dissolved Hg(II) concentrations can increase with increasing sulfide concentrations (Graham et al., 2012; Liem-Nguyen et al., 2017a, 2017b), which is contrary to earlier hypotheses. Despite this positive development, thermodynamic models predict a larger variability of dissolved Hg(II) than is observed (Graham et al., 2012; Liem-Nguyen et al., 2017a, 2017b), indicating that the underlying conceptual model needs improvement. Other potential reasons for a poor simulation of MeHg are simplified assumptions about bioavailable Hg(II) and MeHg and uncertainty in demethylation rate constants. A general

assumption is that dissolved Hg(II) is bioavailable, but there is currently no consensus on which Hg(II) species are most readily taken up by bacteria, and if uptake into cells is active or passive, or both (Adediran et al., 2019; Gerbig et al., 2011; Schaefer et al., 2011, 2014; Schaefer & Morel, 2009; Thomas et al., 2018, 2019; Thomas & Gaillard, 2017). Biotic demethylation rates are an important factor in controlling MeHg concentrations, but demethylation rate constants appear to vary more than methylation rate constants, are more difficult to measure, and are generally associated with higher uncertainties (Helmrich et al., 2021).

A reaction-transport model that combines many processes in a mechanistic way is ideal to test hypotheses, interpret field and laboratory data, and plan management measures. Although Hg models have been applied to lakes (Chen et al., 2008), wetlands (Chen & Herr, 2010; Gilmour et al., 2007; V. Liem-Nguyen, Skyllberg, & Björn, 2017; Van Liem-Nguyen et al., 2021), lagoons (Melaku Canu et al., 2015), groundwater (Johannesson & Neumann, 2013; Richard et al., 2016), and sediment (Bessinger et al., 2012; Leterme et al., 2014; Leterme & Jacques, 2015), only very few are full thermodynamic-kinetic models that simulate Hg and other redox sensitive elements. Gilmour et al. (2007) applied a comprehensive thermodynamic-kinetic model to simulate the depth distribution of Hg methylation in marsh soils. While most studies use a simple pseudo-first order rate formulation for Hg methylation, they employed a rate formulation with multiple parameters including the cell density that might be difficult to transfer to other sites. Other studies used data from controlled conditions to identify the main drivers for MeHg production and estimate model parameters. Leterme & Jacques (2015) conducted a sensitivity analysis (Morris method) of 13 input parameters for a reaction-transport model (Hg speciation and transport) for hypothetical conditions in a contaminated unsaturated soil. However, the model did not include mercury methylation and demethylation or reactions of redox-sensitive elements such as iron and sulfur. Blanc et al. (2018) applied a thermodynamic-kinetic model to column experiments to identify the most important MeHg complexes and test rate formulations for Hg methylation and demethylation. Although, the model included Hg sorption to the mineral mackinawite, it did not include sorption to organic matter.

The aim of this study is to apply a thermodynamic-kinetic model to field data to 1) evaluate how environmental conditions, specifically iron and sulfur species, affect MeHg production, 2) explore how field data can be used to constrain model parameters, and 3) improve model robustness and applicability. The here presented thermodynamic-kinetic model was adapted from Bessinger et al. (2012) and Helmrich et al. (2021) and further extended to include Hg sorption to thiol groups on organic matter and coupling of Hg (II) methylation to iron reduction and methanogenesis. Field data from floodplains in the Cache Creek Settling Basin (CCSB) located in California's Central Valley were chosen because MeHg production had been observed at the site and because a broad range of observed parameters was available to constrain model parameters.

3.3. Model formulation

The thermodynamic-kinetic model written in PHREEQC code simulates aqueous speciation, ion exchange, mineral precipitation and dissolution, primary and secondary redox reactions, and mercury methylation and demethylation using either thermodynamic (equilibrium) or kinetic (rate) constraints, depending on user choice (Figure 3.1). The kinetic model presented by Bessinger et al. (2012) and modified by Helmrich et al. (2021) to describe Hg methylation and demethylation as pseudo first-order rates was further extended in this study by coupling Hg(II) methylation to iron (Fe) reduction and methanogenesis (Table S3.2). Equilibrium aqueous complexation of Hg and MeHg with thiol sites on dissolved organic matter (DOM) and sorption of Hg and MeHg to thiol sites associated with sediment organic matter (SOM) was added to the

database using constants from Liem-Nguyen et al. (2017b). Thermodynamic constants, kinetic reactions, and kinetic parameters are provided in Table S3.1, S3.2, and S3.3 in SI.

The model simulates a one-dimensional 20 cm deep sediment-water interface. The model domain has two cells – one representing the overlying water and the second cell representing the sediment with porewater. The cell with the overlying water has the purposes to supply electron acceptors, which also has the benefit to reduce the computational time. Transport between the cells occurs via diffusion only. A constant concentration boundary conditions was applied at the upper cell and a closed boundary condition was applied at the lower cell. For constituents measured in the sediment that were used to estimate mineral concentrations, the percentage of dry weight per wet weight was used to calculate the moles of minerals per 1 kg water in the sediment-porewater cell.

An exploratory kinetic rate for metacinnabar precipitation was implemented for one simulation scenarios to describe the stabilizing effect of OM:

$$R_{metacin,precip,non-linear} = (k_{metacin,precip,non-linear}^{([S(-II)tot/[RSH_{LMWDOM}])} - 1 \quad (3.1)$$

when

$$logSI_{metacin} = \log(\frac{IAP}{K}) = \log(\frac{[HS^-][Hg^{2+}]}{[HS^-][Hg^{2+}]}) > 0 \quad (3.2)$$

where [S(-II)tot] is the total porewater (PW) sulfide concentration, [$RSH_{LMW\ DOM}$] is the concentration of thiol sites on low molecular weight (LMW) DOM, and $logSI_{matcin}$ is the saturation index of metacinnabar. The saturation index is calculated based on the Ion Activity Product IAP – the activities of in the water samples – and the solubility product K – the activities at equilibrium. Equilibrium is assumed when log $SI_{metacin} < 0$. Setting only one mineral in equilibrium with the solution or adding kinetic rates allows simulation of apparent solubility of metastable phases. The ratio at which metacinnabar precipitation starts is determined by the rate constant $k_{metacin\ precip}$, which was calibrated based on simulated and observed PW Hg(II) and MeHg. The y-intercept was set to zero (by subtracting 1) to have virtually no metacinnabar precipitation when sulfide is ten times higher than the number of thiols sites. Nano-HgS is set in equilibrium with the solution and will set the apparent solubility of HgS(s) when the rate of metacinnabar precipitation is low. Metacinnabar precipitation quickly increases when the sulfide/thiol sites ratio exceeds 10 and is fast enough at a ratio of 100 for metacinnabar to set the apparent HgS(s) solubility.

3.4. Application to field data from CCSB

3.4.1. Site description and dataset

The simulated sites are floodplain areas in the Cache Creek Settling Basin (CCSB) located in California's Central Valley (Figure 3.2). The Cache Creek watershed is contaminated with Hg from legacy Hg and gold mining, and has naturally high background Hg (Domagalski et al., 2004). It contains multiple waterbodies that have Hg fish consumption advisories (Gassel & Brodberg, 2014, 2018). Downstream of CCSB is the Yolo By-Pass area, consisting of ~59,000 acres of seasonal and permanent wetlands with elevated Hg and MeHg that is a source of these contaminants to the Sacramento-San Joaquin Delta (Windham-Myers et al., 2014; Wood et al., 2010).

Ongoing studies by the United States Geological Survey (USGS) and the California Department of Water Resources (CA DWR) are examining the sediment, Hg, and MeHg trap

efficiency of the CCSB. Average trap efficiency for water years from 2010 to 2019 was 67 % for suspended sediment, 63% for particulate THg, and 62 % for particulate THg (Brown & Nosacka, 2020). The apparent trap efficiency was -10 % for filter-passing THg (a net increase across the basin), 55 % for whole-water MeHg, 55 % for particulate MeHg, and -22 % for filter-passing MeHg (also a net increase), indicating production of MeHg within the basin (Brown and Nosacka, 2020). Sediment that is exported from CCSB has higher concentrations of THg and MeHg than sediment that is trapped. The increase in THg concentration of exported particles is likely to be a grain-size effect, whereas the increase in MeHg concentration on exported particles likely reflects MeHg production within the basin (Brown and Nosacka, 2020; C. Alpers, USGS, written communication, 2022). The CCSB has multiple land use types with the most abundant being floodplain and agriculture. It was found that MeHg production is higher in floodplain areas than at agricultural sites. Due to this and a planned conversion of several floodplain areas to agricultural land, simulations focused on floodplains.

The published data (Marvin-Dipasquale et al., 2021) used for simulations in this study are from samples collected between 2010 to 2019, with the majority of data points for wet sediment collected from 2013 to 2016. The data set includes a broad range of observed parameters. However, a limitation of sampling was that typically only one data point per site and flooding event was measured. Therefore, data points from multiple stations with the same land use type and multiple flooding events were aggregated and compared to simulation results based on the estimated number of days since flooding began at a particular site (Marvin-Dipasquale et al., 2021).

3.4.2. Parameter estimation and simulation scenarios

The initial aqueous solution and sediment composition were set to represent average conditions in inflowing water and sediment of the 18 simulated floodplain sites (Table 3.1Table 3.). The floodplain sites are dry for most of the year and can be flooded after rain events. To simulate this flooding process, electron acceptors (oxygen, nitrate, sulfate) at the constant boundary condition and in the cell representing overlying water were set to represent inflowing water based on measured or typical values. Sulfide was assumed to be zero in overlying water. Oxygen and nitrate concentrations were assumed to be zero or a small value in the initial porewater. Initial sulfate and sulfide concentrations in PW were based on observed PW concentrations. Initial mackinawite was based on total reduced sulfur (TRS) and ferrihydrite was set to be always lower than observed sediment Fe(III)a. Total Hg(II) (dissolved and sediment) was based on measured bulk THg in sediment, which was 4 orders of magnitude larger than PW THg. The majority of Hg was initially set to be dissolved Hg, which is redistributed in the first simulation step to HgS(s) and Hg(II) that is sorbed to thiol groups in SOM ($Hg(SOM\text{-}RS)_2$). Dissolved MeHg was initially set to zero because mass balance indicated net production in CCSB.

One kinetic model parameter that was not taken from prior studies was the rate constant for OM degradation k_{OM}. Instead k_{OM} was estimated by matching simulation results with measured PW sulfate and sulfide, and TRS measurement of sediment. The estimated value is a typical value for a 1G sediment diagenesis model applications (Paraska et al., 2014).

The number of thiol sites associated with LMW DOM and SOM, which are known to strongly complex Hg, was determined with a sensitivity analysis within ranges reported in literature (Figure S3.2). The number of thiol sites on LMW DOM are typically 1e-9 mol/l to 1e-7 mol/l (Adediran et al., 2019; Han & Gill, 2005; Hu et al., 2006; Liem-Nguyen et al., 2017a; Zhang et al., 2004). The highest value (1e-7 mol/l) was chosen because the simulated site is high in OM (LOI 5-25 % dry wt., PW DOC 8-186 mg/l). Thiol sites on SOM were calibrated based on PW Hg(II), and (Hg(SOM-RS)2) and HgS(s) estimated from extraction experiments at time point zero when

PW sulfide was zero. Too many thiol sites on SOM would result in underestimation of PW Hg(II) and HgS(s) and overestimation of SOM-bound Hg. Too few thiol sites on SOM would result in underestimation of SOM-bound Hg and overestimation of HgS(s). It was assumed that the number of sorption sites does not change over time. Thermodynamic constants for adsorption of Hg and MeHg to thiol sites were selected from the literature (Table S3.1).

Several simulation scenarios were developed to examine the range of conditions observed within the CCSB floodplain and test which variables improved model simulations (Table 3.2). The first set of scenarios varied initial ferrihydrite amounts in the sediment and dissolved sulfate concentrations in porewater to compare to the observed range of PW sulfide concentrations. The second set of simulations explored the effect of changing HgS(s) equilibrium solubility or adding a kinetic rate for metacinnabar precipitation. Supplementary simulation scenarios to assess the form of Hg in sediment, Hg mineral solubility, and bioavailable DOM are presented in SI.

3.5. Results

3.5.1. Trends in sediment and porewater composition in CCSB floodplain areas

The composition of PW in floodplain areas differed considerably from that of surface water flowing into the basin (Figure 3.3), but conditions were relatively constant after flooding. Boxplots (Figure 3.3) show data related to the flooding events and sites that were simulated. Flooding was simulated for 70 days, but some flooding events were observed to be longer. Boxplots including data points after more than 70 days of flooding are shown in supplemental material (Figure S3.1). On average, PW sulfate concentrations were lower than those in the inflowing water. Sulfide concentration was assumed to be zero in inflowing water. Sulfide was only measured in less than half the collected PW samples. It averaged 0.15 mmol/l in sites flooded less than 70 days (18 sites) and 0.002 mmol/l (Figure S3.1) when including flooding events that lasted longer than 70 days (32 sites). Average PW Hg(II) and MeHg concentrations were almost one and two orders of magnitude higher, respectively, than concentrations in inflowing water. Pore water Hg(II) concentrations ranged from 5e-11 to 5e-10 mol/l and PW MeHg ranged from 5e-12 to 5e-11 mol/l. Bulk Hg and MeHg sediment concentrations were very similar in dry and wet conditions (Figure 3.3).

3.5.2. Base case scenario and varying initial ferrihydrite and sulfate concentrations

Model simulation results with varying initial ferrihydrite and sulfate concentrations (Table 3.2) fell within the range of dissolved and sediment concentrations that were observed at CCSB floodplain sites after flooding (Figure 3.4). Simulated PW sulfate decreases in all scenarios due to sulfate reduction, which matches with the observation that sulfate is higher in the inflowing water than in the PW (Figure 3.4A). Total sediment mackinawite in simulations stays almost constant in the scenario with low Fe/ high S, and slightly increases in the medium and high Fe scenario (Figure 3.4B). Observed PW sulfide concentrations are initially around 2e-6 mol/l and further decrease in the scenario with high Fe/low S (Figure 3.4C). Simulated PW sulfide increases up to two orders of magnitude in the scenarios with low and medium Fe/ low S. The simulated PW sulfide concentrations cover the range of PW sulfide observed in CCSB floodplains. Sediment Hg in simulations consists of HgS(s) and $Hg(SOM\text{-}RS)_2$ (Figure 3.4D, F). The total sediment Hg does not vary over time, but the distribution between HgS(s) and $Hg(SOM\text{-}RS)_2$ changes in simulations. Below around 1e-6 mol/l PW sulfide, there are almost equal amounts of HgS(s) and $Hg(SOM\text{-}RS)_2$.

An increase in PW sulfide results in a shift from $Hg(SOM\text{-}RS)_2$ to HgS(s). Simulated dissolved Hg(II) is initially around 2e-11 mol/l and increases when PW sulfide increases (Figure 3.4F). Simulated dissolved MeHg is initially zero and increases in all three scenarios, but it reaches higher concentrations when simulated dissolved Hg(II) is higher (Figure 3.4G).

3.5.3. Varying Hg mineral solubility

Different scenarios were tested to explore the effect of mineral solubility on the simulation of dissolved Hg and MeHg concentrations. Setting a more soluble phase, nano-HgS (*log K = -36.4* (Drott et al., 2013)) rather than metacinnabar (*log K = -37.3* (Powell et al., 2005)), in equilibrium with the solution gave a better prediction of PW Hg(II) and MeHg at low sulfide concentrations, although simulated values were still lower than observed values (Figure 3.5). In the shown simulation scenario, the simulated dissolved sulfide concentration increases around day 5, which results in overprediction of PW Hg(II) and MeHg by two orders-of-magnitude if nano-HgS is used to set the solubility. Setting metacinnabar in equilibrium with solution instead of nano-HgS gave a better prediction of PW Hg(II) and MeHg at high sulfide concentrations, although simulated values were still higher than observed values (Figure 3.5). Metacinnabar, not cinnabar was selected to set the solubility because it was shown to precipitate after flooding of soils (Barnett et al., 1997).

Setting nano-HgS in equilibrium with solution and including a kinetic rate of precipitation for metacinnabar depending on $[S(-II)tot]/[RSH_{LMW\,DOM}]$ (Equation(3.1)) resulted in approximately one order-of-magnitude higher simulated PW Hg(II) and MeHg under low $[S(-II)tot]/[RSH_{LMW\,DOM}]$ and one order-of-magnitude lower simulated PW Hg(II) and MeHg under high $[S(-II)tot]/[RSH_{LMW\,DOM}]$, which in both cases meant that simulated values were closer to observed values (Figure 3.5). The simulated concentration of $RSH_{LMW\,DOM}$ did not change over time and a change in $[S(-II)tot]/[RSH_{LMW\,DOM}]$ mostly occurred due to a change in sulfide concentration. In the simulation results shown in Figure 3.5 a rapid change in $[S(-II)tot]/[RSH_{LMW\,DOM}]$ occurs around day 5. The same trends were simulated for PW Hg(II) and MeHg (lower and higher depending on $[S(-II)tot]/[RSH_{LMW\,DOM}]$) when $[S(-II)tot]/[RSH_{LMW\,DOM}]$ changed at any other day (not shown). Under low sulfide concentrations and low $[H_2S]/[RSH_{LMW\,DOM}]$, sediment Hg is present as nano-HgS(s) and $Hg(SOM\text{-}RS)_2$ whereas metacinnabar constitutes all sediment Hg under high sulfide concentrations and high $[S(-II)tot]/[RSH_{LMW\,DOM}]$ (Figure 3.6).

3.6. Discussion

3.6.1. Uncertainty in simulating Hg(II) and MeHg bonding to thiol sites on organic matter

Careful selection of thermodynamic constants and estimation of the number of thiol (-RS) sites for aqueous complexation or sorption to sediment OM is important to reduce model uncertainty. However, it was found to have a minor role in improving model fit when sulfide concentrations varied over several orders of magnitude. Potential reasons for the minor role might be the simplified model approaches to represent thiol groups and cycling of OM. Simplified approaches are typically chosen to make models more practical, due to a lack of data and gaps in our basic knowledge. Hg reaction models typically employ a simplified approach by including only the most relevant complexes and average binding constants for complexation with DOM-RS or sorption to SOM-RS (Liem-Nguyen et al., 2017a, 2021). In addition, there is no consensus on the

importance of thiol sites on cell membranes (Song et al., 2020; Thomas et al., 2020), mineral particles coated with organic material (Liem-Nguyen et al., 2021; Zhang et al., 2019) and adsorption kinetics (Jonsson et al., 2012; Liem-Nguyen et al., 2021) to predict Hg cycling. Typically, there is also a simplified approach for OM cycling employed in which OM that is available for degradation via primary redox reaction is supplied in excess and degraded to CO_2 and H_2O (Berner, 1980; Van Cappellen & Wang, 1995). However, OM cycling is highly complex, e.g., OM composition changes with ongoing degradation (Arndt et al., 2013) and microbial biosynthesis of LMW OM (Adediran et al., 2019) are potentially important to quantify Hg cycling. Estimation of model parameters related to Hg bonding to thiol groups for the simulation scenarios of this study are discussed in detail in supplemental information.

3.6.2. Importance of iron and sulfur in controlling MeHg production

Simulation results demonstrate the importance of iron in controlling sulfide concentrations and therefore indirectly affecting Hg bioavailability and MeHg production (Figure 3.4). Based on observed PW sulfate, PW sulfide, TRS and amorphous ferric iron (Fe(III)a) it was inferred that iron reduction and sulfate reduction occurred at flooded floodplains, which was replicated in simulations. Dissolved sulfide was mainly produced from sulfate reduction in model simulations. Fe(II) was produced from reductive dissolution of Fe(III) oxide minerals in sediment. In model simulations, Fe(II) and sulfide precipitate to form the iron sulfide mineral mackinawite (FeS(s)) (Figure 3.4B) (Rickard & Luther, 2007). Iron(III) and sulfate reduction fall into a similar range of thermodynamic potential and can take place simultaneously in aquatic systems depending on the electron acceptor. Sulfide will remain at micromolar concentrations as long as mackinawite is undersaturated and Fe(II) is present. This means that sulfate reduction cannot be equated with changes in sulfide concentration. Direct measurement of dissolved sulfide is a valuable measurement because it strongly affects dissolved Hg(II) concentrations.

Until recently, a common hypothesis in the literature was that MeHg concentration decreases with increasing dissolved sulfide concentration because bioavailable Hg(II) precipitates as HgS(s), which is less bioavailable (Bigham et al., 2016; Driscoll et al., 2013; Zhu et al., 2018). However, the simulations of this study and previous published work shows that dissolved Hg(II) and MeHg concentrations can increase with increasing dissolved sulfide concentrations (Graham et al., 2012; Liem-Nguyen et al., 2017a, 2017b). One mechanism for increasing dissolved Hg(II) and MeHg concentrations with increasing sulfide concentrations is desorption from SOM (Figure 3.4D-G). When sulfide is present, dissolved Hg(II) is predicted to be mostly in the form of strong aqueous Hg-sulfide complexes. Because the methylation rate is first-order with respect to dissolved Hg(II) in the model, simulated MeHg concentrations increase when Hg(II) increases (Figure 3.4G).

One hypothesis is that increasing sulfide concentrations provide conditions that lead to the formation of Hg species that are more important for Hg(II) methylation than other species. Initially it was thought that mostly neutral aqueous HgS complexes are available for methylation (Benoit et al., 1999). A new hypothesis suggests that HgS(s) nanoparticles or polynuclear Hg-S clusters form when dissolved sulfide increases and are readily bioavailable (Gerbig et al., 2011; Thomas et al., 2018, 2019, 2020; Thomas & Gaillard, 2017). This hypothesis is supported by correlations between Hg(II) methylation and dissolved cysteine and sulfide concentrations, and is bolstered through identification of Hg species with EXAFS and XANES (Gerbig et al., 2011; Thomas et al., 2018, 2019; Thomas & Gaillard, 2017). However, in these experiments, dissolved sulfide was a product of the biodegradation of cysteine.

3.6.3. Effect of organic matter on HgS(s) solubility

In this and other thermodynamic simulation studies, aqueous sulfide was shown to outcompete thiol ligands associated with DOM for complexation with Hg(II) at low sulfide concentrations, which results in poor simulation of dissolved Hg(II) and MeHg concentrations (Graham et al., 2012; Liem-Nguyen et al., 2017a, 2017b). In our simulations, dissolved Hg(II) was lower than observed values when dissolved sulfide was below 1e-6 mol/l and higher than observed values when sulfide is above 5e-5 mol/l.

The rate formulation for metacinnabar precipitation tested here (Equation (3.1)) is based on the hypothesis that DOM has a stabilizing effect on HgS(s) formation. It has been observed that HgS(s) nanoparticles are prevented from further growth by DOM, particularly thiol-containing DOM (Deonarine & Hsu-Kim, 2009; Gerbig et al., 2011; Graham et al., 2012; Ravichandran et al., 1999; Slowey, 2010). Graham et al. (2013) found that thiol-containing DOM with high sulfur content were particularly effective at enhancing MeHg production. Liem-Nguyen et al. (2017a) hypothesized that the simulated underprediction of dissolved Hg(II) under low sulfide concentrations is because of underprediction of the solubility of nano-HgS(s). Liem-Nguyen et al., (2017a) were able to improve their model fit by choosing a higher apparent solubility for HgS(s) at low sulfide concentrations to account for inhibition of crystallization due to organic molecules, and using a lower apparent solubility at high sulfide concentrations. However, their model did not automatically change the apparent solubility depending on sulfide concentration. The exploratory metacinnabar rate presented here provides a more general approach.

The simulated variability in Hg(II) and MeHg with our kinetic rate for metacinnabar precipitation was still larger than the observed variability, indicating that additional processes or a modified approach need to be taken into account. Below micromolar sulfide concentrations, simulations did not match observed data because there is partitioning of Hg(II) to SOM-RS, which results in underestimation of Hg(II). One explanation for underestimation of simulated dissolved Hg(II) in comparison to observed filtered Hg (fHg) might be that filter-passing nanoparticulate HgS(s) is included in fHg (Liem-Nguyen et al., 2017a). Increasing crystallinity of HgS(s) has been also linked to increasing Hg(II)/DOM ratio (Graham et al., 2012) and might be another mechanism to improve model predictions. Another potential way to improve model performance might be to include sorption to iron sulfide minerals (Blanc et al., 2018; Hellal et al., 2015). Further model development also needs to address the bioavailability of Hg(II) species.

3.7. Summary

We applied a thermodynamic-kinetic model that simulates Hg speciation, OM degradation, cycling of redox-sensitive elements, and mineral dissolution and precipitation to field data from a Hg mine-impacted floodplain. Initial conditions, model parameters, and reactions were varied to improve the match of simulated and observed data. The range of observed PW sulfide concentrations was reproduced by varying initial sediment ferrihydrite and dissolved sulfate concentrations within observed ranges. In line with previous studies (Graham et al., 2012; Liem-Nguyen et al., 2017a, 2017b), we found that simulated dissolved PW Hg(II) concentrations were underpredicted at low dissolved sulfide concentrations and overpredicted at high dissolved sulfide concentrations. Because total PW Hg(II) was assumed to be available for methylation, the simulated under- and overprediction of PW Hg(II) resulted in under- and overprediction of PW MeHg. Thermodynamic constants for complexation of Hg(II) and MeHg with DOM-RS and sorption to SOM-RS, and the number of thiol (-RS) sites, were varied within ranges reported in the literature, but were found to have a minor role in improving simulated dissolved Hg(II) and MeHg

concentrations. Model simulations of field data were tested by implementing a kinetic rate for metacinnabar precipitation that varies with the ratio of aqueous sulfide concentration to the number of thiol sites on DOM. However, there remained underprediction and overprediction of PW Hg(II) concentrations and thus PW MeHg. Although the simulations were performed for one study site, the findings and revised model are applicable to other, similar freshwater sites that are Hg-mine impacted and seasonally flooded. Additional simulations could help clarify why the observed variability is lower than the simulated variability of PW Hg(II), which could help to elucidate why specific environmental conditions are more favorable for MeHg production than others. The PHREEQC reaction model would be ideal to test such hypotheses because it simulates Hg(II) and MeHg within the context of cycling of major elements and transport.

3.8. References

Adediran, G. A., Liem-Nguyen, V., Song, Y., Schaefer, J. K., Skyllberg, U., & Björn, E. (2019). Microbial biosynthesis of thiol compounds: Implications for speciation, cellular uptake, and methylation of Hg(II). Environmental Science & Technology, 53, 8187–8196. https://doi.org/10.1021/acs.est.9b01502

Alpers, C. N., Hunerlach, M. P., May, J. T., & Hothem, R. L. (2005). Mercury contamination from historical gold mining in California. Publications of the US Geological Survey, 61(October), 7.

Arndt, S., Jørgensen, B. B., LaRowe, D. E., Middelburg, J. J., Pancost, R. D., & Regnier, P. (2013). Quantifying the degradation of organic matter in marine sediments: A review and synthesis. Earth-Science Reviews, 123, 53–86. https://doi.org/10.1016/j.earscirev.2013.02.008

Barkay, T., & Gu, B. (2021). Demethylation─The other side of the mercury methylation coin: A critical review. ACS Environmental. https://doi.org/10.5840/protosociology20011517

Barnett, M. O., Harris, L. A., Turner, R. R., Stevenson, R. J., Henson, T. J., Melton, R. C., & Hoffman, D. P. (1997). Formation of mercuric sulfide in soil. Environmental Science and Technology, 31(11), 3037–3043. https://doi.org/10.1021/es960389j

Benoit, J. M., Gilmour, C. C., Mason, R. P., & Heyes, A. (1999). Sulfide controls on mercury speciation and bioavailability to methylating bacteria in sediment pore waters. Environmental Science and Technology, 33(6), 951–957. https://doi.org/10.1021/es9808200

Berner, R. A. (1980). Early Diagenesis: A theoretical approach. Princeton University Press.

Bessinger, B. A., Vlassopoulos, D., Serrano, S., & O'Day, P. A. (2012). Reactive transport modeling of subaqueous sediment caps and implications for the long-term fate of arsenic, mercury, and methylmercury. Aquatic Geochemistry, 18(4), 297–326. https://doi.org/10.1007/s10498-012-9165-4

Bigham, G. N., Murray, K. J., Masue-slowey, Y., & Henry, E. A. (2016). Biogeochemical controls on methylmercury in soils and sediments : Implications for site management. Integrated Environmental Assessment and Management, 13(2), 249–263. https://doi.org/10.1002/ieam.1822

Blanc, P., Burnol, A., Marty, N., Hellal, J., Guérin, V., & Laperche, V. (2018). Methylmercury complexes: Selection of thermodynamic properties and application to the modelling of a column experiment. Science of the Total Environment, 621, 368–375. https://doi.org/10.1016/j.scitotenv.2017.11.259

Brown, K. J., & Nosacka, J. (2020). Final Loads Determination Report: Mercury Control Studies for the Cache Creek Settling Basin, Yolo County, California. https://www.waterboards.ca.gov/centralvalley/water_issues/tmdl/central_valley_projects/delta_hg/archived_delta_hg_info/#tech_reports

Chen, C., & Herr, J. W. (2010). Simulating the effect of sulfate addition on methylmercury output from a wetland. Journal of Environmental Engineering, 136(4), 354–362. https://doi.org/10.1061/(ASCE)EE.1943-7870.0000176

Chen, C., Herr, J. W., & Goldstein, R. a. (2008). Model calculations of total maximum daily loads of mercury for drainage lakes. Journal of the American Water Resources Association, 44(5), 1295–1307. https://doi.org/10.1111/j.1752-1688.2008.00224.x

Chumney, L., Klasing, S., & Tran Pham, H. (2021). Statewide health advisory and guidelines for eating fish from California's lakes and reservoirs without site-specific advice. California Environmental Protection Agency (Issue August). https://oehha.ca.gov/media/downloads/advisories/fishadvisorystatewidelakesreport2021.pdf

Clarkson, T. W. (1997). The toxicology of mercury. Critical Reviews in Clinical Laboratory Sciences, 34(4), 369–403. https://doi.org/10.3109/10408369708998098

Deonarine, A., & Hsu-Kim, H. (2009). Precipitation of mercuric sulfide nanoparticles in NOM-containing water: Implications for the natural environment. Environmental Science and Technology, 43(7), 2368–2373. https://doi.org/10.1021/es803130h

Domagalski, J. L., Slotton, D. G., Alpers, C. N., Suchanek, T. H., Churchill, R., Bloom, N., Ayers, S. M., & Clinkenbeard, J. (2004). Summary and synthesis of mercury studies in the Cache Creek watershed, California, 2000-2001. In U.S. Geological Survey Water –Resources Investigations Report 03-4355. https://pubs.usgs.gov/wri/wri034335/wri_034335.pdf

Driscoll, C. T., Mason, R. P., Chan, H. M., Jacob, D. J., & Pirrone, N. (2013). Mercury as a global pollutant: Sources, pathways, and effects. Environmental Science and Technology, 47, 4967–4983.

Drott, A., Björn, E., Bouchet, S., & Skyllberg, U. (2013). Refining thermodynamic constants for mercury(II)-sulfides in equilibrium with metacinnabar at sub-micromolar aqueous sulfide concentrations. Environmental Science & Technology, 47(9), 4197–4203. https://doi.org/10.1021/es304824n%0A

Gassel, M., & Brodberg, R. (2014). Health advisory and guidelines for eating fish from Cache Creek (Lake, Yolo, and Colusa Counties) (Issue June). https://oehha.ca.gov/media/downloads/advisories/cachecreekadvisoryjuly2014.pdf

Gassel, M., & Brodberg, R. (2018). Health advisory and guidelines for eating fish and shefffish from Clear Lake (Lake County). https://oehha.ca.gov/media/downloads/advisories/clearlakereport080318.pdf

Gerbig, C. A., Kim, C. S., Stegemeier, J. P., Ryan, J. N., & Aiken, G. R. (2011). Formation of nanocolloidal metacinnabar in mercury-DOM-sulfide systems. Environmental Science & Technology, 45(21), 9180–9187. https://doi.org/10.1021/es201837h

Gilmour, C. C., Roden, E., Harris, R., & Report, F. (2007). Approaches to modeling sulfate reduction and methylmercury production in the Everglades. South Florida water management district report. In The South Florida Environment: Vol. I.

Graham, A. M., Aiken, G. R., & Gilmour, C. C. (2012). Dissolved organic matter enhances microbial mercury methylation under sulfidic conditions. Environmental Science and Technology, 46(5), 2715–2723. https://doi.org/10.1021/es203658f

Graham, A. M., Aiken, G. R., & Gilmour, C. C. (2013). Effect of dissolved organic matter source and character on microbial Hg methylation in Hg-S-DOM solutions. Environmental Science and Technology, 47(11), 5746–5754. https://doi.org/10.1021/es400414a

Han, S., & Gill, G. A. (2005). Determination of mercury complexation in coastal and estuarine waters using competitive ligand exchange method. Environmental Science and Technology, 39(17), 6607–6615. https://doi.org/10.1021/es048667z

Hellal, J., Guédron, S., Huguet, L., Schäfer, J., Laperche, V., Joulian, C., Lanceleur, L., Burnol, A., Ghestem, J. P., Garrido, F., & Battaglia-Brunet, F. (2015). Mercury mobilization and

speciation linked to bacterial iron oxide and sulfate reduction: A column study to mimic reactive transfer in an anoxic aquifer. Journal of Contaminant Hydrology, 180, 56–68. https://doi.org/10.1016/j.jconhyd.2015.08.001

Helmrich, S., Vlassopoulos, D., Alpers, C. N., & O'Day, P. A. (2021). Critical review of mercury methylation and methylmercury demethylation rate constants in aquatic sediments for biogeochemical modeling. Critical Reviews in Environmental Science and Technology. https://doi.org/10.1080/10643389.2021.2013073

Hu, H., Mylon, S. E., & Benoit, G. (2006). Distribution of the thiols glutathione and 3-mercaptopropionic acid in Connecticut lakes. Limnology and Oceanography, 51(6), 2763–2774. https://doi.org/10.4319/lo.2006.51.6.2763

Johannesson, K. H., & Neumann, K. (2013). Geochemical cycling of mercury in a deep, confined aquifer: Insights from biogeochemical reactive transport modeling. Geochimica et Cosmochimica Acta, 106, 25–43. https://doi.org/10.1016/j.gca.2012.12.010

Jonsson, S., Skyllberg, U., Nilsson, M. B., Westlund, P., Shchukarev, A., Lundberg, E., & Bjo, E. (2012). Mercury methylation rates for geochemically relevant Hg(II) species in sediments. Environmental Science & Technology, 46(21), 11653–11659. https://doi.org/10.1021/es3015327%0A

Leterme, B., Blanc, P., & Jacques, D. (2014). A reactive transport model for mercury fate in soil—application to different anthropogenic pollution sources. Environmental Science and Pollution Research, 21(21), 12279–12293. https://doi.org/10.1007/s11356-014-3135-x

Leterme, B., & Jacques, D. (2015). A reactive transport model for mercury fate in contaminated soil—sensitivity analysis. Environmental Science and Pollution Research, 22(21), 16830–16842. https://doi.org/10.1007/s11356-015-4876-x

Liem-Nguyen, V., Skyllberg, U., & Björn, E. (2017a). Thermodynamic modelling of the solubility and chemical speciation of mercury and methylmercury driven by organic thiols and micromolar sulfide concentrations in boreal wetlands. Environmental Science & Technology, 51, 3678–3686. https://doi.org/10.1021/acs.est.6b04622

Liem-Nguyen, V., Skyllberg, U., & Björn, E. (2021). Methylmercury formation in boreal wetlands in relation to chemical speciation of mercury(II) and concentration of low molecular mass thiols. Science of the Total Environment, 755, 142666. https://doi.org/10.1016/j.scitotenv.2020.142666

Liem-Nguyen, V., Skyllberg, U., Nam, K., & Björn, E. (2017b). Thermodynamic stability of mercury (II) complexes formed with environmentally relevant low-molecular-mass thiols studied by competing ligand exchange and density functional theory. Environmental Chemistry, 14, 243–253.

Lim, L., Brodberg, R., Gassel, M., & KLasing, S. (2013). Statewide health advisory and guidelines for eating fish from California's lakes and reservoirs without site-specific advice. California Environmental Protection Agency.

Malm, O., Branches, J. F., Akagi, H., Castro, M. B., Pfeiffer, W. C., Harada, M., Bastos, W. R., & Kato, H. (1995). Mercury and methylmercury in fish and human hair from the Tapajós river basin, Brazil. The Science of the Total Environment, 175, 141–150. https://doi.org/10.1016/0048-9697(95)04910-X.

Marvin-Dipasquale, M. C., Alpers, C. N., Fleck, J. A., Agee, J. L., Kieu, L. H., Kakouros, E., Arias, M., Orlando, J., Bennett, P. A., Stumpner, E., Kinnard, K. D., Ward, A. J., & Rose, S. L.

(2021). Shallow sediment geochemistry in a mercury-contaminated multi-habitat floodplain: Cache Creek Settling Basin, Yolo County, California. https://doi.org/10.5066/P9MDXR3M

Melaku Canu, D., Rosati, G., Solidoro, C., Heimbuerger, L. E., & Acquavita, A. (2015). A comprehensive assessment of the mercury budget in the Marano-Grado Lagoon (Adriatic Sea) using a combined observational modeling approach. Marine Chemistry, 177, 742–752. https://doi.org/10.1016/j.marchem.2015.10.013

Mergler, D., Anderson, H. A., Chan, L. H. M., Mahaffey, K. R., Murray, M., Sakamoto, M., & Stern, A. H. (2007). Methylmercury exposure and health effects in humans: A worldwide concern. Ambio, 36(1), 3–11. https://doi.org/10.1579/0044-7447(2007)36[3:MEAHEI]2.0.CO;2

O'Connor, D., Hou, D., Ok, Y. S., Mulder, J., Duan, L., Wu, Q., Wang, S., Tack, F. M. G., & Rinklebe, J. (2019). Mercury speciation, transformation, and transportation in soils, atmospheric flux, and implications for risk management: A critical review. Environment International, 126(November 2018), 747–761. https://doi.org/10.1016/j.envint.2019.03.019

Paraska, D. W., Hipsey, M. R., & Salmon, U. (2014). Sediment diagenesis models: Review of approaches, challenges and opportunities. Environmental Modelling and Software, 61, 297–325. https://doi.org/10.1016/j.envsoft.2014.05.011

Parks, J. M., Johs, A., Podar, M., Bridou, R., Hurt, R. a., Smith, S. D., Tomanicek, S. J., Qian, Y., Brown, S. D., Brandt, C. C., Palumbo, A. V, Smith, J. C., Wall, J. D., Elias, D. a., & Liang, L. (2013). The genetic basis for bacterial mercury methylation. Science, 339(6125), 1332–1335. https://doi.org/10.1126/science.1230667

Powell, K. J., Brown, P. L., Byrne, R. H., Gadja, T., Hefter, G., Sjoberg, S., & Wanner, H. (2005). Chemical speciation of environmentally significant heavy metals with inorganic ligands. Part 1: The Hg 2+ –Cl– , OH– , CO 32– , SO 42– , and PO 43– aqueous systems. IUPAC Technical Report. In Pure Appl. Chem. (Vol. 77, Issue 4). https://doi.org/10.1351/pac200577040739

Ravichandran, M., Aiken, G. R., Ryan, J. N., & Reddy, M. M. (1999). Inhibition of precipitation and aggregation of metacinnabar (HgS) by humic substances isolated from the Florida Everglades. Abstracts of Papers of the American Chemical Society, 217(9), 105-ENVR. https://doi.org/10.1021/es9811187

Richard, J.-H., Bischoff, C., & Biester, H. (2016). Comparing modeled and measured mercury speciation in contaminated groundwater: Importance of dissolved organic matter composition. Environmental Science & Technology, 50, 7508–7516. https://doi.org/10.1021/acs.est.6b00500

Rickard, D., & Luther, G. W. (2007). Chemistry of Iron Sulfides. Chemical Reviews, 107(2), 514–562. https://doi.org/10.1021/cr0503658

Schaefer, J. K., & Morel, F. M. M. (2009). High methylation rates of mercury bound to cysteine by Geobacter sulfurreducens. Nature Geoscience, 2(2), 123–126. https://doi.org/10.1038/ngeo412

Schaefer, J. K., Rocks, S. S., Zheng, W., Liang, L., Gu, B., Morel, F. M. M. M., Zhang, W., Liang, L., Gu, B., & Morel, F. M. M. M. (2011). Active transport, substrate specificity, and methylation of Hg(II) in anaerobic bacteria. Proceedings of the National Academy of Sciences of the United States of America, 108(21), 8714–8719. https://doi.org/10.1073/pnas.1105781108

Schaefer, J. K., Szczuka, A., & Morel, F. (2014). Effect of divalent metals on Hg(II) uptake and methylation by bacteria. Environmental Science & Technology, 48(5), 3007–3013. https://doi.org/10.1021/es405215v

Slowey, A. J. (2010). Rate of formation and dissolution of mercury sulfide nanoparticles: The dual role of natural organic matter. Geochimica et Cosmochimica Acta, 74(16), 4693–4708. https://doi.org/10.1016/j.gca.2010.05.012

Song, Y., Adediran, G. A., Jiang, T., Hayama, S., Björn, E., & Skyllberg, U. (2020). Toward an internally consistent model for Hg(II) chemical speciation calculations in bacterium-natural organic matter-low molecular mass thiol systems. Environmental Science and Technology, 54(13), 8094–8103. https://doi.org/10.1021/acs.est.0c01751

Thomas, S. A., Catty, P., Hazemann, J., Michaud-soret, I., & Gaillard, J. (2019). The role of cysteine and sulfide in the interplay between microbial Hg (II) uptake and sulfur. Metallomics, 11(7), 1219–1229. https://doi.org/10.1039/C9MT00077A

Thomas, S. A., & Gaillard, J. (2017). Cysteine addition promotes sulfide production and 4-fold Hg(II)–S coordination in actively metabolizing Escherichia coli. Environ. Sci. Technol., 51(8), 4642–4651. https://doi.org/10.1021/acs.est.6b06400

Thomas, S. A., Mishra, B., & Myneni, S. C. B. (2020). Cellular mercury coordination environment, and not cell surface ligands, influence bacterial methylmercury production. Environmental Science and Technology, 54(7), 3960–3968. https://doi.org/10.1021/acs.est.9b05915

Thomas, S. A., Rodby, K. E., Roth, E. W., Wu, J., & Gaillard, J. F. (2018). Spectroscopic and microscopic evidence of biomediated HgS species formation from Hg(II)-cysteine complexes: Implications for Hg(II) bioavailability. Environmental Science and Technology, 52(17), 10030–10039. https://doi.org/10.1021/acs.est.8b01305

Van Cappellen, P., & Wang, Y. (1995). Metal cycling in surface sediments: Modeling the interplay of transport and reaction. In Metal contaminated aquatic sediments (pp. 21–62).

Windham-Myers, L., Fleck, J. A., Ackerman, J. T., Marvin-DiPasquale, M., Stricker, C. A., Heim, W. a., Bachand, P. a M., Eagles-Smith, C. A., Gill, G., Stephenson, M., & Alpers, C. N. (2014). Mercury cycling in agricultural and managed wetlands: A synthesis of methylmercury production, hydrologic export, and bioaccumulation from an integrated field study. Science of the Total Environment, 484(1), 221–231. https://doi.org/10.1016/j.scitotenv.2014.01.033

Wood, M. L., Foe, C., & Cooke, J. (2010). Sacramento – San Joaquin Delta Estuary TMDL for Methylmercury Staff Report. Draft Report for Scientific Peer Review (Issue April). https://www.waterboards.ca.gov/centralvalley/water_issues/tmdl/central_valley_projects/delta_hg/archived_delta_hg_info/april_2010_hg_tmdl_hearing/apr2010_tmdl_staffrpt_final.pdf

Zhang, J., Wang, F., House, J. D., & Page, B. (2004). Thiols in wetland interstitial waters and their role in mercury and methylmercury speciation. Limnology and Oceanography, 49(6), 2276–2286. https://doi.org/10.4319/lo.2004.49.6.2276

Zhang, L., Wu, S., Zhao, L., Lu, X., Pierce, E. M., Gu, B., Wu, S., Zhao, L., Lu, X., Pierce, E. M., & Gu, B. (2019). Mercury sorption and desorption on organo-mineral particulates as a source for microbial methylation [Research-article]. Environmental Science & Technology, 53(5), 2426–2433. https://doi.org/10.1021/acs.est.8b06020

Zhu, S., Zhang, Z., & Žagar, D. (2018). Mercury transport and fate models in aquatic systems: A review and synthesis. Science of the Total Environment, 639, 538–549. https://doi.org/10.1016/j.scitotenv.2018.04.397

3.9. Figures and Tables

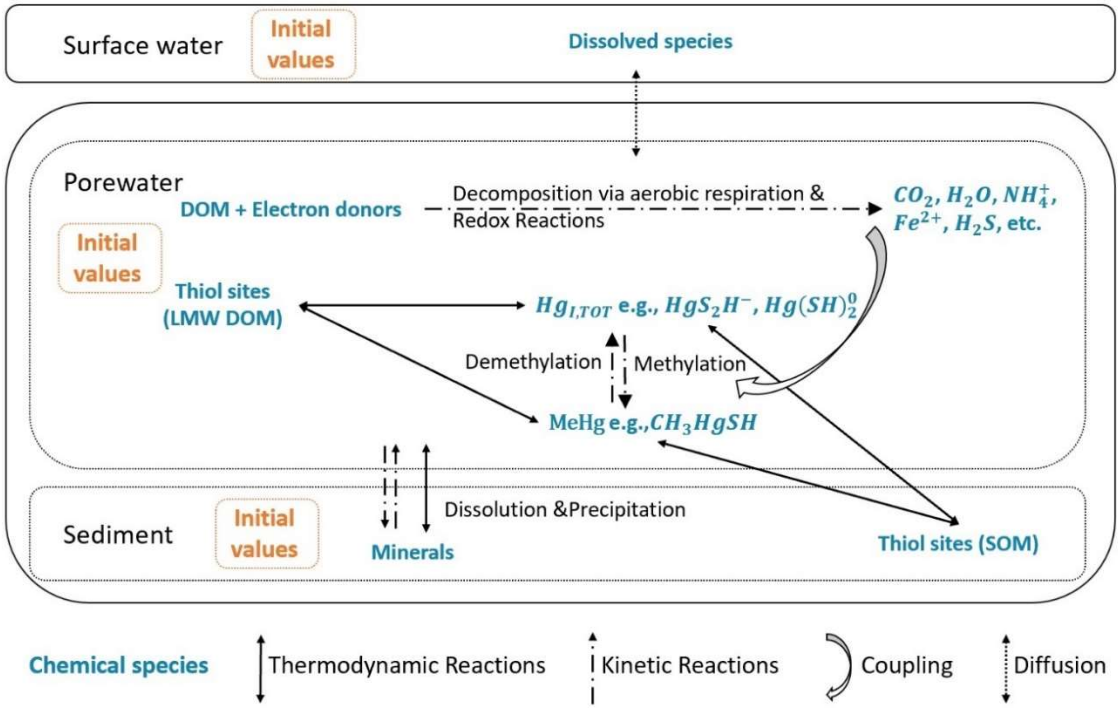

Figure 3.1. Conceptual model for PHREEQC mercury model showing diffusion between overlying surface water and porewater, and reactions that are happening in porewater and sediment. The surface water and the sediment (including porewater) are each represented by one cell in PHREEQC. DOM, dissolved organic matter; SOM, sediment organic matter; LMW, low molecular weight; CO_2, carbon dioxide; H_2O, water; NH_4^+, ammonium; Fe^{2+}, ferrous ion; H_2S, hydrogen sulfide; $Hg_{I,TOT}$, total inorganic mercury; MeHg, methylmercury.

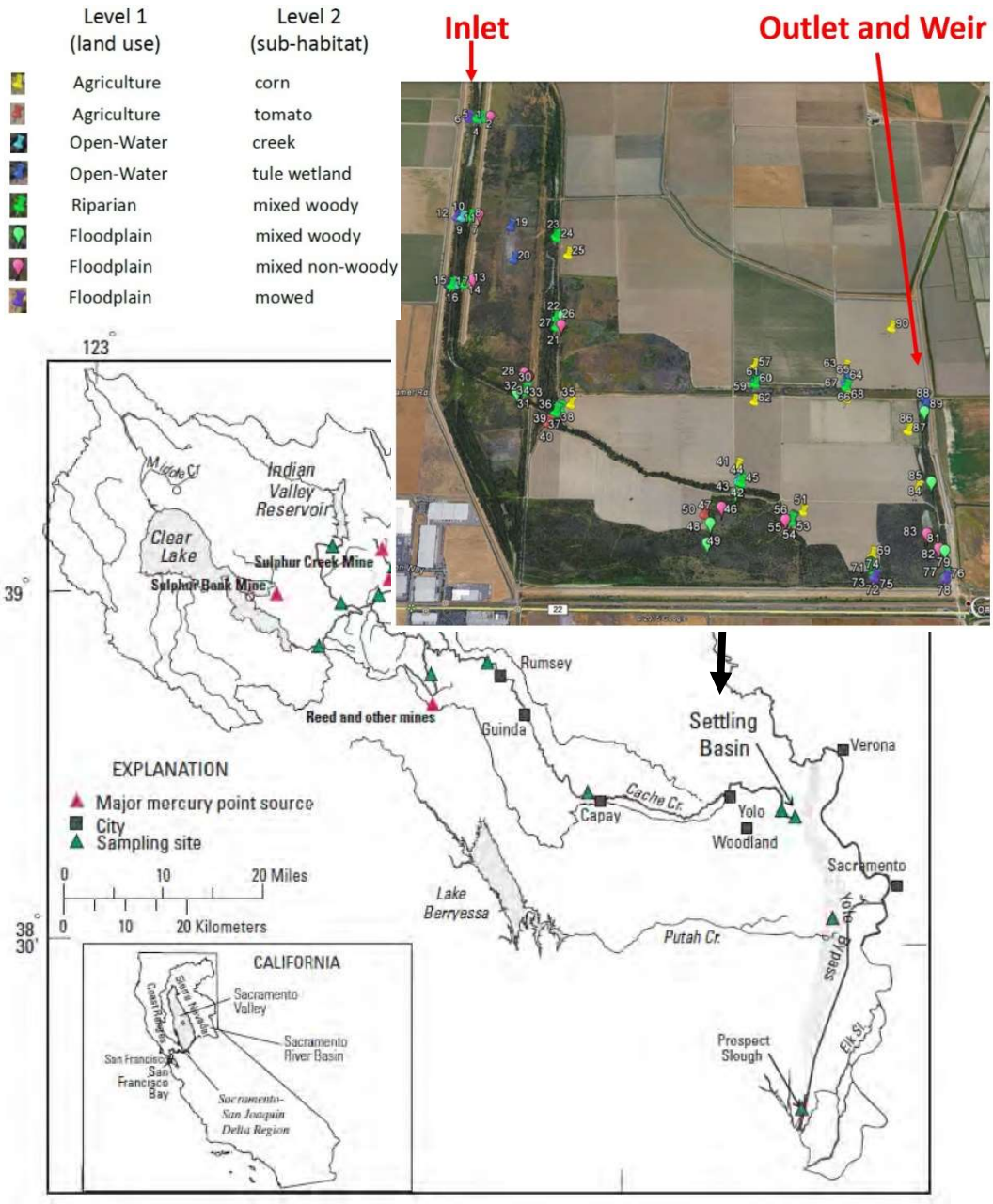

Figure 3.2. Map of the Cache Creek Settling Basin study area used in simulations (Brown & Nosacka, 2020). Sampling locations are classified according to land use and sub-habitat.

Table 3.1. Initial conditions in the PhreeqC model for overlying water and pore water and sediment constituents for the base case scenario of floodplain sites in the Cache Creek Settling Basin.

Parameter	Overlying water	Porewater	Unit	Comment
Aqueous solution (porewater)				
pH	8.2	8.2	Log activity (H^+)	a
p*e*	12	4	Log activity (e^-)	b
HCO_3^-	$6.9 \cdot 10^{-3}$	$6.9 \cdot 10^{-2}$	mol L^{-1}	a
Cl	$5.5 \cdot 10^{-5}$	$5.5 \cdot 10^{-5}$	mol L^{-1}	a
Na	$5.5 \cdot 10^{-5}$	$5.5 \cdot 10^{-5}$	mol L^{-1}	a, c
$O_2(g)$	$2.0 \cdot 10^{-4}$	0	mol L^{-1}	d
N (total)	$1.0 \cdot 10^{-4}$	$1.0 \cdot 10^{-6}$	mol L^{-1}	d
S(VI)	$6.0 \cdot 10^{-4}$	$6.0 \cdot 10^{-4}$	mol L^{-1}	a, f
S(-II)	0	$1.0 \cdot 10^{-10}$	mol L^{-1}	e, f
Hg	0	$2.0 \cdot 10^{-6}$	mol L^{-1}	a, g, h
MeHg	0	0	mol L^{-1}	a, g
RSH (LMW DOM)	$1.0 \cdot 10^{-7}$	$1.0 \cdot 10^{-7}$	mol L^{-1}	i
Sediment				
Ferrihydrite	-	$5.0 \cdot 10^{-3}$	moles	a, j
Mackinawite	-	$5.0 \cdot 10^{-3}$	moles	a, k
Calcite	-	1	moles	l
Metacinnabar	-	$2.0 \cdot 10^{-10}$	moles	e, h
DOM	-	$5.0 \cdot 10^{-3}$	moles	m
SOM-RS	-	$3 \cdot 10^{-6}$	moles	n

a Estimated to replicate trends observed at all floodplain sites
b Estimated based on redox active species concentrations
c Species used for charge balance
d Estimated based on typical values in freshwater
e Small starting value needed for simulation of porewater
f S(-II) and S(VI) defined as separate master species in PHREEQC to allow kinetic reactions

g Hg and MeHg defined as separate master species in PHREEQC to allow kinetic reactions
h Equilibration step will redistribute Hg from aqueous phase to sediment
i RSH – thiol group, LMW DOM – low molecular weight organic matter; Based on concentrations reported in literature (Han & Gill, 2005; Liem-Nguyen et al., 2017a; Zhang et al., 2004)
j Amount was high enough to precipitate all sulfide as FeS(s); measured bulk sediment Fe(III)a: $6.5 \cdot 10^{-3}$ moles (scaled to PHREEQC)
k Based on measured total reactive sulfide (TRS)
l pH buffer
m Derived by model fitting, observed LOI: 5 – 25 % dry wt., PW DOC: 8 – 186 mg/l
n Was determined in sensitivity analysis that compared simulated and observed Hg associated with SOM

Table 3.2. Overview of initial conditions and reactions for simulation scenarios that deviate from base case scenario.

Varying initial concentrations of ferrihydrite and sulfate (Figure 3.4.)[a]		
	Ferrihydrite(s) (moles)	Sulfate(aq) (mol/l)
High Fe/ Low S	5e-3	6e-4
Medium Fe/ Low S	5e-4	6e-4
Low Fe/ High S	1e-4	6e-3
Hg mineral solubility (Figure 3.5. and 3.6.)		
Thermodynamic, variation of most stable phase		
Either metacinnabar (log K = -37.3) (base case scenario) or		
nano-HgS(s) (log K= –36.4) in equilibrium with porewater		
Thermodynamic and kinetic		
Nano-HgS is in equilibrium; kinetic metacinnabar precipitation:		
$\boldsymbol{R_{metacin\ precip\ \ non-linear}} = (\boldsymbol{k_{metacin\ precip}}^{([H_2S]/[RSH_{LMW\ DOM}])}) - \mathbf{1}$ when log SI>0[b]		

[a] Other sources for Fe and S are present in model, but do not necessarily affect simulated mercury
[b] Dissolution when log saturation index (SI)<0

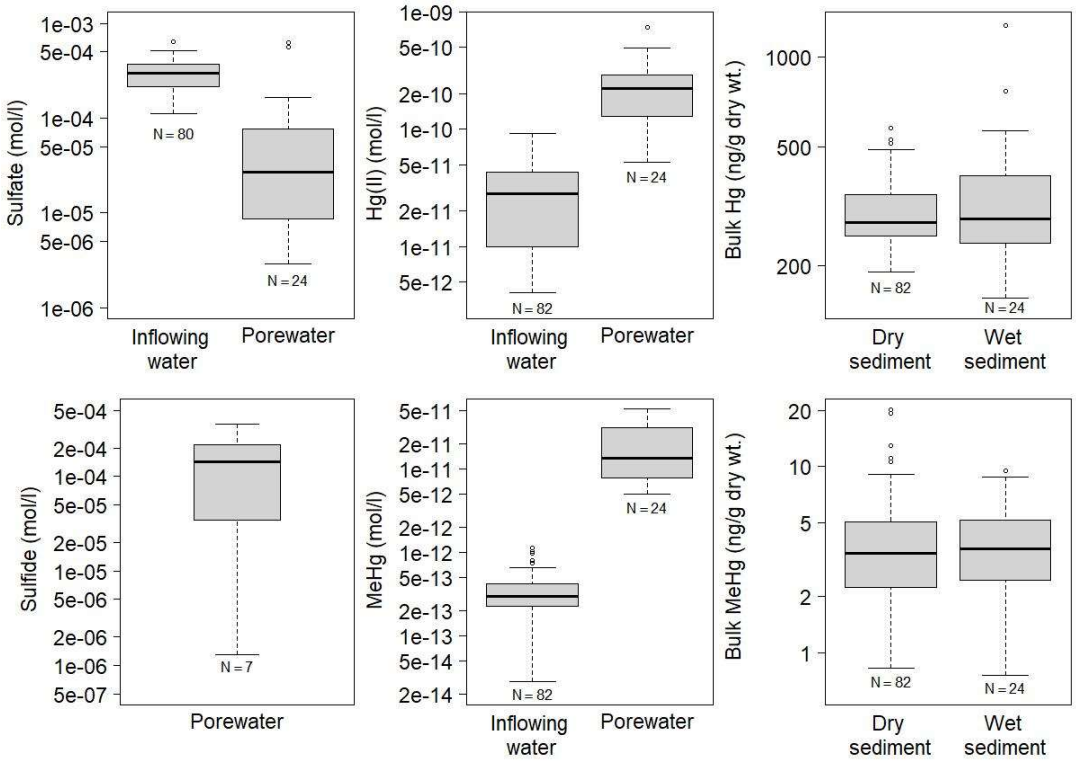

Figure 3.3. Boxplots (log-scale) showing sulfate, sulfide, Hg(II), and MeHg concentrations for inflowing water and porewater, and bulk Hg and MeHg concentrations in dry and wet sediment at floodplain sites at CCSB that were flooded for up to 70 days (data for sediment and porewater from Marvin-Dipasquale et al. (2021); data for inflowing water from https://waterdata.usgs.gov). Only inflowing water that resulted in flooding and data from dry sediment that was later flooded were included. The solid line of the boxplot shows the median, the box shows the first and third quartile, and dots show maximum and minimum data points.

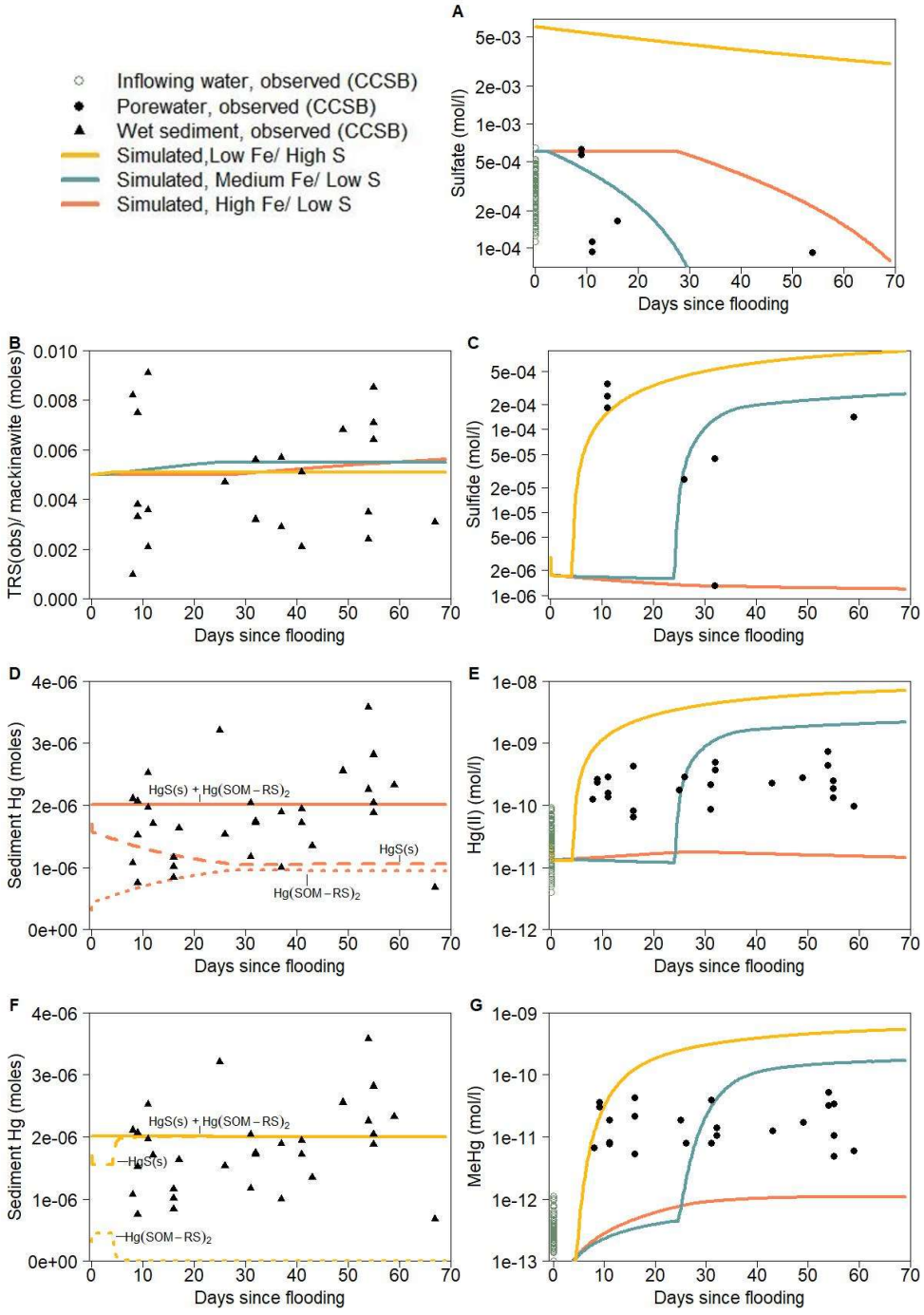

Figure 3.4. Simulated aqueous species (log-scale) A) sulfate, C) sulfide, E) Hg(II), and G) MeHg, and B) simulated mackinawite (FeS(s)) and observed TRS, D) simulated sediment Hg for the scenario high Fe/ low S, F) sediment Hg for the scenario low Fe/ high S plotted as a function of the number of days since flooding. Sediment Hg shows HgS(s) and Hg(SOM-RS)$_2$. Simulated aqueous species and mackinawite are shown for three scenarios with varying initial ferrihydrite and sulfate concentrations that result in different sulfide concentrations at day 70. Observed data are shown for comparison.

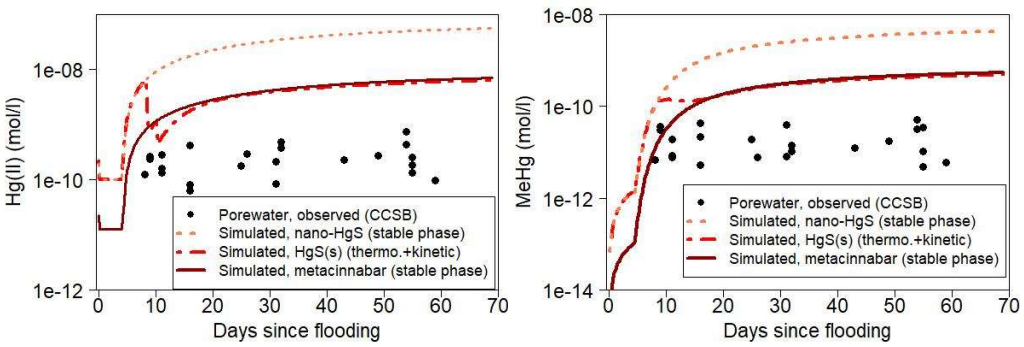

Figure 3.5. Simulated dissolved Hg(II) and MeHg compared with observed porewater Hg(II) and MeHg (points) concentrations (log-scale) for scenarios with either nano-HgS(s) or metacinnabar in equilibrium with the solution, and with a non-linear rate for metacinnabar precipitation to dynamically switch solubility for log SI > 0 depending on the sulfide/RSH(LMW DOM) ratio. Initial ferrihydrite and sulfate are the same as in scenario low Fe/high S.

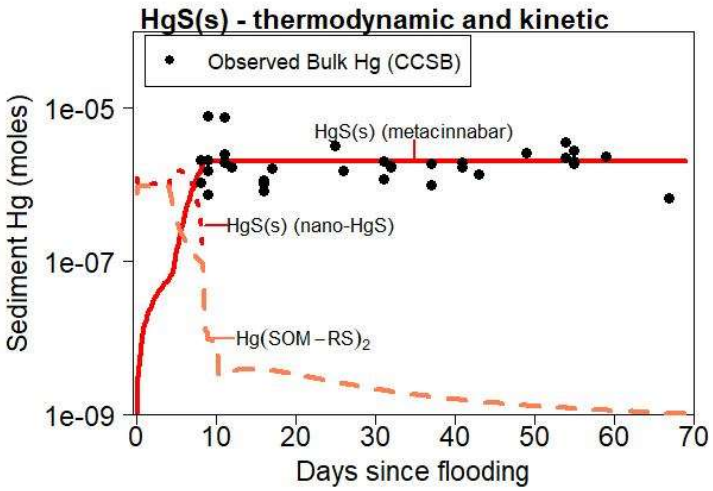

Figure 3.6. Simulated moles of metacinnabar, nano-HgS(s) and $Hg(SOM\text{-}RS)_2$ compared with observed sediment bulk Hg (log-scale) when using a non-linear rate for metacinnabar precipitation (Equation(3.1)) to dynamically switch solubility depending on $[S(-II)tot]/[RSH_{LMW\ DOM}]$ ratio. Initial ferrihydrite and sulfate are the same as in scenario low Fe/high S.